

**Theoretical and lab based studies of fluorescence anisotropy
toward the analysis of multiple homo-FRET pairs**

Zahra Zolmajd Haghighi

School of Science and Technology

Nottingham Trent University

Director of Study:

Dr. Quentin S. Hanley

Thesis submitted for the Degree of Doctor of Philosophy (PhD)

November 2014

This research is a part of the project:

“Nanoactuation of plasma membrane protein clusters”

Acknowledgements

Hereby I would like to convey my sincere gratitude to my competent and caring supervisor Dr. Quentin Hanley. I appreciate his patient guidance, continued support and great care of my family life.

I also greatly thank Dr. Haida Liang as my second supervisor whose great support helped me pass the “hard time”.

I would like extend my gratitude and appreciation to Dr. David Hughes for his help with electrophoresis of my DNA samples.

I express my gratitude to Dr. Homanaz Ghafarifar for her invaluable help during my first days in the UK and Dr. Mostafa Moghisi for the support that he provided for me. I would also like to thank my friends and sisters; Dr. Masoumeh Nazarian, Motahatreh Habibi and Dr. Zahra Gholami who were my angels during my life in the UK.

I acknowledge funding from NanoSci-E+ as a part of the NanoActuate consortium. In the UK Nano Actuate was administrated by EPSRC EP/H00694X/1.

I am indebted to Professor Carole Perry’s lab and I would like to thank Mithun Parambath for his help.

I would specially like to thank my sisters Maryam and Nazanin and my beloved daughter, Nikki, for all the hope and joy she brought to my life and last but not least my dear mother, whose prayer for me was what sustained me so far.

List of symbols

r	Anisotropy
r_{FRET}	Anisotropy of the dye in the presence of the energy transfer
r_o	fundamental anisotropy in the absence of rotational diffusion
G	correction factor for anisotropy measurements
I	steady-state intensity or fluorescence
I_{mono}	fluorescence intensity of a cluster labelled with one dye
E	efficiency of energy transfer
θ	rotational correlation time
R_o	Förster distance in resonance energy transfer
R	distance between fluorophores
N	number of subunits in a cluster
Q	quantum yield
η	Viscosity
τ	lifetime
κ^2	orientation factor in resonance energy transfer
Φ_i	fluorescence intensity of a cluster with i labels

λ	wavelength (nm)
λ_{em}	maximum emission wavelength
λ_{ex}	maximum excitation or absorption wavelength
F_D	relative fluorescence intensity of donor
F_{DA}	intensity of donor in the presence of acceptor
$\pi_m(t)$	the probability that m th molecule is excited at time t
f	fraction of labelled subunits
VH, I_{\perp}	intensity measured when the polarizers are perpendicular
VV, I_{\parallel}	intensity measured when the polarizers are parallel
A	acceptor or absorption
z_i	correction factor for intensity measurements
q_N	correction factor for N considering the distances between the dyes
A_{iN}	the i^{th} element of the N^{th} row of Pascal's triangle

Abstract

Many biological functions, involve assembly of proteins. Protein clustering has an important role in signal transduction through the cell membrane. Model systems that simulate receptor aggregation can be used to monitor oligomerization. Techniques based on homo-FRET can reveal the aggregation state of receptor proteins because homo-FRET causes the fluorescence anisotropy of the system to decrease when the number of identical fluorophores within energy transfer distance increases. Theories that describe these systems apply an assumption of equal fluorescence efficiency for all sites [1, 2], that means emission intensity of fluorophores do not change when in close proximity with each other in a cluster. However, most fluorophores in close proximity show either self-quenching or emission enhancement. Previous theories that were devised to study fractional labelling of proteins were only applicable to cases where the distances between the labels were less than $0.8R_0$, while in practice the distances between the dyes are more in protein aggregates.

Three different systems were chosen to mimic aggregation of fluorescently labelled receptor proteins and analytical expressions were presented for fully labelled and fractionally labelled clusters and the experimental results from the three systems were analyzed. The systems were: a)stochastically labelled BSA containing up to 24 FITC, b) DNA fused trimeric clusters of fluorescein (stochastically labelled), and c)DNA Holliday junctions labelled with fluorescein (in a range of sizes). The inter-probe distances on the DNA constructs were designed to be up to $1.5 R_0$ to cover cluster sizes of larger protein clusters. The experimental results showed that: 1) none of the clustered species followed the assumption of equal fluorescence efficiency, 2) by applying the assumption of equal fluorescence efficiency, anisotropies were under-predicted and cluster sizes were under-estimated in systems that show quenching and 3) anisotropy behaviour of a multiply labelled cluster of a particular size depends on the behaviour of the fluorophores and their distance in a cluster.

As a result of the theory presented here, the size of larger clusters than currently considered possible can be determined; if they are strongly quenched and their fractional labelling is carefully selected.

Table of Contents

Acknowledgements	2
Abstract	5
Publications.....	10
1 Protein Aggregation and Fluorescence	11
1.1 Introduction	11
1.2 Protein Aggregation in Living Cells	14
1.3 Fluorescence Emission.....	15
1.4 Anisotropy.....	15
1.5 Förster Resonance Energy Transfer (FRET).....	17
1.6 Distance measurement by multiple FRET	20
1.7 Homo-FRET	21
1.7.1 Fluorescence depolarization and cluster size	22
1.7.2 Depolarization curve as a function of labelling.....	26
1.8 Homo-FRET and fluorescently labelled proteins.....	29
1.9 Self–Quenching	31
1.10 Enhancement of fluorescence emission	32
1.11 Size of Clusters in living cells	33
1.12 Conclusion.....	34
1.13 Aims	35
2 Design, Synthesis and Characterization of Model Systems of Multiple Fluorophores	36
2.1 Introduction	36

2.2	Bovine Serum Albumin	37
2.3	Dendrimers	39
2.4	DNA Constructs	40
2.4.1	DNA strands	41
2.4.2	Four-way junctions	41
2.4.2.1	Geometry.....	43
2.4.2.2	Fluorescein labelled DNA.....	44
2.5	Instrument Validation	45
2.5.1	G-factor	46
2.5.2	Intensity.....	46
2.6	Materials and Methods.....	49
2.6.1	BSA.....	49
2.6.1.1	Labelling reaction	49
2.6.1.2	Removing the unreacted Dye	50
2.6.2	Intensity and Anisotropy measurements.....	50
2.6.3	UV-Visible absorption spectroscopy.....	51
2.6.3.1	Dye to protein ratio	51
2.6.4	DNA Strands	53
2.6.5	Four-way junctions	54
2.7	Results.....	57
2.7.1	BSA.....	57

2.7.2	Dendrimers	58
2.7.3	DNA strands	59
2.7.4	Four-way junctions	60
2.8	Conclusion.....	61
3	Fluorescence Efficiency in Aggregates	62
3.1	Introduction	62
3.2	Theory	63
3.3	Results and discussions.....	65
3.3.1	Model System Verification	68
3.4	Conclusion.....	74
4	Distance Dependent Non-Additivity of Fluorescence Emission and Its Effect on Anisotropy Measurements. ...	75
4.1	Introduction	75
4.2	Theory	76
4.2.1	The emission intensity of individual species in stochastic mixtures ...	76
4.2.2	Finding effective N in clusters labelled with fluorophores undergoing self quenching.....	76
4.3	Results and Discussion	78
4.3.1	DNA Strands	78
4.3.1.1	Intensity.....	78
4.3.1.2	Anisotropy.....	82
4.3.2	Four-way junctions	86

4.3.3	Distances	92
4.3.4	Self-quenching.....	93
4.3.4.1	Intensity.....	93
4.3.4.2	Fitting anisotropy data	95
4.4	Conclusion.....	100
5	Conclusion.....	101
	References	104

Publications

1. Zolmajd-Haghighi, Z. and Q. S. Hanley. Enhancement, Equal Fluorescence Efficiency, and Quenching in the Interpretation of Fluorescence Anisotropy Data. Biophysical Society 58th Annual Meeting, February 15-19, 2014, San Francisco CA.
2. Zolmajd-Haghighi Z. and Q. S. Hanley. When One Plus One Does Not Equal Two: Fluorescence Anisotropy in Aggregates and Multiply Labelled Proteins, *Biophysical Journal*, 106(7):1457-1466 (2014).

1 Protein Aggregation and Fluorescence

1.1 Introduction

The aggregation of biomolecules in living cells via self-assembly is involved in many biological processes and disruption of those processes can lead to malfunction and disease [3-5]. For example, Alpha-synuclein is a protein made of 140 amino acids and exists at the tips of nerve cells in the human brain. Recent studies have shown that long-term exposure to manganese promotes α -synuclein aggregation in neuronal cells and leads to degeneration in the frontal cortex gray and white matter. Such nervous system dysfunction associated with is due to protein misfolding in endoplasmic reticulum[6, 7].

Measurement of aggregations *in vivo* remains a challenge. Ideally, aggregation measurements should be done *in vivo* with methods sensitive to low concentrations due to clustering events leading to activation of signalling involving less than 10^4 protein molecules.

Many biophysical techniques can reveal the size and distribution of aggregates including NMR spectroscopy, gel electrophoresis, X-ray crystallography, optical spectroscopy and electron microscopy [8-10]. These methods cannot be used for *in vivo* studies because they need extensive sample preparations during which the cell structure is destroyed. Fluorescence methods do not suffer from this limitation

allowing the study of live cells in a minimally invasive manner. Biomolecules can be labelled with fluorescent probes and fluorescent imaging techniques subsequently used to study their behaviour [11-14]. A further advantage of fluorescence methods is their high sensitivity. For example, fluorophores give reproducible signals at concentrations below 1 nM extending, to the single molecule level. These techniques are capable of identifying interactions of target molecules against a background of many other molecules in a living cell[14, 15]. Methods, such as total internal reflection fluorescence microscopy (TIRF) and fluorescence correlation spectroscopy (FCS), use one or two-photon excitation to identify single molecules within living cells[15].

Fluorescence techniques such as fluorescence lifetime imaging microscopy (FLIM)[16] and FCS[17] are widely used to study nanometre sized clusters. Fluorescence can be characterized by its intensity, position, wavelength, lifetime, and polarization or anisotropy. Changes in molecule structure, interaction and environment may be assessed by monitoring changes in these parameters as well as, Förster resonance energy transfer(FRET) efficiency and collisional quenching rate [14].

FRET is the non-radiative transfer of excitation energy between dyes. FRET is distance-sensitive on the nanometre scale making it a compatible with protein studies. FRET can be used to determine the spatial separation between two residues in the same or different proteins. A wide variety of FRET methods are suitable for specific problems and upon choosing appropriate fluorophores successful FRET experiments can be designed [14, 18]. FRET imaging combined with state-of-the-art microscopy and spectroscopy has made significant advances in the life sciences as it allows researchers to study phenomena causing changes in molecular proximity[19]. fluorescence resonance energy transfer between identical fluorophores is called homo-FRET and is often used to study molecular self-assembly, the number of subunits in a cluster [5, 20], the distribution of cluster sizes, and the extent of polymerization [4, 21]. Homo-FRET is detected by a decrease in the anisotropy of the fluorescence and is proportional to the number of contributing fluorophores. This allows the application of homo-FRET to measure aggregate formation in cells.

Homo-FRET is a convenient method due to a simplified labelling strategy [22] and has been studied for nearly 50 years beginning with the pioneering work of the Weber group[1]. Theories and methods have evolved to quantify the number of subunits as a function of homo-FRET [1, 23, 24]. These advances in homo-FRET techniques allow researchers to more precisely detect and measure the size of oligomers in living cells which could have a great impact on the study of disorders such as the early stages of neurodegenerative diseases. If the theory can be expanded to study clusters of larger size, its applicability would be considerably widened [5, 25, 26]. Current methodologies are based on a number of simplifying assumptions that either limits their application or causes discrepancies with experimental results. One such simplifying assumption supposes equal fluorescence efficiency for all sites [23, 24], meaning each fluorophore has the same brightness when free in solution as they do in close proximity to each other in a cluster. However proximity dependent quenching and enhancement are known.

FRET involves the transfer of excited-state energy between fluorophores located within approximately 10 nm of each other and the method can be used to measure distances at such scales [27]. Formulae based on homo-FRET that are used to estimate the size of clusters and determine the number of subunits, are simplest on shorter scales (less than 80% of the R_0). For most fluorophores R_0 for homo-FRET is usually less than 4nm [23, 24, 28]. However, most plasma membrane proteins organize in larger clusters [29-31]. Well defined model systems mimicking larger oligomers may be used to study the behaviour of homo-FRET systems with $R > 0.8R_0$ and applicability of the theories.

In the present work models such as bovine serum albumin (BSA) were chosen to mimic large oligomers and simulate clusters with varying numbers of subunits of labelled proteins. Dye binding to BSA has been well studied but techniques that are commonly used to determine the levels of labelling are not precise [32-34].

The study of depolarization behaviour of labelled BSA as a function of labelling was undertaken previously but the number of the fluorophores bound to BSA was not quantified [35] nor was a thorough comparison of results to existing theory carried out. BSA has been fractionally labelled with FITC and the intensity and anisotropy measurements were done and the existing theories were used to fit and analyse the

data and the limitations of the existing theories were examined. Labelled DNA molecules were other model systems that were chosen to simulate labelled oligomers undergoing homo-FRET. Data gathered in each case were analysed by the existing theories and the limitations of the theories were examined.

1.2 Protein Aggregation in Living Cells

Clustering of proteins plays an important role in many biological processes such as signalling networks. For example, G-protein coupled receptors have an important role in signal transduction through the cell membrane and there is considerable evidence that they form oligomers activation[36, 37]. Aggregation of CUL3-modified caspase-8, leads to full activation and processing of cullin3 (CUL3)-based E3 ligase and leads to cell death. The mechanism that positively controls apoptosis signalling by poly ubiquitination includes aggregation of a key initiator (caspase) [38]. The oligomerization of serotonin_{1A} receptors has been monitored and the presence of constitutive oligomers of the serotonin_{1A} receptor is proposed [39];as a mechanism for that the activation of the epidermal growth factor receptor (EGFR) involves the formation of ligand-induced oligomers of the receptor[20, 40, 41]. Misfolding and accumulation of proteins are characteristic signs of some age-related, neurodegenerative conditions such as Alzheimer's, Parkinson's, Creutzfeldt-Jakob and Huntington's[42, 43].Aggregation of β -amyloid peptide and homodimerization of amyloid precursor protein are thought to have a key role in the development of Alzheimer's disease [42, 44, 45]. In Parkinson's disease, the protein α -synuclein (AS) aggregates and forms deposits that containing the proteins in an amyloid fibrillar form in special regions of the brain [46]. Aggregation of poly(Q) protein causes disorders such as Huntington's disease [47]. Age-related cataracts are caused by aggregation of crystalline proteins that exist in the centre of the lens of the eyes[48]. α -crystalline interacts with partially folded T4 lysozyme to prevent its aggregation and possible precipitation. The proposed mechanism states that there is equilibrium between dimeric and oligomeric states of α -crystalline that is coupled to the equilibrium between the folded and unfolded form of T4 lysozyme. It is also thought that the dimeric form of α -crystalline is the activated state that interacts with T4 lysozyme [49].

Elucidating varied multimerisation and clustering processes is challenging particularly *in vivo* and the present work aims to assist to resolve the cluster sizes

1.3 Fluorescence Emission

Fluorescence is emitted when an electron relaxes from the first excited electronic singlet state of the species to its ground electronic energy level (figure 1.3.1) with emission of a photon, while in non-fluorescent substances the energy that is absorbed by the electrons dissipate as heat. Information about the alignment, size and environment of the molecules can be obtained from investigating the extent of polarization of this emission [22, 50, 51].

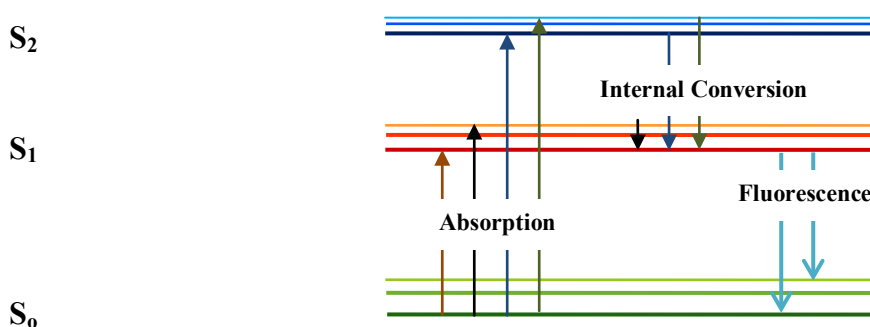


Figure 1.3.1: The diagram shows different electronic energy levels of a fluorophore. Electrons may be excited and jump to any of the vibrational energy levels within each of the higher electronic energy levels, but before they relax back to the ground state and fluoresce, they will fall to the lowest vibrational energy level of the excited state[52].

1.4 Anisotropy

Light is linearly polarized when the orientation of its electric vector (the component of light that interacts with matter) does not change during propagation[53].

The emission anisotropy, r , is a measure of the polarized response of a fluorescent substance to plane polarized excitation light and gives information about the substance and its environment (equation 1.4-1) [22, 54]:

Equation 1.4-1

$$r = \frac{I_{\parallel} - GI_{\perp}}{I_{\parallel} + 2GI_{\perp}}$$

For a sample excited with vertically polarized light (figure 1.4.1), I_{\parallel} and I_{\perp} represent the fluorescence intensities of the vertically and horizontally polarized emission. I_{\parallel} is the emission when the polarisers are set to Vertical-Vertical (VV) orientation and I_{\perp} is the emissions when the orientation is Vertical-Horizontal (VH). G is the ratio of the responsiveness of the detection system to vertically and horizontally polarized light. Monochromators usually have lower transmission efficiencies for horizontally polarized light and they get even less efficient at higher wavelengths [22]. The G factor is a number greater than one and tends to increase with wavelength and corrects for the differential transmission[54, 55].

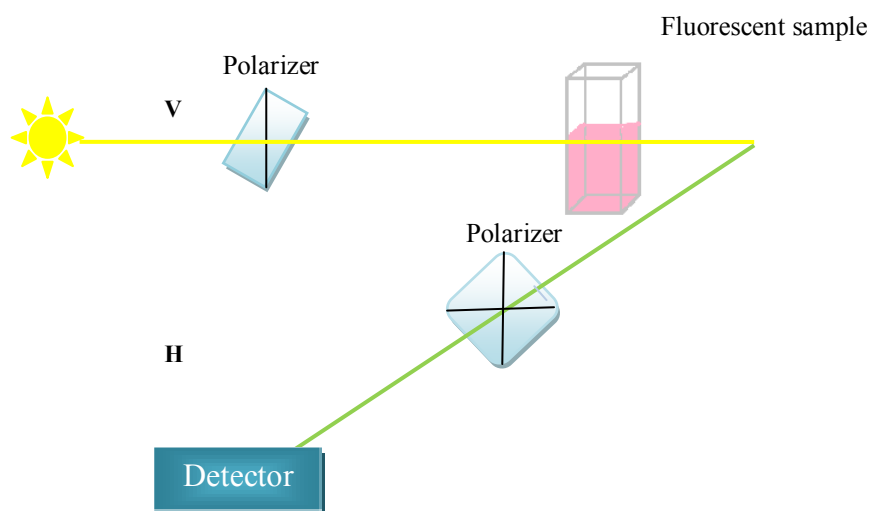


Figure 1.4.1: Geometry of fluorescence anisotropy measuring system. The polarizer in the emission path rotates from the vertical (V) to the horizontal (H) position and the intensity of vertically and horizontally polarized light is measured.

Steady state anisotropy measurements can be used to study physical processes such as rotational diffusion, extent of denaturation, and orientation at surfaces[56]. Anisotropy is ideal for measuring the association of biomolecules such as DNA or proteins with each other or other macromolecules, because the anisotropy always changes with changes in the rotational correlation time [57, 58] or proximity to an acceptor [20, 23].

The probability for excitation of a fluorescent molecule when exposed to linearly polarized light depends on the orientation between the transition moment of the molecule and the electric vector of the photon. Molecules whose absorption dipole moments are orientated parallel to the polarization plane are most efficiently excited. The extent of the polarization of the emitted light or the value of r_0 , be measured in the absence of rotational diffusion, depends on the size of the angle between the emission and excitation transition dipole moments of the molecule, θ , and is a maximum (the theoretical value of 0.4 for single photon excitation), if they are parallel (equation 1.4-2)[54].

Equation 1.4-2

$$r_0 = \frac{3 \cos^2 \theta - 1}{5}$$

However, if the excited state life time of the fluorophore is long enough to allow energy transfer or molecular rotation to take place, the emitted light will depolarize.

If a sample contains several emitting species with anisotropy values of r_i and fractional intensities of f_i , the average anisotropy of the mixture is given by (equation 1.4-3)[53]:

Equation 1.4-3

$$\bar{r} = \sum_i f_i r_i$$

The relationship is sometimes called the sum law of anisotropies.

1.5 Förster Resonance Energy Transfer (FRET)

FRET occurs when a fluorophore in its excited state (donor) transfers its energy via long range dipole-dipole interaction to a molecule in its ground state (acceptor). The distance for a specific donor-acceptor pair at which the energy transfer is 50% efficient is named the Förster distance (R_0) and is 2-5nm for typical fluorophores.

Resonance energy transfer is only significant if a) the molecules are close to each other (within $<1.5R_0$), b) the quantum yield of the donor is high, c) there is a considerable overlap of the donor emission and the acceptor absorption spectrum and d) the absorption and emission transition moments are properly aligned. The rate of FRET changes inversely with the sixth power of the distance between the interacting fluorophores, providing a useful tool for nanoscale distance measurement[22]. The energy transfer rate $k_T(R)$ is given by (equation 1.5-1):

Equation 1.5-1

$$k_T(R) = \frac{1}{\tau_D} \left(\frac{R_0}{R} \right)^6$$

where τ_D is the lifetime of the donor in the absence of FRET, lifetime is the time that the excited electrons of the donor spend in the excited state and is typically around 10ns [22]. R is the donor to acceptor distance and R_0 is the Förster distance. The Förster distance that can be estimated from theoretical and measured parameters (equation 1.5-2):

Equation 1.5-2

$$R_0^6 = \frac{9000(\ln 10)Q_D\kappa^2}{128\pi^5 N n^4} J(\lambda)$$

In this expression, Q_D is the quantum yield of the donor in the absence of the acceptor, n is the refractive index of the medium, N is Avogadro's number, $J(\lambda)$ is the extent of spectral overlap between the donor emission and the acceptor absorption, and κ^2 describes the relative orientation in space between the transition dipoles of the donor and acceptor[22].

R_0 provides a window comparable to the scale of typical proteins, protein clusters, and the thickness of cell membranes. In practice, proteins are tagged with fluorophores and the distance between them (R) estimated from the experimentally measured FRET efficiency (equation 1.5-3) [4, 50]:

Equation 1.5-3

$$E = 1 - \frac{F_{DA}}{F_D}$$

F_D is the relative fluorescence intensity of donor in the absence of acceptor and F_{DA} is the intensity of donor in the presence of acceptor. FRET efficiency can also be calculated based on anisotropy changes during energy transfer (equation 1.5-4)[59]:

Equation 1.5-4

$$E = 1 - \frac{r_{FRET}}{r_o}$$

r_{FRET} and r_o are the anisotropy of the dye in the presence and absence of the energy transfer. Dependence of the energy transfer efficiency on the sixth power of the distance (R) between the chromophores is particularly important in distance measurement (equation 1.5-5) [22]:

Equation 1.5-5

$$E = \frac{1}{1 + (R/R_o)^6}$$

There are numerous methods to measure FRET. The most common methods are those that are based on monitoring changes in fluorescence lifetime and intensity. Some methods monitor changes in donor fluorescence while others examine changes in fluorescence of the acceptor. By means of spectral imaging changes in both donor and acceptor fluorescence can be measured simultaneously[60, 61].

FRET phenomena have turned into powerful tools for biomedical research due to their compatibility in scale with biological molecules the development of novel fluorophores and optical detection techniques[18, 62] has greatly expanded the scope of problems amiable to FRET methods. The highest accuracy of imaging the spatiotemporal interaction of proteins in cells is achieved by FRET techniques such

as lifetime imaging[63]. One of the most common applications of FRET is assessing proximity of sites on macromolecules [22]. Changes in conformation of macromolecules and their cleavage can also be determined by FRET measurements [64]. FRET may be observed between nonidentical (hetero-FRET) and identical (homo-FRET) fluorophores. FRET can be used to identify the co-localization of fluorescent macromolecules on a nanometre scale. For example, FRET techniques were used to analyze the oligomeric state of the core component (BioY) of a bacterial biotin transporter. BioY was labelled by fluorescent proteins and their hetero- and homo-FRET signals were analyzed allowing the functional state of the core unit of BioY oligomers to be identified [65]. In another study, FRET techniques were used to measure the size and stability of G-protein coupled receptors and to distinguish the monomeric receptor from its dimeric form[37]. Both hetero- and homo-FRET can be used to study protein aggregation. However, for these types of measurements, hetero-FRET is much less sensitive than homo-FRET because if the aggregates are made up of identical subunits they cannot be detected by usual hetero-FRET methods. To study protein or lipid clustering by hetero-FRET, molecules must be labelled with donor and acceptor fluorophores and the exact ratio of the pair as well as the fractional labelling of each must be known. However in homo-FRET studies one type of fluorophores is sufficient. The interpretation of hetero-FRET is more complicated [66] than homo-FRET (especially when clusters are large)[67]. Further studies have shown that the rate of energy transfer between a single donor–acceptor pair in a multimeric system is measured in the absence of other acceptors. The individual transfer rates are used to predict the FRET efficiency of the ensemble. A kinetic model in which the sum of all FRET transfer rates is divided by the sum of all radiative and non-radiative transfer rates has been used to do the prediction[68].

1.6 Distance measurement by multiple FRET

The relationship between the efficiency of energy transfer and the distance between sites when more than two fluorophores are present is not as well described as the case of a single pair of fluorophores [69]. There are a number of studies showing how resonance energy transfer can be used to measure distances between multiple fluorophores in hetero-FRET systems with complex geometries[23, 68-70]. These

studies show that in multimeric complexes, de-excitation of donors through energy transfer depends on the number of donors and acceptors and there are several pathways for de-excitation. Acceptors can be excited by several donors and there is a non-zero probability for all donors to transfer energy to the same acceptor. In such complexes the transfer of the excitation energy happens sequentially from one molecule to another. The simultaneous transfer of energy from more than one donor to an acceptor or from one donor to more than one acceptor is quantum mechanically forbidden[70].

The rate of energy transfer between a single donor-acceptor pair in a multimeric system has been measured in the absence of other acceptors and the individual transfer rates used to predict the FRET efficiency of the ensemble by a kinetic model in which the sum of all FRET transfer rates is divided by the sum of all radiative and non-radiative transfer rates[68].

The measured energy transfer efficiency is the weighted average of different transfer efficiencies (equation 1.6-1) [71, 72]:

Equation 1.6-1

$$E = \sum_{i=1}^n f_i E_i$$

E_i and f_i are respectively the energy transfer efficiency and the population fraction of the i^{th} homo-FRET pair. In the present study the populations of all the FRET pairs were assumed to be the same.

1.7 Homo-FRET

Homo-FRET refers to the transfer of excitation energy between identical fluorophores. Fluorescent molecules that have significant overlap between their emission and excitation spectra (small Stokes' shift) are prone to homo energy transfer. Homo-FRET happens between differently oriented fluorophores that are in close proximity and it always results in depolarization of the emission. Homo-FRET

is detected by measuring the changes in anisotropy as it is believed not to have any detectable impact on intensity or the lifetime of the fluorophores because whatever intensity or lifetime is lost from the donor, is exactly compensated for by the acceptor [22, 67, 73]. The reduction in anisotropy is proportional to the contributions of these indirectly excited molecules to the emission, so homo-FRET induced depolarization increases with the number of contributing fluorophores [23]. This is why homo-FRET is widely used to study molecular assembly [5] and quantification of cluster sizes [4]. For example self-assembly of Annexin A4, a cytosolic protein that has been implicated in regulation of exocytosis and ion-transport at the plasma membrane in living cells. This system was studied via homo-FRET using total internal reflection microscopy (TIRF). Number-and-brightness analysis revealed the predominant form of the protein is trimeric in the plasma membrane [74]. To better understand and control carcinoembryonic antigen-related cell adhesion molecule 1 (CEACAM1) roles in cell metabolism, immune response, and tumorigenesis, it was labelled with EYFP and studied using steady-state TIRF homo-FRET imaging in living cells. The active form of the molecule proved to be a mixture of monomers and oligomers, with a slightly more monomeric population [75]. In some studies, however, homo-FRET is an undesirable “energy trap” or “sink for the excitation energy” as it reduces the fluorescent emission of the fluorophores [76-78].

1.7.1 Fluorescence depolarization and cluster size

Quantitative biological fluorescence studies of multiply labelled proteins using polarization method were pioneered by Gregorio Weber in the 1960's [53, 79]. The relationship between fluorescence anisotropy and cluster size was further developed (by Knox [2] and Runnels [23]). Terms that describe the motion of excitation energy and its duration for a cluster of N identical molecules undergoing homo-FRET are described by a differential equation (equation 1.7.1-1) [2]:

Equation 1.7.1-1

$$\frac{d\pi_m(t)}{dt} = -\frac{\pi_m(t)}{\tau} - \sum_{m=1}^N F_{m \rightarrow n} \cdot \pi_m(t) + \sum_{n=1}^N F_{n \rightarrow m} \cdot \pi_n(t)$$

where,

Equation 1.7.1-2

$$F_{m \rightarrow n} = \frac{1}{\tau} \cdot \left(\frac{R_o}{R_{mn}} \right)^6$$

$\pi_m(t)$ is the probability that m th molecule is excited at time t (equation 1.7.1-1). This probability will decay at a rate relative to $\pi_m(t)$. The term $(-\pi_m(t)/\tau)$ explains the excitation decay in the absence of energy transfer (duration of excitation). The next terms describe the migration energy as a sum over all Förster energy transfer rates, $F_{m \rightarrow n}$, (equation 1.7.1-2) from molecule m to the rest of the molecules in the homo-cluster and the sum of all Förster energy transfer rates back to molecule m . R_o is the Förster distance and R_{mn} is the inter-probe distance. The transfer of energy between identical molecules reduces the fluorescence anisotropy. For the case of non-rotating, randomly oriented molecules of parallel excitation and emission dipoles, excited with vertically polarized light, the effect of homo-FRET on anisotropy may be calculated[80]. For example, the emission anisotropy of the directly excited molecules and the molecules that are excited by energy transfer might be 0.4 and 0.016 respectively. For the more common case of molecules of non-parallel excitation and emission dipoles the emission anisotropy of indirectly excited molecules can be even less, so it is usually assumed that the fluorescence emission is completely depolarized after one energy transfer step.

When considering homo-FRET it is possible for the excitation energy to transfer back to the initially excited molecule. Eventually, all the molecules in a cluster will reach equilibrium of electronic energy exchange. The emission anisotropy of such a system is composed of two constituents: the anisotropy of directly excited molecules

and the anisotropy of the molecules excited by homo-transfer. All interacting molecules have linear differential equations that describe the movement and decay of excitation energy inside the system [23, 81]. For a cluster of N equally interacting molecules $F_{mn} = F_{nm}$ and for all m and n and $F_{1N} = (N - 1)F$ and $F_{N1} = F$ (equation 1.7.1-3):

Equation 1.7.1-3

$$r_N = r_1 \cdot \frac{(1 + F \cdot \tau)}{(1 + N \cdot F \cdot \tau)} + r_{RET} \cdot \frac{(N - 1) \cdot (F \cdot \tau)}{(1 + N \cdot F \cdot \tau)}$$

By substituting the right side of the Förster energy transfer rate equation in equation 1.7.1-2, it can be written (equation 1.7.1-4):

Equation 1.7.1-4

$$r_N = r_1 \cdot \frac{1 + (R_o/R)^6}{1 + N \cdot (R_o/R)^6} + r_{RET} \cdot \frac{(N - 1) \cdot (R_o/R)^6}{1 + N \cdot (R_o/R)^6}$$

As mentioned before, a common assumption is that the second term of equation 1.7.1-4 is zero, as the emission of molecules excited by energy transfer is depolarized [23, 24, 80, 82]. There are some cases where this assumption is not valid and the contribution of the second term is considered [4, 67]. This is mainly the case with fluorescent proteins when the rotational correlation times are high in comparison with lifetime and the energy is not completely depolarized through rotational diffusion.

A simulation (figure 1.7.1.1) following equation 1.7.1-4 shows changes of anisotropy in a cluster of $N=2-10$ subunits over a range of distances from $0.2R_0$ to $3R_0$. The simulation shows that when the distance between subunits is greater than $3R_0$ there is no energy transfer and as they get closer the anisotropy decreases.

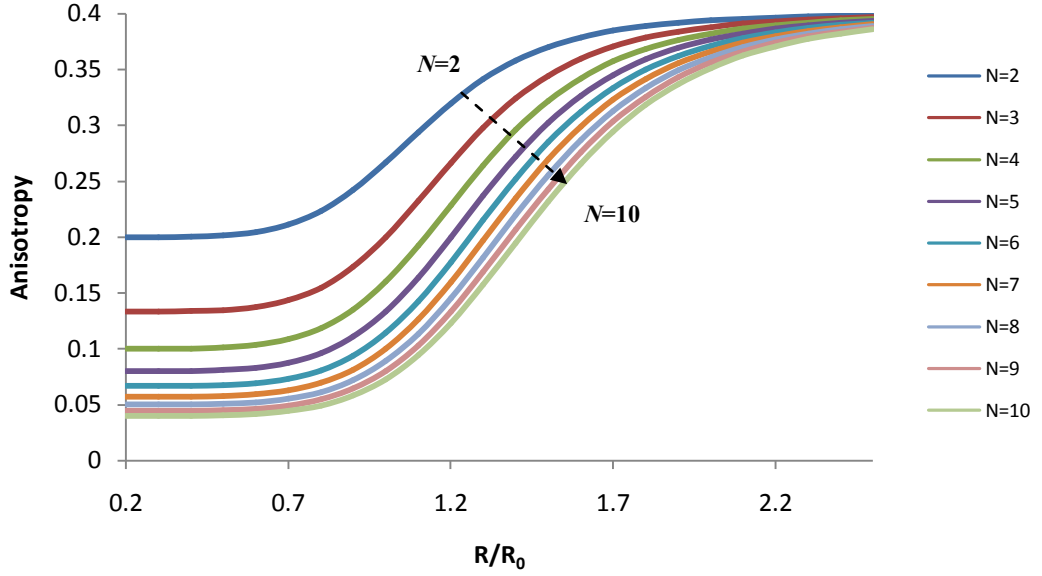


Figure 1.7.1.1:Theoretical curves for emission anisotropy of cluster sizes from two to ten obtained from equation 1.7-4, with $r_1 = 0.4$ and $r_{RET} = 0$ [23].

The results of anisotropy measurements for clusters larger than 6-mer, and at inter-probes distances shorter than $0.8 R_0$ and longer than $2R_0$ are ambiguous. Below $0.8R_0$, where the anisotropies are stable, homo-clusters of different sizes can be clearly discriminated, however the difference in distances cannot be determined. Subunits that are close ($R/R_0 \leq 0.8$) to each other within a cluster of any size lead to efficient redistribution of the excitation energy (homo-FRET efficiency $\approx 95\%$). Eventually, all molecules will have equal shares of the excitation energy and the apparent emission anisotropy of the N-mer would be the average of all the anisotropies (equation 1.7.1-5). Considering all the other species rather than the directly excited one, as depolarized ($r \approx 0$) (equation 1.7.1-5).

Equation 1.7.1-5

$$r_N = \frac{r_1}{N}$$

Equation 1.7.1-5 is specific to instances when $R/R_0 < 0.8$. The gradual decrease in total anisotropy gets less noticeable as the number of the participant fluorophores in the cluster increases. Although the technique may be used to detect large clusters [46], it has been mainly used to quantify clusters of sizes $N < 4$ [5] (figure 1.7.1.1).

For ($\frac{R}{R_0} \geq 0.8$) where the FRET efficiency is low the total anisotropy is mainly determined by the directly excited molecule and is calculated by equation 1.7.1-4 [67].

Based on the existing theory, detailed above, experiments may be designed to assess the extent of protein oligomerization in cells. For example homo-FRET was used to study plasma membrane and nanoscale organization (rather than random concentration clustering) of fluorescent protein tagged GPI-anchored proteins[83]. Homo-FRET studies on dimer and tetramers of human erythrocyte band 3 have shown that the receptor does not form higher order oligomers in native membranes[84]. Dimerization and oligomerization of GFP have been studied and its cluster size determined based on FRET efficiency and relative depolarization values ($\frac{r_{cluster}}{r_{monomer}}$)[67]. Erb1 cell signalling was investigated and the existence of homo-dimers reported[85]. Cluster size of α -synuclein are quantified in pathogenic aggregation of the protein (a model of Parkinson's disease) [46] and the existence of oligomers of serotonin_{1A} receptors upon the presence of the stimulant in cells was proven[86]. In all cases, the biomolecules have been labelled with a single kind of fluorophore and then the loss of anisotropy upon aggregation of the molecules or anisotropy enhancement after photobleaching of the fluorophores was measured with fluorescence anisotropy imaging microscopy [73, 87] or fluorescence spectroscopy [88, 89]. Novel methods have been developed to record and process micro images to obtain quantitative information about homo-FRET between (GFP)-labelled proteins in a living cell[90].

1.7.2 Depolarization curve as a function of labelling

When the anisotropy of proteins labelled with fluorophores changes upon self-association, it is due to changes in rotational correlation time, homo-transfer, or both. This ambiguity makes the analysis of anisotropy results difficult[91].

Nevertheless, altering the extent of labelling proteins with fluorophore lets processes leading to homo-FRET to be tracked separately from rotational diffusion. On this basis some experiments in which proteins (subunits of clusters) were fractionally

labelled[83, 84]or fractionally photobleached [67, 86, 92] were designed. As the extent of labelling increases, clusters exchange unlabelled molecules for labelled ones so the probability for transfer of energy increased while the motional characteristics of the clusters were constant. Labelling experiments often result in incomplete saturation of sites that leads to mixtures consisting of a distribution of fluorophores in the cluster and the overall anisotropy is a weighted average of the anisotropies of the clusters within the distribution as predicted by the sum law of anisotropies[53]. This type of experiment provides evidence of both proximity and the distribution of cluster sizes[4]. Weber and Daniel [1] were the first to introduce the idea of studying the polarization of the fluorescence emission as a function of the average number of ligand molecules attached to a protein. They studied depolarization of 1-aniline-8-naphthalene sulfonate (ANS) bound to bovine serum albumin (BSA) as a function of increasing labelling frequency. They assumed a random distribution of the dyes among sites of equal binding affinity on the protein. It was also assumed that a single transfer of the excitation energy was responsible for the depolarization of the fluorescence emission. A final assumption was an assumption of equal fluorescence efficiency for all sites. The assumption states that fluorophores have the same brightness when free in solution as they do in close proximity to each other in a cluster. The assumption simplifies descriptions of anisotropy trends as the fractional labelling of the cluster changes. Their theory suggests that the fractional fluorescence of these N species could be given by the successive terms of the binomial distribution of order $(N-1)$. The binomial theory implies that if there are N binding sites on a protein (P) and \bar{i} is the average number of labelled sites, then the fraction, f_i , of the protein that exists in the form of PX_i ($0 \leq i \leq N$), in which i fluorescent molecules or ligands (X) are bound to P , is given by the successive terms of the binomial distribution (equation 1.7.2-1) in which $\binom{N}{i}$ shows the number of i out of N choices :

Equation 1.7.2-1

$$f_i = \binom{N}{i} \left(\frac{\bar{i}}{N} \right)^i \left(1 - \frac{\bar{i}}{N} \right)^{N-i}$$

Note that in this representation the overall fractional labelling, f , is given by \bar{i} / N . If the fraction associated with PX_i has a contribution of ϕ_i to the total fluorescence intensity and its emission anisotropy is r_i , the observed emission anisotropy r of the ensemble, based on the sum law of anisotropies [1, 24, 50, 53] is (equation 1.7.2-2):

Equation 1.7.2-2

$$r(N) = \sum_{i=1}^N \phi_i r_i$$

Then they applied an assumption of equal fluorescence efficiency of all sites which gives ϕ_i by the expression (equation 1.7.2-3):

Equation 1.7.2-3

$$\phi_i = \frac{i f^i}{\sum_{i=0}^N i f^i}$$

The equal fluorescence efficiency assumption states that a species containing i fluorophores is weighted by i (e.g. a tetramer contributes 4 times as much per molecule as a monomer). Therefore, when equation 1.7.2-1 is expanded and replaced in equation 1.7.2-3, it reduces from N to $N-1$ yielding (equation 1.7.2-4):

Equation 1.7.2-4

$$\phi_i = \binom{N-1}{i-1} (f)^{i-1} (1-f)^{(N-1)-(i-1)}$$

Consequently, when equation 1.7.2-4 is applied to equation 1.7.2-2, the average anisotropy of the N species PX_i , is (equation 1.7.2-5):

Equation 1.7.2-5

$$r(N) = r_1 + \sum_{i=1}^{N-1} (-1)^i \binom{N-1}{i} (f)^i \times \left[\binom{i}{0} r_1 - \binom{i}{1} r_2 + \dots \pm \binom{i}{i} r_{i+1} \right]$$

The assumption of equal fluorescence efficiency of all sites allows the equations to be simplified to a reduced expression based on the binomial distribution of order ($N-1$).

1.8 Homo-FRET and fluorescently labelled proteins

Weber and Daniel also suggested that if random occupancy of binding sites could be approached, their method could be applied to proteins made up of identical subunits and results on both orientation and distance among subunits would be obtained. This method was then used by Yeow and Clayton [24] to quantify protein clusters and determine size distribution in oligomers of limited sizes where the distance between the sub units is $<0.8R/R_0$. The enumeration was done by linking the steady-state anisotropy and fractional labelling of the subunits of the protein cluster. The same discrete probability distribution is written to describe the distribution of the fraction of labelled monomers f between clusters, F_i (equation 1.8-1):

Equation 1.8-1

$$F_i(i, f, N) = \frac{N! f^i (1-f)^{N-i}}{i! (N-i)!}$$

The observed emission anisotropy of the ensemble, r , is given by (equation 1.8-2):

Equation 1.8-2

$$r(f, N) = \frac{\sum_i^N i F_i r_i}{\sum_i i F_i}$$

This allows equation 1.7.2-5 to be rewritten to include fractional labelling of a stochastically generated cluster (equation 1.8-3):

Equation 1.8-3

$$r(f, N) = A_1 f^0 (1-f)^{N-1} r_1 + A_2 f (1-f)^{N-2} r_2 + \dots + A_N f^{N-1} (1-f)^0 r_N$$

Where (A_1, A_2, \dots, A_N) are the elements of the $(N-1)$ row of Pascal's triangle and f is the fraction of labelled subunits. This expression may be simulated (figure 1.8.1) as a function of labelling:

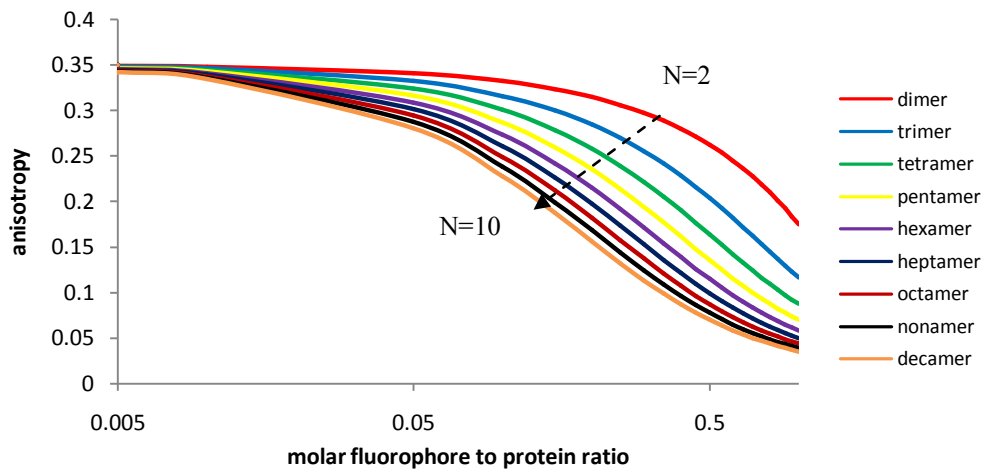


Figure 1.8.1: Simulation of the anisotropy as a function of labelling according to equations 1.8-3 with $r_1 = 0.35$, N -values in order from top to bottom: $N = 2, 3, \dots, 10$. The curvature reveals the oligomerization state of the cluster[24].

1.9 Self–Quenching

As noted previously, it is usually assumed that homo-FRET does not change intensity or lifetime and that a fluorophore's intensity is not affected by the extent of labelling in clusters. In other words when studying clusters of biomolecules containing multiple subunits, the subunits are labelled with fluorescent probes and when the subunits combine to form clusters, the fluorescence intensity is expected to be the sum of the individual probes. However, this is not usually observed. Instead intensity does not increase in proportion to the number of bound fluorophores and sometimes the intensity decreases. This phenomenon is due to homo-FRET between the fluorophores, leading to self-quenching [2, 93-96]. As noted above, a dye showing efficient homo-FRET, will have a small Stokes shift. The problem with such dyes is that they usually show self-quenching. For example, fluorescein is widely used as an extrinsic label for antibodies because of its favourable properties such as broad absorption band, high molar extinction coefficient, high quantum yield and having a variety of reactive derivatives such as isothiocyanate, iodoacetamide and maleimide [97, 98]. However fluorescein tends to self-quench due to having a small Stoke shift, formation of non-fluorescent fluorescein dimers and energy transfer from active fluorescein to such dark dimers [22, 23, 80].

By increasing the extent of labelling in fluorescein-labelled molecules, it might be expected that the fluorescence emission intensity increases linearly with label but self-quenching causes the brightness of fluorescein-labelled molecules to eventually decrease. When a number of fluorescein molecules are bound to a host molecule leading to high local concentration they move within a suitable Förster distance from each other to allow efficient energy transfer and therefore the fluorescence intensity decreases. Alexa dyes with similar small Stokes shift show less self-quenching than fluorescein derivatives but these also quench at high ratios of fluorophore to protein (F/P) [22, 99].

An example of self-quenching is the emission intensity changes of a 2.4 nM solution of Bodipy-biotin upon titration with avidin solution. Avidin is a relatively large protein and has four binding sites for biotin that are approximately 3nm apart. Before addition of avidin, bodipy molecules were far apart and self-quenching was not

observed. When avidin was added, the fluorescence intensity of Bodipy decreased. There was a little decrease in intensity when the avidin concentration is low because there was not enough avidin to bind with more than a small fraction of the Bodipy and the intensity of free Bodipy molecules was dominant. When concentration of avidin was high (0.8 nM) there were approximately 3 Bodipy probes bound per avidin and homo-FRET was more probable. At this point the Bodipy was 70% quenched.[100]BODIPY dyes also have a very small Stokes shift[101]. Similar quenching behaviour has been observed in a wide range of fluorescent dyes including: FITC [93, 99, 102-104], Cy3[34], Cy5[34, 105], Cy7[34], Alexa 488, Alexa 532, Alexa 546, Alexa 594[99] and Alexa 647 [105].

Fluorescent proteins may also show self-quenching behaviour. As an example, template directed assembly of monomeric teal fluorescent protein (mTFP) exhibited quenching as a tetrameric assembly formed. This system consisted of mTFP fused to a short PNA sequence and assembled along a complementary DNA strand with regular repeats. By titrating mTFP-PNA with DNA containing 4 repeats of the complementary sequence, the behaviour of a tetrameric system over a range of fractional labelling values was studied and the result was that a 4:1 mTFP:DNA had a brightness of only 1.82 that of free mTFP in solution indicating some self-quenching[106]. In the absence of quenching the brightness would be expected to be 4.

1.10 Enhancement of fluorescence emission

Although quenching of fluorescence emission upon proximity of fluorophores is well known, there are also cases where fluorophores in close proximity show enhanced emission intensity. In addition to energy transfer when in the excited state, fluorophores can have other interactions with each other such as excimer formation. Excimer formation is a short-range interaction of an excited-state fluorophore with another ground-state molecule of the same type. The term "excimer" is an abbreviation for an excitedstate dimer[22]. Excimer formation is widely used in biotechnology for detection of an insertion mutation in DNA[107, 108] and in nanotechnology for following self-assembly processes[109].The best known

example of a fluorophore that forms an excimer is pyrene. Pyrene exhibits different spectral behaviour at different concentrations. At low concentrations pyrene shows a structured emission near 400 nm. However if an excited pyrene molecule contacts another ground-state pyrene molecule it forms an excimer that displays an unstructured emission at 470 nm. One study[110] showed that at low concentrations pyrene is invisible at 470 nm but as the concentration increases from approximately 0.1 M to 1 M the emission at 470 nm increases approximately 10 fold. This long-wavelength emission is known to be the result of excimer formation[22, 110]. In another study it is reported that DNA doubly labelled with pyrene on adjacent bases gave over 6 times the brightness of DNA with only a single label [102].

The impact of self quenching and emission enhancement on fluorescence anisotropy of fractionally labelled clusters was not understood before the present study[28].

1.11 Size of Clusters in living cells

Many plasma membrane proteins organize into larger clusters with submicron sizes. For example, syntaxins are a group of membrane integrated Q-SNARE proteins that participate in exocytosis and their clusters are 50-60 nm[29, 111]. HIV-1 envelope glycoprotein (Env) mediates the fusion of viral and cellular membrane. These clusters have diameters around 65 to 105 nm[30]. Clusters of epidermal growth factor in cell membrane were found to have sizes ranging from 32 to 56 nm[31]. By fluorescence anisotropy decay microscopy, the spatial monomer-dimer distribution and oligomeric state of the herpes simplex virus thymidine kinase, TK₂₇ and TK₃₆₆ tagged with GFP, were determined in both cytoplasm and the nucleus. The upper intermolecular limit between the two fluorescent tags, was calculated from the energy transfer rate to be 7nm [112].

Investigations of homo-FRET induced depolarization at distances larger than $0.8R_0$ are needed to resolve structures of clusters such as above mentioned systems.

1.12 Conclusion

As explained in section 1.4, FRET involves the transfer of excited-state energy between fluorophores that are located within approximately 10 nm of each other and the method can be used to measure distances at this scale [27]. General formulae to explain homo-FRET phenomenon in clusters are available to assess the size of clusters and determine the number of subunits (equation 1.7-10) upon fractional labelling. However in practice they are most often restricted to scales less than 80% of the R_0 . For typical fluorophores this is around 4nm [23, 24, 28].

Widely applied theory assumes equal fluorescence efficiency this is known to be incorrect when dealing with typical fluorophores. Fluorescein displays strong self-quenching properties, while the fluorescence emission from DNA molecules doubly labelled with pyrene was strongly enhanced [102].

The first model chosen was bovine serum albumin (BSA). BSA has many sites for attaching fluorophores such as fluorescein isothiocyanate (FITC) to simulate clusters with varying numbers of subunits of labelled proteins and to test theories related to anisotropies of stochastic mixtures [1, 24]. Experiments were also done with DNA systems as more robust structures in which the number of the reacting sites and the distances between them are more controllable.

The next three chapters are as follows:

Chapter 2 presents synthesis and characterization of a range of materials created to explore the effect of clustering and distance on anisotropy. Chapter 3 presents a detailed study of quenching and enhancement of intensity on clustering including modification and generalization of existing theory. Chapter 4 presents quenching and distance effects in DNA strands and DNA four-way junctions. Chapter 5 presents a summary and introduces the areas for further works on the theory

1.13 Aims

The goal of the present work was to work toward methods to directly visualize clusters *in vivo*. Model systems were required to be developed to explore the limits of the existing theories. To investigate these issues, a) the impact of the assumption of equal fluorescence efficiency on anisotropy and cluster size was studied. In the present study it was shown how non-additivity of fluorescence emission in clusters affects interpretation of anisotropy data and calculation of the cluster size. b) homo-FRET over longer distances than $0.8 R/R_0$ was studied, to cover a range of distances that are more realistic relative to the size of protein clusters.

2 Design, Synthesis and Characterization of Model Systems of Multiple Fluorophores

2.1 Introduction

Studying homo-FRET induced depolarization required a set of defined model systems which could be used to test the limits of the existing theories [1, 23, 24]. Once created, they could be used to observe while varying distances or fractional labelling. The idea initially was to determine the number of fluorophores on fully labelled proteins as defined by N in equation (1.8-3). Bovine serum albumin (BSA) was the first model system selected for labelling because it has a well known structure, Weber [1] presented theory based on observations of fractional labelling of BSA with ANS, and it is low cost and readily available.

In addition to fractional labelling, assessing resonance energy transfer between identical fluorophores at distances $> 0.8R/R_0$ (figure 1.7.1.1) was a second aim. The main challenge of such studies was generating a geometric structural model system in which the distances between the fluorophores were fixed and known. BSA was not a good choice for this part of the study because it has too many reacting sites to simulate a protein cluster, the distances between the reacting sites in some cases are less than $0.8R/R_0$, these distances are not well known in solution, and it does not have the diversity needed to study homo-FRET over a controlled range of distances. Systems to study this distance regime need the flexibility to be designed in different

sizes and have a known and controllable number of labelled sites. Models meeting these specifications are not readily available. Proteins, polypeptides, dendrimers and DNA molecules were considered as possible models as they all have adjustable size and architectures [113-115]. Among these choices, however, DNA molecules presented the most diverse structures. DNA tertiary structures are better known and the number of reacting sites is controllable in comparison to dendrimers and was available at reasonable cost relative to polypeptides. Fractional labelling is also much easier with DNA molecules because they self-assemble, a feature that the other two structures lacked. Oligonucleotides with semi-complementary sequences can hybridize to make three and four way junctions [114].

2.2 Bovine Serum Albumin

BSA is one of the most extensively studied proteins and because of its ease of isolation, abundance in serum and structural features, has been widely used as a model protein to understand the structure-function relationship in proteins [1, 116-119]. Another aspect of this protein, due to a large number of exposed lysine groups, is its capacity to react with a variety of compounds [120, 121], one of which is FITC [35].

¹H NMR studies [122] and X-ray crystallographic data [123] have revealed BSA to be a heart-shaped structure with dimensions of 14 × 4nm. BSA has 60 lysine residues out of which approximately 51% are buried in the protein interior and the rest 49% are located on the surface [121, 124, 125] with an average distance between these reactive lysine residues around 2-2.4nm [126]. The distance between the lysine groups makes BSA a good choice as a model system because, upon labelling, the distance between the probes will be within the desired limit of 0.8 R/R_0 . The presence of the dyes on the surface of the molecule makes them readily exposed to the solution so it can be assumed that the dyes are randomly oriented.

BSA as a model system to study homo-FRET as a function of fractional labelling has already been used in different studies. Polarization of the ligand fluorescence and quenching of protein fluorescence have been studied using ANS/BSA conjugates.

BSA was fractionally labelled with ANS and the depolarization of ANS upon increasing the ANS/BSA ratio was investigated [1]. The anisotropy of FITC/BSA conjugates over a range of BSA concentrations have been measured and a rapid method to determine fluorophore to protein molar ratio has been presented [127]. To study the effect of labelling ratio on photophysics of FITC, it is bound to BSA and its absorption, anisotropy and lifetime changes over a range of FITC to BSA ratios are studied [35].

The exposed lysines in BSA and the primary amines populating the surface of a dendrimer provide a target for amine reactive dyes. Fluorescein isothiocyanate (figure 2.2.1) is a commonly used fluorescent compound to label biomolecules and its functional group (isothiocyanate, $-N=C=S$) target exposed amine groups of lysine [78]. The photophysical characteristics of FITC such as: a) pH dependency of emission [128]; b) reasonable overlap between absorption and emission spectra [129] (small Stoke's shift); and c) a critical energy transfer distance for homo-FRET in the range of 4.2 to 5.6 nm [35] have been well studied making it a suitable and commonly used probe for studying protein conformation [130-132]. These same features make it an attractive reagent for labelling other molecules containing primary amines.

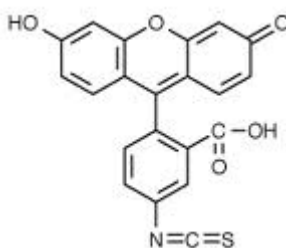


Figure 2.2.1: Isothiocyanate derivative of Fluorescein [78]

The FITC conjugation reaction is relatively easy to control so it can be applied to reactions that require a precise degree of conjugation [133]. FITC also presents convenient excitation-emission characteristics, exciting at approximately 495 nm and its maximum emission at approximately 520 nm [35].

The reaction between FITC and an exposed primary amine takes place when a nucleophile such as the free amine group of the protein attacks the electrophilic carbon of the isothiocyanate group, the electrons then shift to the nitrogen of isothiocyanate and a thiourea bond between FITC and the protein is made [78, 134] (figure 2.2.2).

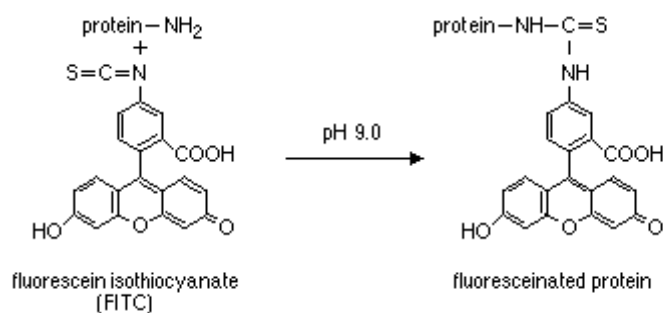


Figure 2.2.2: FITC reacts with free amino groups of proteins to form stable conjugates and binds to the lysine residues and N-terminal amine of BSA[78].

Fluorescein isothiocyanate hydrolyses rapidly in aqueous solution to give amino fluorescein reducing the efficiency of the labelling [135, 136].

2.3 Dendrimers

Dendrimers are hyperbranched, three-dimensional molecules with well defined size and architecture[113]. They are synthesized by stepwise repetitive reaction sequence that guarantees a complete control over several molecular design parameters, such as size, shape, surface chemistry, and flexibility[137]. At each subsequent growth step the diameter of the molecule becomes larger; the dendrimer finds a new layer and belongs to a new "generation" with twice the number of reactive surface sites of the preceding generation. This synthesis process results in their size and architecture being both regular and well-defined[138]. Dendrimers have a nearly perfect hyperbranched topology that starts from a central core and grows generation by generation and can be designed to have any desirable size[137]. Dendrimers have a high degree of molecular uniformity and can be designed to have highly functionalized terminal surface to react with any molecule of interest, e.g.

fluorophores. For example in Polyamidoamindendrimer, PAMAM, the end groups are primary amines that can react with amine reactive dyes such as FITC.

2.4 DNA Constructs

DNA molecules can be designed to have any desirable lengths and can also be labelled with fluorophores. To fulfil the need for simulations and they have been used to build a variety of nanoscale structures [139, 140]. Over the past 30 years DNA sequence specificity and the resulting spatial addressability of DNA molecules have allowed the creation of a variety of biomimetic nanoscale structures [141]. DNA is one of the most programmable self-assembling materials to have been used in nanotechnology [142].

Synthetic DNA molecules of defined sequence and length have already been used to build model systems. For example, to extend the sensitivity of FRET measurements to the single molecule level, resonance energy transfer was measured between single tetramethyl rhodamine and a single Texas Red molecule attached to the 5' ends of hybridized, complementary DNA strands. This work resolved conformational changes, such as rotation and distance changes on a nanometre scale [143]. In the present study, DNA molecules labelled with fluorescein were designed to provide a model system to mimic a trimer cluster.

Both DNA duplexes and DNA four-way junctions have already been labelled with fluorescent dyes and the resonance energy transfer between the dyes has been used to study the structures of the DNA constructs and to obtain information about the dyes structural and dynamical heterogeneity. In fact, Förster resonance energy transfer is the only tool that has been used to study the handedness, sequence dependent bending and helicity of DNA molecules in a qualitative manner [140, 144-147].

2.4.1 DNA strands

Linear geometry and a regular helical structure make DNA an excellent construct for structural investigation by FRET techniques. The energy transfer efficiencies between a FRET pair bound to both 5' ends of a series (from 8 to 20 bp) of double stranded DNA molecules have been studied and found to be in agreement with helical structure [145]. The distances calculated from FRET efficiencies were in good agreement with the known helical geometry of double stranded DNA in solution. The thermal dissociation of DNA strands has also been followed by FRET and it allowing FRET to be used to study conformational transitions. Systems of template directed DNA assembly have been reported to study the DNA hybridization process[148], to determine the geometry of DNA molecules in solutions [149] to investigate the structure, stability, and dynamics of nucleosome [150], and to create DNA-based photonic wires able to transfer excitation energy over distances exceeding 15 nm [151].

2.4.2 Four-way junctions

Branched DNA structures play critical roles as an intermediate in DNA replication, repair, and recombination and were first discovered by Robin Holliday [152]. Holliday junctions are DNA structures in which two duplex DNA molecules are joined to each other by a reciprocal single-stranded cross-over [153]. These molecules have been produced *in vitro* to study their physical and biological behaviour [153-157]. Stable Holliday (four-way) junctions, incapable of branch migration[158] have been built from synthesized DNA molecules by hybridizing four oligonucleotides with semi-complementary sequences [156]. Single molecule studies have shown that the structure of DNA four-way junctions have a dynamic and polymorphic character [159, 160]. Although the structure of four-way junctions is dynamic, when salt concentration is controlled, the general features of their structures have been confirmed by a variety of experimental methods[161]. In the absence of metal cations, the centre of the junction is open and the structure is more square planar with the axes of the junctions approximately perpendicular [162, 163], to give the four arms of the junction enough space to minimize electrostatic

repulsion between phosphate groups [163-166]. Upon addition of positive metal ions with a single or double positive charge (e.g. Mg^{2+} , Na^+ , etc) the negative charges of the phosphate groups become shielded and the helical arms fold to form stacked, right-handed, anti-parallel X-Shaped structure [167-169]. DNA four-way junctions have different stacking conformers and their structures are determined by both the sequences of the strands and the salt concentration of their environment [154]. During transitions between these alternative stacking conformers in the folded form, the extended form has been found to be a transient structure [158, 160] (figure 2.4.2.1.1). The existence of the conformers has also been confirmed by X-ray crystallography, sedimentation velocity, and computational modelling techniques [170-172].

Methods based on labelling the DNA junctions with fluorescent molecules and studying intensity, polarization and lifetime of the dyes to find clues about the structures of the junctions have widely been used [16, 154, 155, 164, 173]. The three-dimensional arrangement of DNA junctions has been probed by covalently binding FRET pairs to known positions on the arms. For example, Förster resonance energy transfer measurements were carried out to study the helical configurations of the arms of a number of four-way DNA junctions. Two of the four strands were labelled with fluorescent dyes (one with fluorescein and one with rhodamine) and the compounds titrated with metal cations. The efficiency of energy transfer between the two dyes depended on the distance of the arms and the conformation of the compound. This has been confirmed by measuring the enhanced emission of the acceptor (rhodamine), decrease of the quantum yield of the donor (fluorescein), and changes in donor lifetime and the anisotropy of the acceptor. Low FRET efficiencies at low ion concentrations indicated an extended structure in which the helical arms, and consequently the FRET pair, had the maximum distance [155, 164]. The arms of four-way junction follow the same rules as DNA duplexes and they form helices if they have more than 10base pairs [174, 175]. Multi parameter fluorescence detection of single molecule fluorescence resonance energy transfer has also been used to study branched DNA [173].

The idea of generating sequences of oligonucleotides which would associate to form migrationally immobile junctions [176], rather than linear duplexes, was first

suggested by Seeman [141, 177]. Such structures have already been constructed as model systems to study three-color FRET by labelling three of the arms with three different fluorophores, and devising techniques to detect the complex dynamics of biomolecules and observe binding events between multiple components [178].

2.4.2.1 Geometry

In the absence of positive metal ions in solutions, the arms of four-way junctions are stretched and give the molecule tetrahedral or square planar structures (figure 2.4.2.1.1, conformer 2) to minimize the repulsion of the phosphate groups of the nucleotides at the centre of the junction (branch point) [153, 155, 179]. The fluorescein molecules are usually assumed to be on the surface of a tetrahedron or on four corners of a square. Arms of DNA junctions that are longer than 10 base pairs were assumed to make helices [164, 174, 175]. To calculate the arm lengths of these molecules the cylindrical properties of a DNA helix must be considered [144, 145]. High-resolution nuclear magnetic resonance (NMR) and time-resolved fluorescence resonance energy transfer experiments have proven that immobilized four-way junctions must be viewed as an equilibrium mixture of two conformations (crossover isomers) the distribution ratio of which, depends on their sequences [180, 181]. During the transitions between these alternative stacking conformers in the folded form, the open or planar form is the transient structure and single-molecule measurements have shown that the open form is stably populated (hundreds of times a second) even when the concentration of the doubly charged metal ions is relatively high (figure 2.4.2.1.1) [160]. The interaction of cations might reduce the mutual repulsions of the negative charges in the region of the exchanging strands [164].

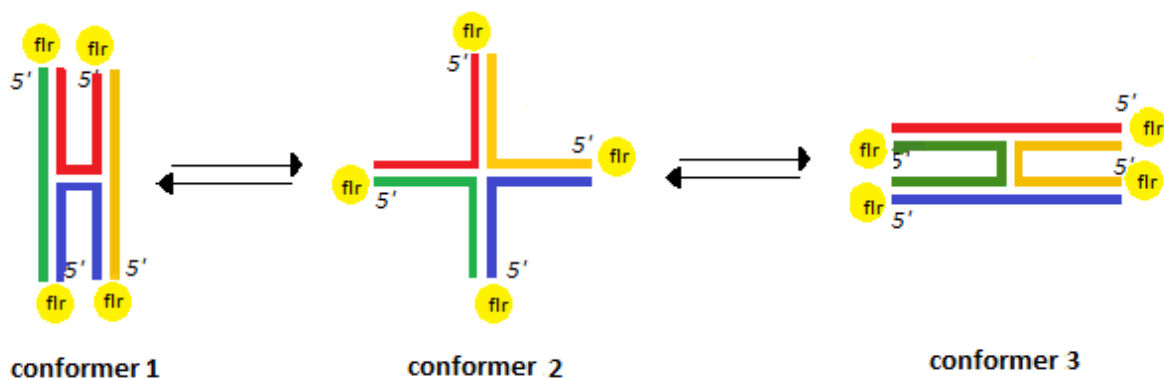


Figure 2.4.2.1.1: The fluorophores are attached to the ends of four arms and the ion-dependent folding of the junction changes their distances. Conformers 1 and 3 bring fluorescein molecules to the same distance and show the same FRET efficiency that is different from efficiency of energy transfer in conformer 2. In the absence of the metal ions conformer 2 is the most stable form.

2.4.2.2 Fluorescein labelled DNA

The spectroscopic behaviour of fluorescein is not known to change when bound to DNA (figure 2.4.2.2.1) because of electrostatic repulsions between phosphate groups of DNA molecules and fluorescein which inhibit the interaction between fluorescein and DNA molecules [182]. The anisotropy of fluorescein is not influenced significantly by the size of the DNA or its rotational motion either [182, 183] because the fast local twisting of the DNA molecule around its helix axis causes rapid decay of anisotropy [184] and the anisotropy of fluorescein tagged to DNA is typically around 0.04 [185].

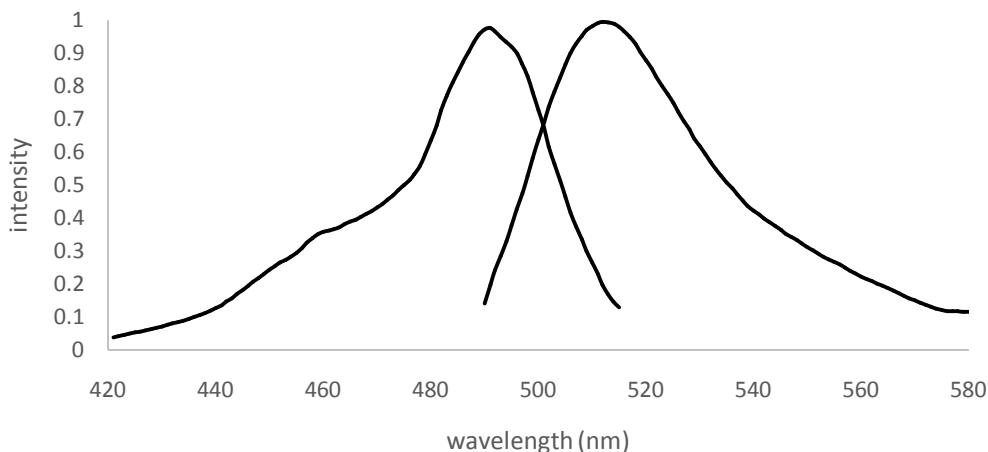


Figure 2.4.2.2.1: Normalized emission and excitation spectra of fluorescein labelled DNA measured by Carry-Eclipse: fluorescein is not influenced by DNA and its excitation and emission maxima occur at 494 nm and 512 nm respectively.

When labelling DNA molecules with fluorophores, to ensure that the dyes are randomly oriented, they are bound to the oligonucleotides via a linker that is usually 5 to 6 carbons long and in such cases anisotropy measurements have indicated the dyes were very mobile [145, 155, 164]. However in a similar study in which DNA strands are bound with donors and acceptors with the distances of 5, 15, 25 and 35 base pairs, and the dyes are directly bound to DNA, anisotropy measurements have shown that none of the dyes can be observed as a free rotor. In a study done by Runnels and Scarlata however, fluorescein is directly attached to a polypeptide (melittin) is known as randomly oriented and the emission of indirectly excited fluorescein molecules is regarded as completely depolarized $r_{RET} = 0.016$ [23]. Fluorescein undergoes a fast rotational diffusion and its rapid movement within its excited state lifetime approves its random static orientation [155].

2.5 Instrument Validation

All intensity and anisotropy measurements were done using Varian Cary Eclipse Fluorescence Spectrophotometer and Tecan microplater readers (Infinite 200 PRO). G-factor was determined for both machines and blank reading was done too. With Cary Eclipse fluorometer that is based on L-format reading (figure 1.4.1) and uses a Xenon flash lamp, the blank reading was zero.

Calculations were done to correct the intensity readings in Tecan. Tecan microplate readers have UV Xenon flash lamp too and the wavelength accuracy was $< \pm 2$ nm. All the measurements were done with the “reading from top” mode.

2.5.1 G-factor

G factor was calculated based on the known anisotropy of fluorescein (0.017) using equation 2.5.1-1. The G-factor was found to depend on the PMT setting (gain, an amplification factor for the photomultiplier tube) and was done at different PMT voltages:

Equation 2.5.1-1

$$G = \left(\frac{VH}{VV} \right) \left(\frac{1 + 2r}{1 - r} \right)$$

The procedure was repeated at each working PMT setting in order to obtain best results. For the gain of 30-50 (Tecan) a G-factor of 1.256 worked well while at 50-60 a G factor of 1.241 was the best. Once the G-factor was found the anisotropies of all samples were calculated manually using the raw parallel and perpendicular intensity (equation 1.4-1).

The same measurements were done with Cary Eclipse fluorometer at different PMT voltages.

2.5.2 Intensity

To prevent artefacts, control experiments were carried out. The contribution of scattered light to the measured intensity and anisotropy is high in the Infinite 200 PRO and all the measured intensity values had to be corrected by subtracting the emission intensity of a blank [186]. The issue was critical for dilute samples where the contribution of the scattered light is greater. In some instances the samples had to be prepared at the lowest possible concentration of labelled oligonucleotide. The sensitivity of the instrument, however, decreased with the concentration of the sample and the consequent drop in intensity. Therefore the lower limit of the concentration range was measured as a dilution series of fluorescein labelled

oligonucleotide with concentrations from 100 μM to 1 nM. These were measured at a gain of 50 to test the consistency of measurements. Although the anisotropy was supposed to be constant at different concentrations, as shown in figure (2.5.2.1) the measured values showed marked inconsistency at concentrations below 1 μM and were completely unusable below 0.1 μM .

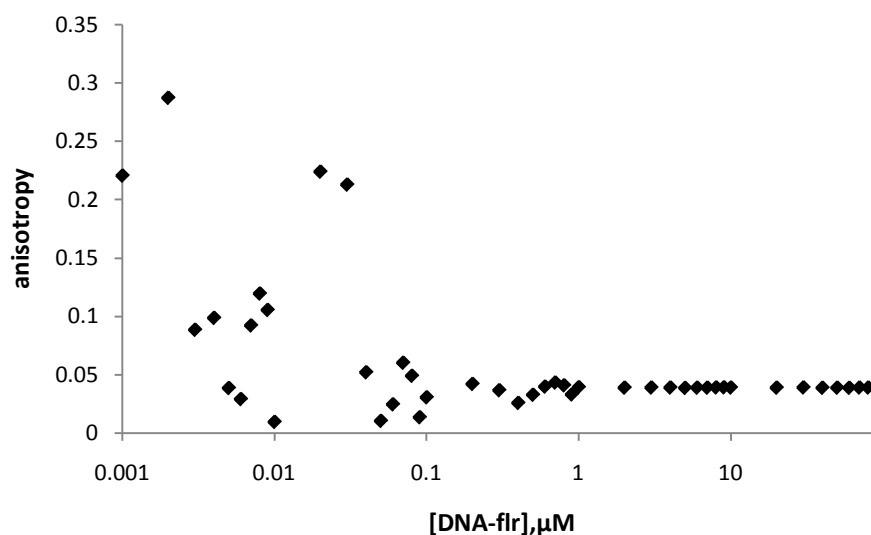


Figure 2.5.2.1: The anisotropy measurement of the dilution series show that for the present sample the results are only reliable if the concentration of the sample is more than 1 μM .

The intensity data revealed non-linear changes with decreasing concentration of fluorescein labelled oligonucleotide (table 2.5.2-1). Below 0.1 μM the instrument is not sensitive to changing concentrations (figure 2.5.2.1) and reading below 700 at PMT setting of 50 are mainly scattered light.

concentration (μM)	intensity	anisotropy	concentration (μM)	intensity	anisotropy
100	135950	0.0384	0.5	1211	0.0324
90	123148	0.0387	0.4	1081	0.0254
80	108503	0.0386	0.3	962	0.0363
70	94518	0.0386	0.2	840	0.0417
60	81430	0.0384	0.1	727	0.0302
50	68912	0.0385	0.09	944	0.0131
40	54895	0.0384	0.08	575	0.0487
30	41786	0.0387	0.07	550	0.0599
20	27858	0.0385	0.06	595	0.0242
10	14925	0.0386	0.05	583	0.01
9	12110	0.0388	0.04	580	0.0517
8	11212	0.0387	0.03	666	0.2128
7	9717	0.0385	0.02	644	0.2239
6	8371	0.0385	0.01	749	0.0091
5	7247	0.0383	0.009	562	0.1052
4	5807	0.0386	0.008	592	0.1193
3	4612	0.0386	0.007	586	0.0919
2	3291	0.0385	0.006	586	0.0287
1	2021	0.0389	0.005	579	0.0382
0.9	1673	0.0327	0.004	606	0.0984
0.8	1527	0.0405	0.003	594	0.0882
0.7	1445	0.0429	0.002	625	0.2873
0.6	1327	0.0394	0.001	646	0.2205

Table 2.5.2-1: For all the measurements the excitation wavelength was 485nm, emission wavelength was 535 and the integration time was 20 μs . All the samples were in the same 96 well-plate.

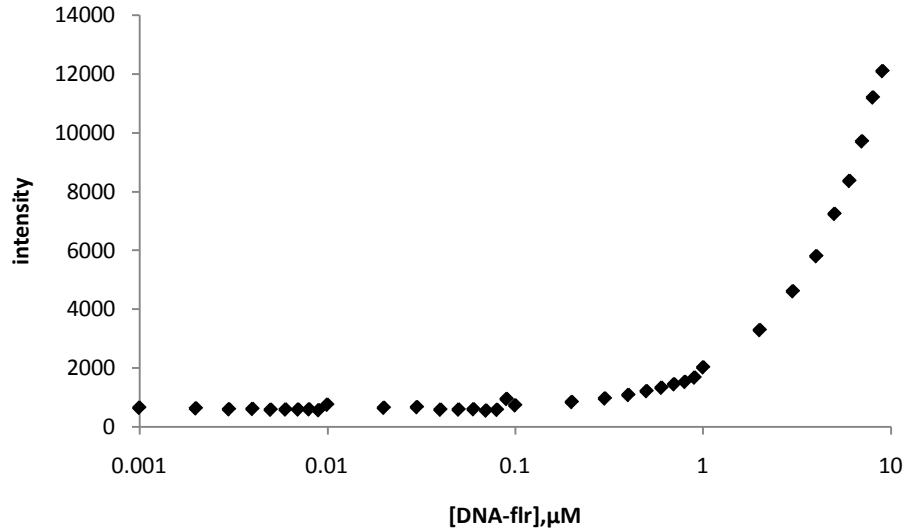


Figure 2.5.2.2: Measured intensity with concentration, measured with Tecan 200 PRO. For the fluorescein labelled oligonucleotides, the instrument was only sensitive to concentrations above 0.1 μM , below this level the fluorescence intensity didn't alter with changing concentration.

2.6 Materials and Methods

2.6.1 BSA

2.6.1.1 Labelling reaction

BSA (0.48 g) (Sigma, MW=66000) was dissolved in 120 ml of 0.1 M carbonate-bicarbonate buffer (Sigma), pH=9, at a concentration of 4 mg/ml and the solution was then divided into 20 vials (3000 μl each), to react with FITC (Thermo-Fisher, MW=389.38).

The lab was darkened when making fluorophore solutions. FITC solution (1 mg/ml) was prepared by dissolving 0.05g of FITC in a few drops of DMF and then immediately brought up to 50ml using the bicarbonate buffer. The reaction vessels were protected from light by wrapping them in aluminium foil. FITC solutions were immediately added to 20 vials of BSA solution and they were gently stirred. The samples were left on stirrer to react for 8 hours at room temperature in the dark.

2.6.1.2 Removing the unreacted Dye

When the reaction is complete it is very important to remove the unreacted dye because the free dye will have contributions to absorbance and depolarization of the emission and introduces considerable errors to measurements. Free unreacted dye was separated from the reaction mixture by dialysis against buffer. The dialysis membranes (Medicell International Ltd, cut-off 12-14000 Da) were soaked in distilled water for 4 hours prior to use and were rinsed every hour. They were then boiled for approximately an hour in 10 mM sodium bicarbonate solution and approximately 30 min in distilled water. The membranes were then extensively washed in distilled water and were immediately used [187].

Samples were processed in tissue culture flasks (Sarstedt, 175 cm²) containing 300-600 ml of the 0.01 M bicarbonate buffer. There was a range of buffer changes depending on the concentrations of the samples from 3 changes (2 within the first five hours and 1 after leaving overnight) for very dilute samples to more than 30 changes, done in a week followed by labelling reaction, for highly concentrated samples.

To preserve the protein from bacteria, 1% solution of sodium azide(Sigma, MW=74) was added to all buffer solutions and the dialysis stages were done at 4°C in cold room while the containers of the dialysis bags (flasks) were on the stirrer.

To avoid the error from the unreacted dye, the separation was regarded as complete only when the emission intensities of the supernatants measured by the fluorometer (Carry Eclipse) at the PMT voltage of 850V were below 40.

2.6.2 Intensity and Anisotropy measurements

Purified protein conjugates were characterized by measurements of, their fluorescence spectra and steady-state emission anisotropy. Samples concentrations were adjusted for the anisotropy measurements because the most precise anisotropy data are obtained if the solutions are optically dilute so that depolarization due to radiative reabsorption is avoided [22].

The fluorescence spectra and steady-state emission anisotropies of all the samples were measured by a Cary Eclipse Fluorometer, equipped with removable polarisers. The excitation and emission bandwidths were both set to 5nm (default). Plastic cuvettes (usable at 340-900nm, Fisher Scientific) were used for all the measurements. To avoid any inconsistency in adjustment of the polarisers for different measurements, the polarisers were set to VV orientation and the emissions of all the samples were measured. The same was done for all VH measurements as well. All anisotropy measurements were done at the λ_m of the emission peak, at the maximum intensity, to have the most precise results[22].

2.6.3 UV-Visible absorption spectroscopy

The absorption spectra of all samples were measured by Jasco V530 spectrophotometer. All the measurements were done in a range from UV to Visible (270-600nm) using 1 cm quartz cuvettes (Hellma, Fisher) containing approximately 3 mL of conjugated protein solution against sodium bicarbonate (solvent) as reference. Some samples of high optical densities were diluted such that the optical density was below 0.05[22].

2.6.3.1 Dye to protein ratio

The levels of fluorophore conjugation with protein are usually resolved by finding the ratios of the fluorophore concentration to protein concentration, F/P. The concentrations are determined by measuring the absorbance (Beer-Lambert law) [188] of protein and the dyes at or near their characteristic excitation maximum (279 nm for BSA and 495 nm for FITC), using the following formula (Equation 2.6.3.1-1):

Equation 2.6.3.1-1

$$F/P = \frac{A_{495}}{A_{279} - 0.34 \times A_{495}} \times \frac{\epsilon_{279}}{\epsilon_{495}}$$

A_{495} and A_{279} are the maximum absorbance for FITC and BSA, and ϵ_{279} and ϵ_{495} are molar absorptivity of BSA and FITC respectively. The absorbance spectrum of the unreacted FITC shows that it has absorption at UV region as well and to find the protein concentration the contribution of the dye at this region ($0.34 \times A_{495}$ in the case of FITC)[189] must be deduced from the total absorbance. However this method is not very accurate because the characteristics of the spectra of a free dye are different from the conjugated ones [35, 76] (figure 2.6.3.1.1) and the fluorophore to protein ratios, especially for highly conjugated proteins, are usually lower than the actual value if the dye concentration is calculated solely based on the height of the absorbance peak [33].

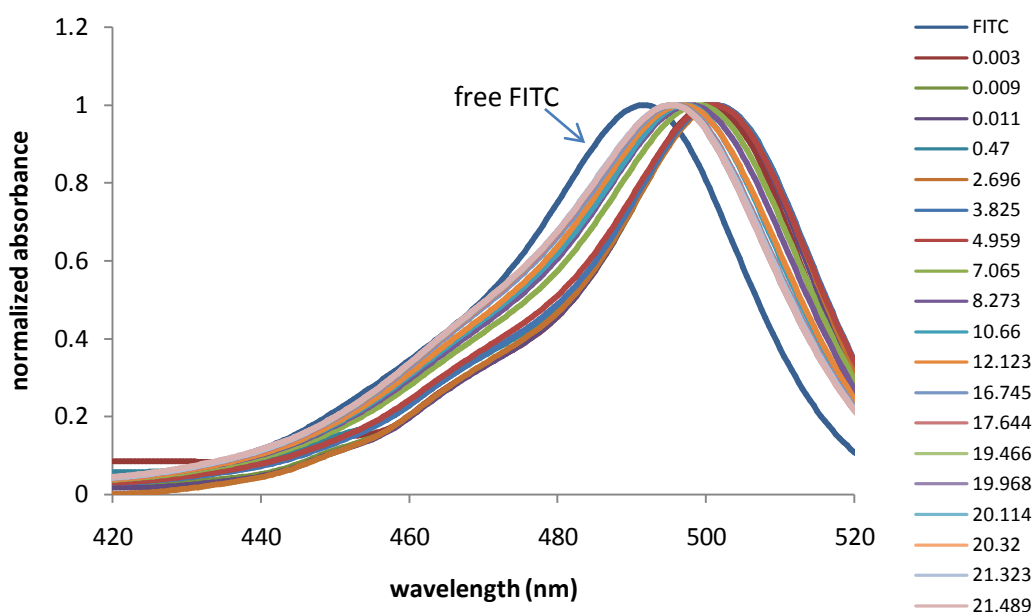


Figure 2.6.3.1.1: Bound FITC shows red-shift of the absorption maxima but as the molar ratios increase the peaks shift back to left

To fix this error the area under the curve (AUC) of the normalized absorbance spectra in the visible region of both conjugated and unconjugated dye were estimated (by means of trapezoidal rule [190]) because the integrated intensity that can be obtained by integrating the area under the absorption peak is relative to the amount of the absorbing substance and their ratios, were used as a correction factor, ξ [33, 191] (equation 2.6.3.1-2):

Equation 2.6.3.1-2

$$\int_{\lambda_{\kappa}}^{\lambda_n} I(\lambda) d\lambda \approx \frac{1}{2} \sum_{\kappa}^n (\lambda_{(\kappa+0.5)} - \lambda_{\kappa}) (I_{(\kappa+1)} + I_{\kappa})$$

λ_n to λ_{κ} is the range of wavelength over which the area of the peak is calculated.

2.6.4 DNA Strands

All custom oligonucleotides were synthesized commercially (*Life Technologies, UK*) and provided in concentrated form. The oligonucleotides were dissolved in a buffer solution of 10 mM Trizma hydrochloride (MW=157.6), 1 mM EDTA (MW=292.24) and 50mM NaCl (MW=58.44). To prepare the buffer the component materials were first dissolved in water and had a pH of 2.7. The pH of the buffer was adjusted using NaOH to pH=8. Stock solutions (100 μ M) of all oligonucleotides were prepared in this buffer.

To fractionally label the template oligonucleotides, a concentration range of fluorescein labelled oligonucleotide solutions were prepared such that the upper limit of the range was sufficient to allow them to react with the complementary sequences on the template DNA. Finding the lower limit was more complicated, as it needed to allow the templates to be hybridized sub-stoichiometric fluorescence for robust measurement of the anisotropy. To determine such a low concentration of fluorescein labelled oligonucleotide, where the sensitivity of the instrument (Tecan Infinite 200 PRO), would allow precise and accurate measurements of intensity and anisotropy a dilution series of fluorescein labelled oligonucleotide solution with concentrations from 100 μ M to 1nM were prepared and their fluorescence emission intensity and anisotropy were measured.

Each template was titrated under DNA annealing conditions with the short complementary sequence over a molar ratio from 0.05:1 up to 3:1.

2.6.5 Four-way junctions

To build migrationally immobile [176]four-way Holliday junctions, four semi-complementary strands (indexed a-d) of DNA of different sizes (12-28 mer oligonucleotides) were obtained commercially in concentrated form (Life Technologies; Paisley, UK). The samples (figure 2.6.5.1) were dissolved in a buffer solution of 10 mM Trizma hydrochloride (MW=157.6) and 50mM NaCl (MW=58.44) to a final concentration of 100 μ M for all oligonucleotides.

32-mers

<i>a</i>	flr	T	G	C	C	C	A	G	T	G	C	G	T	A	G	A	C	G	T	G	T	T	A	T	C	A	G	T	C	G	T	C	A
<i>b</i>	flr	T	A	C	T	A	T	C	A	G	C	G	C	T	C	A	C	G	T	C	T	A	C	G	C	A	C	T	G	G	G	C	A
<i>c</i>	flr	T	G	A	C	G	A	C	T	G	A	T	A	A	C	A	C	G	A	G	T	G	C	A	C	T	G	T	A	C	G	T	A
<i>d</i>	flr	T	A	C	G	T	A	C	A	G	T	G	C	A	C	T	C	G	T	G	A	G	C	G	C	T	G	A	T	A	G	T	A

30-mers

<i>a</i>	flr	T	C	C	C	A	G	T	G	C	G	T	A	G	A	C	G	T	G	T	T	A	T	C	A	G	T	C	G	T	A
<i>b</i>	flr	T	C	T	A	T	C	A	G	C	G	C	T	C	A	C	G	T	C	T	A	C	G	C	A	C	T	G	G	G	A
<i>c</i>	flr	T	A	C	G	A	C	T	G	A	T	A	A	C	A	C	G	A	G	T	G	C	A	C	T	G	T	A	C	G	A
<i>d</i>	flr	T	C	G	T	A	C	A	G	T	G	C	A	C	T	C	G	T	G	A	G	C	G	C	T	G	A	T	A	G	A

28-mers

<i>a</i>	flr	T	C	C	A	G	T	G	C	G	T	A	G	A	C	G	T	G	T	T	A	T	C	A	G	T	C	G	A
<i>b</i>	flr	T	T	A	T	C	A	G	C	G	C	T	C	A	C	G	T	C	T	A	C	G	C	A	C	T	G	G	A
<i>c</i>	flr	T	C	G	A	C	T	G	A	T	A	A	C	A	C	G	A	G	T	G	C	A	C	T	G	T	A	C	A
<i>d</i>	flr	T	G	T	A	C	A	G	T	G	C	A	C	T	C	G	T	G	A	G	C	G	C	T	G	A	T	A	A

26-mers

<i>a</i>	flr	T	C	A	G	T	G	C	G	T	A	G	A	C	G	T	G	T	T	A	T	C	A	G	T	C	A
<i>b</i>	flr	T	A	T	C	A	G	C	G	C	T	C	A	C	G	T	C	T	A	C	G	C	A	C	T	G	A
<i>c</i>	flr	T	G	A	C	T	G	A	T	A	A	C	A	C	G	A	G	T	G	C	A	C	T	G	T	A	A
<i>d</i>	flr	T	T	A	C	A	G	T	G	C	A	C	T	C	G	T	G	A	G	C	G	C	T	G	A	T	A

24-mers

<i>a</i>	flr	T	A	G	T	G	C	G	T	A	G	A	C	G	T	G	T	T	A	T	C	A	G	T	A
<i>b</i>	flr	T	T	C	A	G	C	G	C	T	C	A	C	G	T	C	T	A	C	G	C	A	C	T	A
<i>c</i>	flr	T	A	C	T	G	A	T	A	A	C	A	C	G	A	G	T	G	C	A	C	T	G	T	A
<i>d</i>	flr	T	A	C	A	G	T	G	C	A	C	T	C	G	T	G	A	G	C	G	C	T	G	A	A

22-mers

<i>a</i>	flr	T	G	T	G	C	G	T	A	G	A	C	G	T	G	T	T	A	T	C	A	G	A
<i>b</i>	flr	T	C	A	G	C	G	C	T	C	A	C	G	T	C	T	A	C	G	C	A	C	A
<i>c</i>	flr	T	C	T	G	A	T	A	A	C	A	C	G	A	G	T	G	C	A	C	T	G	A
<i>d</i>	flr	T	C	A	G	T	G	C	A	C	T	C	G	T	G	A	G	C	G	C	T	G	A

20-mers

<i>a</i>	flr	T	T	G	C	G	T	A	G	A	C	G	T	G	T	T	A	T	C	A	A
<i>b</i>	flr	T	A	G	C	G	C	T	C	A	C	G	T	C	T	A	C	G	C	A	A
<i>c</i>	flr	T	T	G	A	T	A	A	C	A	C	G	A	G	T	G	C	A	C	T	A
<i>d</i>	flr	T	A	G	T	G	C	A	C	T	C	G	T	G	A	G	C	G	C	T	A

18-mers	<i>a</i>	flr	T	G	C	G	T	A	G	A	C	G	T	G	T	T	A	T	C	A
	<i>b</i>	flr	T	G	C	G	C	T	C	A	C	G	T	C	T	A	C	G	C	A
	<i>c</i>	flr	T	G	A	T	A	A	C	A	C	G	A	G	T	G	C	A	C	A
	<i>d</i>	flr	T	G	T	G	C	A	C	T	C	G	T	G	A	G	C	G	C	A
16-mers	<i>a</i>	flr	T	C	G	T	A	G	A	C	G	T	G	T	T	A	T	A		
	<i>b</i>	flr	T	C	G	C	T	C	A	C	G	T	C	T	A	C	G	A		
	<i>c</i>	flr	T	A	T	A	A	C	A	C	G	A	G	T	G	C	A	A		
	<i>d</i>	flr	T	T	G	C	A	C	T	C	G	T	G	A	G	C	G	A		
14-mers	<i>a</i>	flr	T	G	T	A	G	A	C	G	T	G	T	T	A	A				
	<i>b</i>	flr	T	G	C	T	C	A	C	G	T	C	T	A	C	A				
	<i>c</i>	flr	T	T	A	A	C	A	C	G	A	G	T	G	C	A				
	<i>d</i>	flr	T	G	C	A	C	T	C	G	T	G	A	G	C	A				
12-mers	<i>a</i>	flr	T	C	T	C	A	C	G	T	C	T	A	A						
	<i>b</i>	flr	T	A	A	C	A	C	G	A	G	T	G	A						
	<i>c</i>	flr	T	C	A	C	T	C	G	T	G	A	G	A						
	<i>d</i>	flr	T	T	A	G	A	C	G	T	G	T	T	A						

Figure 2.6.5.1: 11 sets of 4 semi-complementary sequences labelled with fluorescein at 5' end were used to generate 11 different four-way junctions, figure 4.4.2.1.

Samples were diluted to 25 μ M and equal volumes (25 μ L) of oligonucleotides a-d were mixed in an Eppendorf tube. Three replicates of each sample were made. The mixtures were incubated at 95°C for 5 minutes, then moved to an insulated box and left on a water bath, overnight to allow slow annealing down to ~ 5°C below the melting temperature of the lowest melting arm and then moved to an ice bath.

To plan the most efficient annealing protocol and as the majority of the junctions had short arms and low melting temperatures, the melting temperature of each individual arm was calculated (table 2.6.51). In some cases, where the calculated melting temperatures of the arms were very low, a different buffer with a higher salt concentration, 450mM NaCl, was used for making samples.

FJ \ arm, °C	A	B	C	D
16	54	46	48	48
15	49	41	46	46
14	38	44	41	40
13	40	36	38	40
12	36	32	36	38
11	34	30	34	36
10	30	26	30	32
9	28	24	28	30
8	24	26	24	20
7	22	18	20	22
6	18	16	18	16

Table 2.6.5.1- Melting temperature of the arms of 11 four-way junctions, the Tms were calculated based on "salt adjusted" method. Naming the arms A to D was arbitrary and for all junctions in figure 2.6.5.1 followed the same pattern as shown for FJ 16.

The melting temperatures were estimated using OligoCalc[192], based on the DNA sequences, DNA concentrations and the salt concentration Oligocalc provides the results of three common melting temperature calculations named "basic", "salt adjusted" and "nearest neighbour method". As the lengths of the arms of different junctions were between six to sixteen base pairs, the melting temperatures were calculated based on the "nearest neighbour method" that was used as the most accurate method for oligonucleotides of these lengths[192-194]. However the method failed to calculate the Tms of a number of arms of small junctions, to keep the consistency, all the melting temperatures were calculated by salt-adjusted method. The software was also used to confirm that none of the sequences would self dimerize or make hairpins.

In the present study, four-way junctions, FJ, were named based on the number of the base pairs of their arms, from FJ6 to FJ16 (figure 4.4.2.1).

Six 30µL replicates for each four-way junction were then made up in a 384-well glass bottomed plate (Nunc). The fluorescence intensity and anisotropy of each well was measured on an automated reader (Infinite 200 PRO, Tecan, UK Ltd, Reading, UK). In the next step, unreacted oligonucleotides were separated from four-way

junctions by electrophoresis in 10% (w/v) non denaturing polyacrylamide in 90 mM Tris borate solution. The formation of four-way Holliday junction structures was investigated by their slow mobility on gel electrophoresis. The assembled oligonucleotides moved as single fluorescent bands which were excised and the DNA junctions recovered by electroelution and ethanol precipitation. The pure four-way junctions were dissolved in buffer (90 mM Trizma hydrochloride pH=8.3[155]) without salt and their emission intensity and anisotropy measured. Samples of all strands (a-d) at a concentration of 25 μ M were tested and the intensity and anisotropy measured to assess the changes that take place upon junction formation.

All measurements were under taken at the same PMT setting (gain of 50) excitation band at 485 nm with the bandwidth of 20 nm. Fluorescence emission was monitored at 535 nm (band width of 25nm).

To verify homo-FRET it is common to do fractional labelling or red-edge excitation anisotropy measurements[4, 195]. To ensure that the reduction in anisotropy was due to homo-FRET, the experiment was repeated with a buffer with a higher concentration of salt and the consequent changes in anisotropy were also studied. The emission anisotropy of two of the constructs, FJ16 with the arm length of 16 bp (the biggest) and FJ6 with 6 bp (the smallest), were measured in both low and high salt conditions.

The experimental results showed that anisotropy increased as the size of four-way junction got bigger. To ensure that the increase was solely due to the failure of homo-FRET in molecules of bigger sizes, and not because of having a lower rotational diffusion, all samples were left in -30°C freezer and the anisotropy was measured again.

2.7 Results

2.7.1 BSA

In the present study BSA was fractionally labelled with FITC and its UV absorption, fluorescence intensity and anisotropy were measured.

The anisotropy of FITC is 0.0495 [127] and when it is bound to BSA (MW=66 KD, Dimensions=14nm, 4nm, 4nm) [196], its rotational correlation time increases and its anisotropy raises to approximately 0.32 [127]. By increasing the number of FITCs labelled to BSA however, the slight increase in the mass and the rotational correlation time, was not expected to make a detectable change in the anisotropy of the molecule. (Table 2.7.1) On the contrary, as BSA gets labelled with more of FITC molecules, its anisotropy decreases. This is due to the fact that homo transfer of the excitation energy (homo-FRET), happens between the fluorophores as the distance between them becomes less and gets closer to their Förster distance[64].

BSA(MW)= 66000 FITC(MW) = 389.38		Perrin equation $r = r_0 / (1 + \tau/\theta)$ $r_0 = 0.37\tau$ (ns) = 3.8	
Number of FITC on BSA	molecular weight	rotational correlation time, θ (ns)	anisotropy (r)
1	66389.38	39.83	0.2911
2	66778.76	40.06	0.2913
3	67168.14	40.3	0.2914
4	67557.52	40.53	0.2916
5	67946.9	40.76	0.2917
6	68336.28	41	0.2918
7	68725.66	41.23	0.2919

Table 2.7-1: Using Perrin equation the anisotropy (r) of the labelled BSA is calculated. Mass of BSA is approximately 170 times bigger than the mass of FITC and the changes in the rotational correlation time of the molecule are negligible.

2.7.2 Dendrimers

Poly-amidoaminedendrimers (PAMAM G6-NH₂) labelled with FITC. The diameter of PAMAM G6-NH₂ is 6.7 nm which was in the range of interest ($1.37R/R_0$) and it has 256 amine groups on the surface.

The trend of decrease in anisotropy clearly showed the increase of homo-FRET upon addition of FITC to dendrimer ratio, however saturation of all sites seemed impossible and the exact quantification of the extent of labelling was hard and

beyond the limits of the model. On the other hand such a huge ensemble of dyes did not make a useful model to mimic protein clusters in cell membrane.

2.7.3 DNA strands

The conventional DNA system in the present study consisted of two types of primers; i) single stranded template DNAs with a specific repeating sequence (6 nucleotides long) along the chain, and ii) short complementary sequences to the repeating sections of the template. The short strand was fused to fluorescein at the 5' end. The design was to allow titration the DNA template with the fluorescein labelled short complementary sequences. The DNA templates were engineered a range of lengths, such that the repeating sequence, and consequently the short complementary sequence, could be distributed over a range of distances separated by a gap of 0-12nucleotides (figure 2.6.3.1).The template containing three repeats of the complementary sequence were designed to assemble the short complementary sequences giving stochastic mixtures of differently labelled DNA molecules when the template was unsaturated. DNA molecules, at the lengths that suits the present study (<100 bp), can be assumed as rigid rods that do not bend in solutions [114, 184].

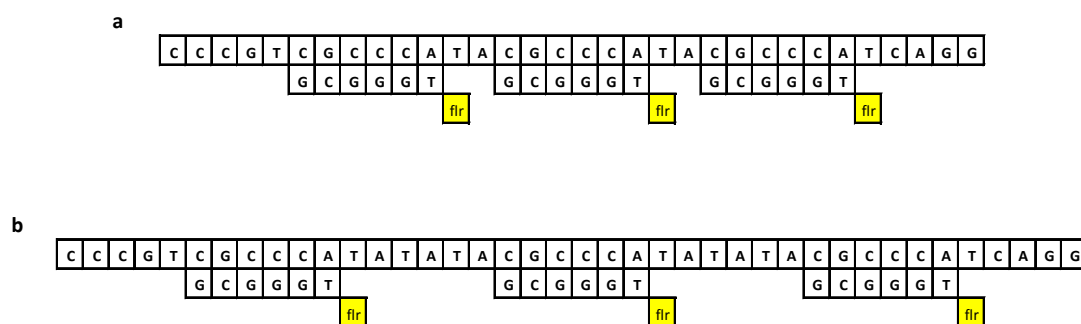


Figure 2.6.3.1: Two examples of linear DNA constructs. Both templates (long, unlabelled oligonucleotides) had 3 sequences of CGCCCA that hybridized with GCGGGT-flr,(short, labelled oligonucleotides) to form two trimers of fluorescein with different sizes. The distance between two neighbouring fluorescein in compounds **a** and **b** are 2.72 and 4.08 nm respectively.

2.7.4 Four-way junctions

In the present study, fluorescently labelled DNA four-way junctions were designed to study homo-FRET over varying distances. Four separate oligonucleotides were tagged with fluorescein at the 5' end, and had matching sequences to form the four-way junctions. The oligonucleotides have different lengths to generate a set of four-way junctions of a range of inter-fluorophore distances (figure 2.7.4.1).

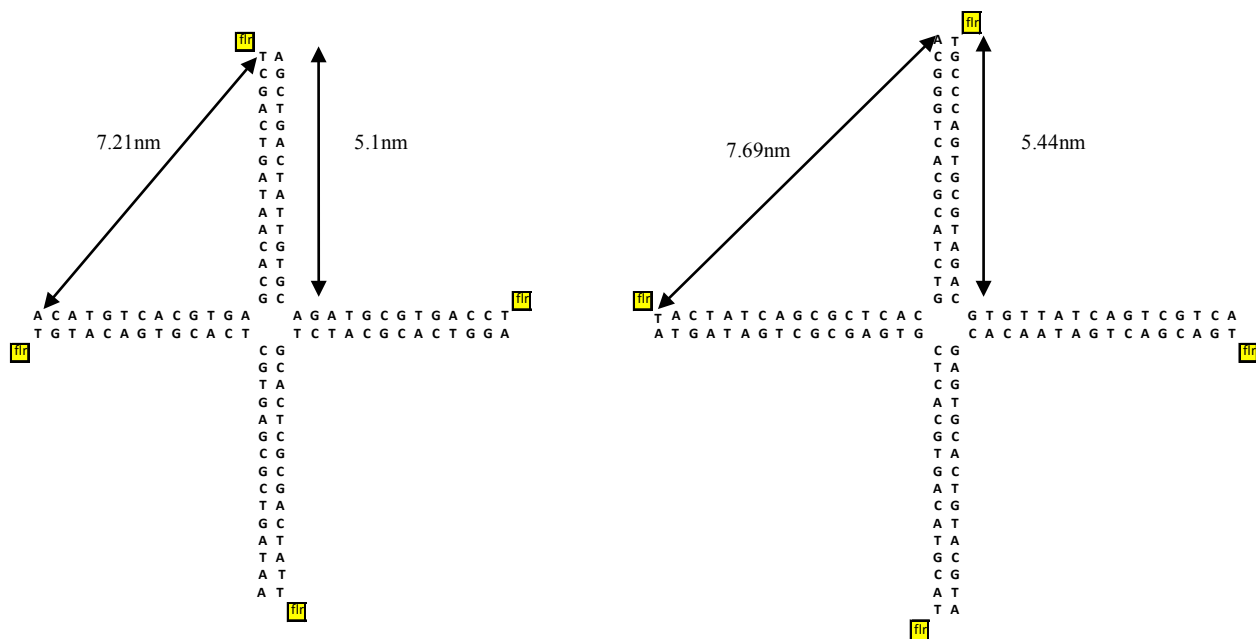


Figure 2.7.4.1: Two four-way junctions with the arm length of 15 base pairs (left) and 16 base pairs (right). The average distance between the fluorescein molecules, calculated based on square planar configuration [164], is 8.2 nm for the smaller junction and 8.85 nm for the bigger one, the length of each base is 0.34 nm [197].

In the present study however the conformational changes was not an issue, because a) the fluorescence anisotropy of the pure four-way junctions had been measured at no/low salt condition, where the majority of the conformational population would be in the extended unstacked form (conformer 2), b) the four arms of each four-way junction were similar to each other because all the oligonucleotides were labelled with fluorescein at their 5' end and were designed to generate four-way junctions with four equal arm lengths, so even if conformers 1 and 3 existed and were not equally populated, the average distances between fluorescein molecules would be similar it could be assumed that conformational changes would not alter the average

distances between the dyes. To figure out the exact inter-probe distances in this case conformer 2 and one of the other two conformers would be considered. Two structural models of square planar and tetrahedral were compared.

2.8 Conclusion

To investigate the accuracy of the assumption of equal fluorescence efficiency of the theory initiated by Weber [1], BSA was chosen as a model system as it was already used by him to devise the formula. BSA is a suitable model system to study homo-FRET in multiply labelled systems because upon labelling it fulfils the assumptions of the inter-probe distances ($\leq 0.8R/R_0$) and the randomness of the probes orientation. BSA was labelled with FITC, which was available at a reasonable cost and its conjugates with BSA were well studied in similar investigations.

Among different systems revised for the study of homo-FRET on distances greater than $0.8 R/R_0$ (up to $2.2R/R_0$), DNA constructs were chosen. DNA constructs are programmable materials, they self assemble and their lengths are adjustable. The constructs were composed of two sets of oligonucleotides with complementary sequences and upon hybridizing could give the desired distances to dyes. Oligonucleotides can be designed in to give duplexes or 2D structures such as four-way Holliday junctions upon hybridization.

3 Fluorescence Efficiency in Aggregates¹

3.1 Introduction

Theories and formula based on the effects of homo-FRET on fluorescence anisotropy in clusters, explained in chapter 1 (sections 1.7-1.8), have been applied to study aggregation of proteins in cells and resolving cluster sizes for nearly 50 years. For example, the effect of KCl on association and dissociation of yeast enolase was investigated [198], the geometric arrangement of fluorophore binding sites on CaATPase was studied and its coordination number determined [199], rotational correlation time of the phosphorylation domain of CaATPase was determined [200], the average oligomeric state of phospholamban molecules enumerated [201], the size of lysozyme oligomers in an anionic lipid membrane was calculated [202] and it was shown that oligomeric complexes of membrane-bound Lz-A488, possibly have a stoichiometry of $k = 6 \pm 1$ [203].

All of these studies have invoked the assumption of equal fluorescence efficiency either directly or implicitly. The assumption, however, needs to be treated more carefully as dyes in close proximity in clusters are prone to interact, producing either

¹The material in this chapter is based substantially on the publication: Zolmajd-Haghighi, Z., Hanley, Q.S., *When One Plus One Does Not Equal Two: Fluorescence Anisotropy in Aggregates and Multiply Labelled Proteins*. Biophysical Journal, 2014. **106**: p. 1457–1466.

self-quenching or emission enhancement. Both of these phenomena may result in non additive behaviour of the dyes in the emission intensity observed from a cluster.

The aim of the present work was to study the effect of self quenching and emission enhancement on fluorescence anisotropy and to investigate how the assumption of equal fluorescence efficiency may affect the interpretation of anisotropy data. A combination of theoretical treatment, numerical simulations, and measurements of a model system containing multiple fluorophores was used to study the relationship between cluster formation and anisotropy. BSA, as a model system, was fractionally labelled with FITC and its fluorescence intensity and anisotropy were measured at each stage of labelling. The theory was then applied to interpret the data and the accuracy of the assumption was examined.

3.2 Theory

As explained in section 1.7, in a stochastic mixture of fractionally labelled protein the contribution of the species PX_i to total emission intensity is ϕ_i , (equation 1.7.2-3). The equal fluorescence efficiency assumption states that a species containing i fluorophores is weighted by i , however as noted in (sections 1.9-1.10) many studies report non-additivity of fluorescence emissions. This non-additivity can be treated using a specific factor of the emission of individual subunit. Such a factor, z_i , replaces i in equation 1.7.2-8 to account for the relative intensity of the cluster PX_i containing i fluorophores. Equation 1.7.2-3 can be rewritten as equation 3.2-1:

Equation 3.2-1

$$\phi_i = \frac{z_i f_i}{\sum_{i=0}^N z_i f_i}$$

If in any rare case the assumption of equal fluorescence intensity is correct for a system then $z_i=i$, and $z_i= (1, 2, 3 \dots N)$, this means the general formula in equation 3.2-1 has reduced to equation 1.7.2-3.

“In systems with fluorophores that quench or enhance emission, $z(i)$ can be defined with the general model of $z(i) = i^p$, which considers quenching or enhancement to be multiplier. If fluorophores do not interact, $p = 1$ and the assumption of equal fluorescence efficiency applies. If the fluorophores interact and show self-quenching $p < 1$ and if the emission is enhanced due to the interaction $p > 1$. These simple models show the impact of quenching and enhancement on the predicted anisotropy of stochastic mixtures. Depending on the type of behaviour that the dyes have with themselves, $z(i)$ may take on any value. If $z(i)$ follows a known functional progression $z(i)$, this can be conveniently substituted into the equation. A related parameter providing information about the behaviour of individual fluorophores in the cluster may be defined by dividing z_i by i (e.g.: $\zeta_i = z_i/i$).

In general, the anisotropy of an N -mer cluster with i labelled subunits when a fraction, f , of the monomers are labelled is given by equation 3.2-2:

Equation 3.2-2

$$r(f, N) = \frac{\sum_{i=1}^N A_{i,N} z_i f^i (1-f)^{N-i} r_i}{\sum_{i=1}^N A_{i,N} z_i f^i (1-f)^{N-i}}$$

where, $A_{i,N}$ is the i^{th} element of the N^{th} row of Pascal's triangle indexed such that the first element, 1, is given by $A_{0,0}$, and r_i is the anisotropy of the cluster with i fluorophores. If measured values of r_i are available, these should be used. Otherwise, as in the case for equation 1.7.1-4, the considerations of Runnels and Scarlata may be applied [204]. The index begins at 1 due to the fact that the unlabelled fraction does not contribute directly to the anisotropy.

It is challenging to recover the values of z_i in the absence of a known equation predicting its value. One approach is to measure fluorescence intensity while titrating a fluorescent ligand, X , with a clustering agent or protein, P , over a range of

fractional labelling. Total fluorophore concentration should be held constant while investigating over the range $[P] = N[X]$ to $[P] \gg \gg N[X]$. Let I be normalized intensities of solutions at each fractional labelling (f) value. A system of equations can be set up which may allow z_i to be estimated. In general intensity is given by equation 3.2-3:

Equation 3.2-3

$$I(f, N) = \sum_{i=1}^N A_{i, Ni} z_i f^i (1-f)^{N-i}$$

This approach requires knowledge of f and N and assumes each labelling site is independent of the others. Other approaches might be to construct the individual species forming a mixture [205] or using synthetic biology approaches [206]. Once the z_i are known, anisotropy can be computed.”

3.3 Results and discussions

To compare the conventional predictions ($z(i) = i^1$) to cases where z_i values follow progressions other than expected from the assumption of equal fluorescence efficiency, using simple power law models (Figure 3.3.1). Although these models are simplistic, they illustrate general trends for cases where interactions between clustered fluorophores result in brightness changes. Under these conditions, as the fractional labelling increased, the predictions diverged with the quenched models consistently yielding higher anisotropy either $z(i) = i$ or $z(i) = i^2$. For the tetramer, the maximum difference in predicted anisotropy Δr , between the two conditions ($p = 0$ and $p = 1$) was 0.048 with the models converging as f approached 0 and 1. This Δr is greater than what is expected going from a cluster with $N = 3$ to one with $N = 4$ in a saturated cluster ($\Delta r = 0.033$). The under-prediction of anisotropy when applying the assumption of equal efficiency to a system exhibiting strong self-quenching will result in under-predicting cluster size. Similarly, in cases where the clustering of

fluorophores results in enhanced brightness, the conventional assumptions will over-predict anisotropy and overestimate cluster

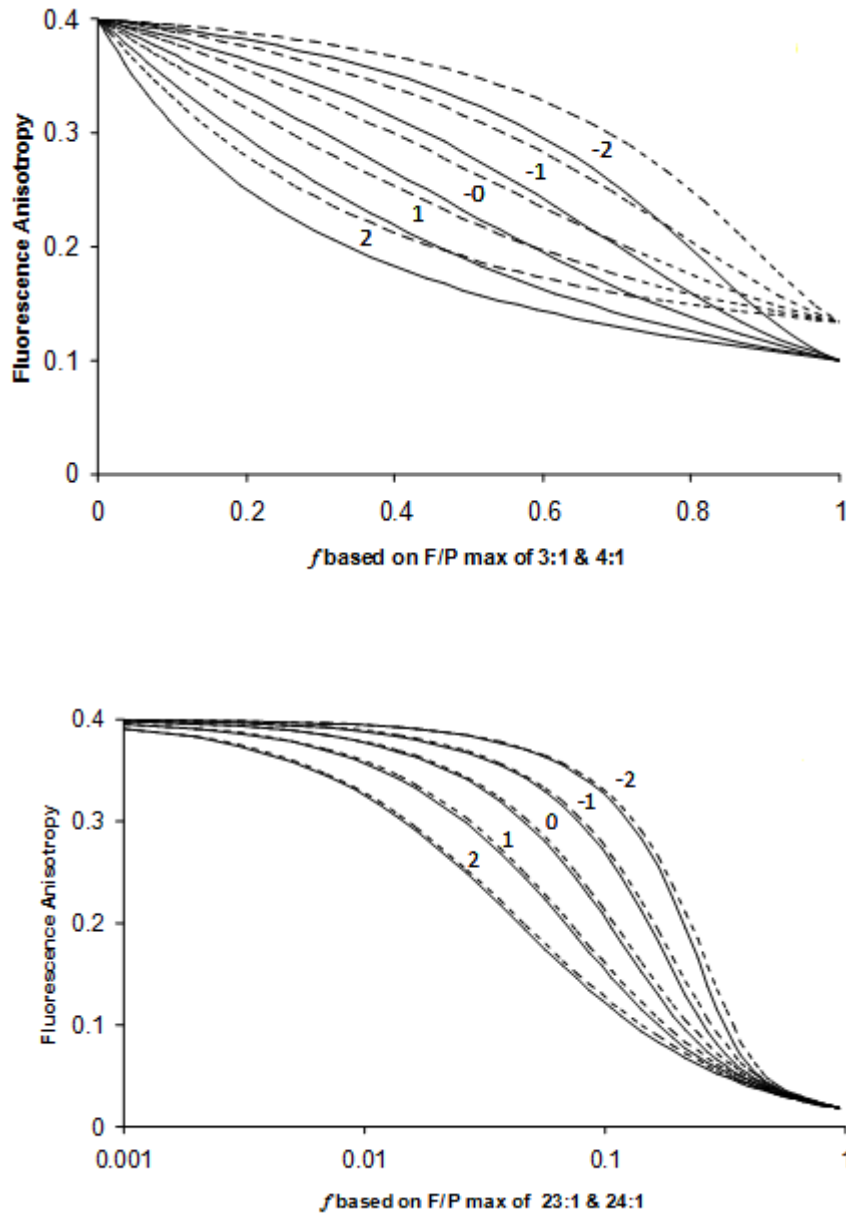


Figure 3.3.1: Predicted anisotropy for different fluorophore interaction terms (z_i) in stochastic mixtures in which each molecule within the mixture follows the rules of Runnels and Scarlata and $R < 0.8 R_0$. In both the graph with $N = 3$ (dashed lines) and $N = 4$ (solid lines) (panel a) and the one with $N = 23$ (dashed lines) and $N = 24$ (solid lines) (panel b), all models of fluorophore interaction converge in the limits of high (100%) and low (0%) fractional labelling. In both sets of data, the variations in anisotropy due to model assumptions exceed the difference expected due to changing the cluster size by one.

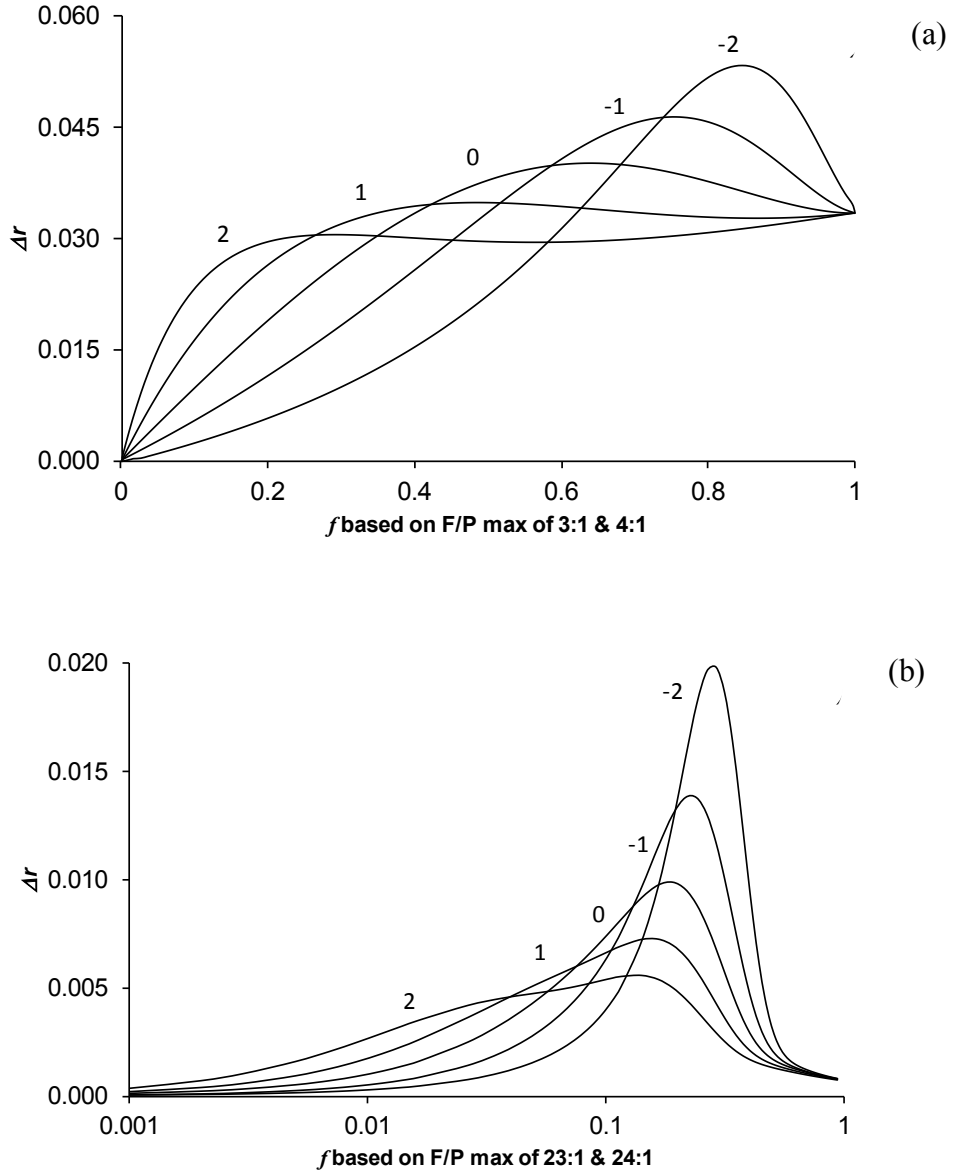


Figure 3.3.2: The lowest anisotropy for each cluster size is given by $0.4/N$ in these simulations. The interaction models shown are for power laws ($z(i) = i^p$) with values of p indicated next to the corresponding curves. The curves labelled with 1 correspond to the equal fluorescence efficiency model. Panels (a) and (b) illustrate the differences due to cluster size changing by one. The quenched systems show greater resolving power based on anisotropy difference than do either the enhanced model or the equal fluorescence efficiency model. Note: the y-axis scale with r_0 (e.g. using $r_0 = 0.32$ leads to a 20% reduction relative to $r_0 = 0.4$).

To better understand the impact of fluorophore interaction on the anisotropy of mixtures of clusters, Δr was computed for $p = 1$ (equal fluorescence efficiency) vs. $p = 0$ (quenched) for cluster sizes over the range $N = 2$ to $N = 26$. The models differed systematically with the magnitude of Δr and the fractional labelling corresponding to

the maximum difference changing with cluster size (Figure 3.3.3). As the cluster size increased, the fractional labelling at maximum Δr approached 0 and the magnitude of Δr increased. For example in a dimer, taking $z_i = 1$ yields an anisotropy that is 0.034 higher at a fractional labelling of 0.59. For a decamer, Δr is expected to be 0.055 higher at a fractional labelling of 0.146. Extrapolation of a reciprocal plot (not shown) indicates the maximum Δr to be 0.06 at the limit of infinite cluster size.

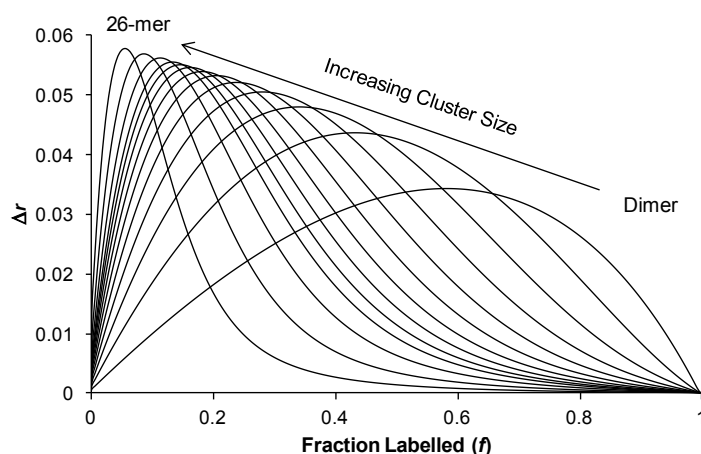


Figure 3.3.3: Difference between $p = 1$ and $p = 0$ as a function of cluster size and fractional labelling. The predictions include clusters made up of 2, 3, 4, 5, 6, 7, 8, 9, 10, 11, 13, 17, and 26 units. The maximum difference increases with the cluster size, but has impact over a wider range of fractional labelling in the smaller clusters.

For all cases, the anisotropy predicted for the simple quenched model was lower than predicted using the assumption of equal fluorescence efficiency. Consequentially, applying this assumption will systematically under-estimate cluster sizes when fluorophores exhibit reduced brightness in clusters.

3.3.1 Model System Verification

“[28]To study the impact of fluorophore interaction on larger clusters, exhaustive labelling of BSA was studied. BSA has 60 lysine residues with approximately half buried in the interior and additional residues in hydrophobic pockets leaving a subset to react [207, 208]. Dye binding to BSA has been studied previously [209-211].

Estimates of the F/P ratio for BSA under potentially saturating levels of FITC and other similarly reactive dyes vary widely in the literature and reflect the conditions used in individual laboratories [212-214]. The maximal F/P ratio under our conditions was determined by varying the ratio of FITC to protein in the reaction mixture while keeping the amount of protein and the reaction time constant (Figure 3.3.1.1). The saturation of FITC reactive sites on the surface of BSA was treated using a Langmuir type binding model (equation 3.3.1-1):

Equation 3.3.1-1

$$F = \frac{F_{max} [C]}{K_D + [C]}$$

F is the fitted values for F/P, F_{max} is F/P_{max} , K_D is Langmuir constant and $[C]$ is the initial concentration of FITC. F/P_{max} (F_{max}) was found to be $23.94 \approx 24$ FITC/BSA and the good correspondence to the Langmuir model suggests all FITC reactive sites on BSA reacted independently. The F/P_{max} for the FITC:BSA system fell within the range of 15-25 reported for similar experiments with FITC [212, 213] and similar amine reactive dyes [214]. $F/P_{max} = 24$ was used subsequently to scale the fractional labelling of BSA.

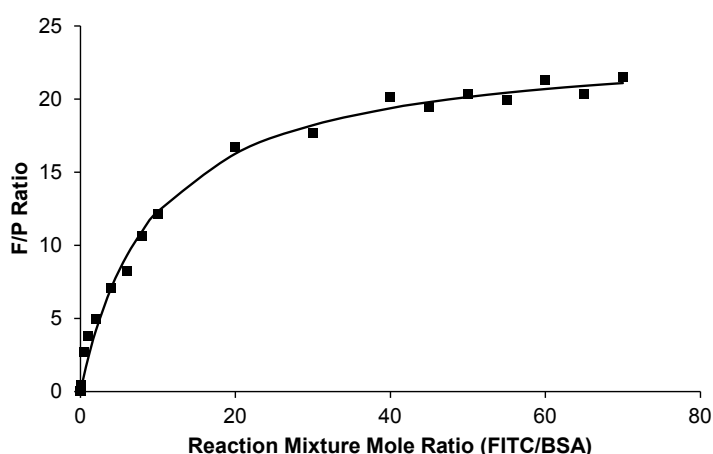
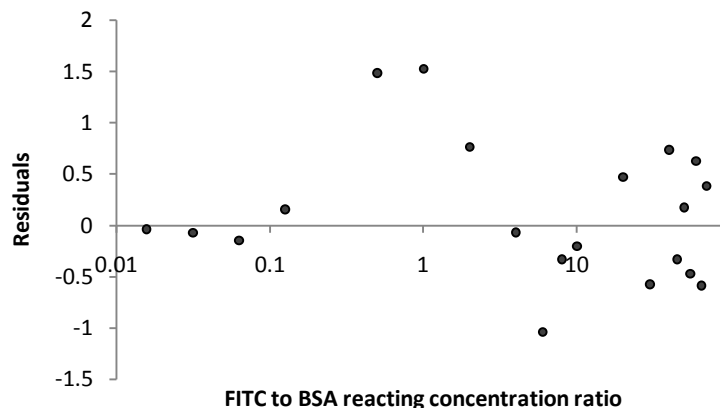


Figure 3.3.1.1: Spectroscopically determined F/P ratio with increasing mole ratio of FITC during reaction. Data (•) were measured up to a mole ratio of 70. A Langmuir type fit (solid line) indicated a maximum F/P ratio of 24.



Examination of the normalized intensity of a series of labelled BSA samples revealed a clear maximum followed by reduced intensity as f increased (figure 3.3.1.2). The equal fluorescence efficiency ($z(i) = i^1$) and simplified self-quenching ($z(i) = i^0$) models were computed and compared to the data. At the highest F/P ratios, FITC was highly quenched in agreement with previous reports (c.f. [212]). It is notable that the progression of intensity does not follow any of the simple power law models (Figure 3.3.1.2) and clearly does not conform to the assumption of equal fluorescence efficiency. There is an initial rise in intensity per BSA for f between 0 and 0.1. In this system when f reaches 0.1, molecules with 3 or fewer FITCs account for 77% of the total and dominate the fluorescence. The fluorescence per BSA dropped over the range $f = 0.1$ to 0.5. For $f > 0.5$ (samples dominated by BSA molecules with more than 10 FITCs attached) the normalized intensity was essentially constant. Similarly, the high levels of quenching as f approaches 1 are consistent with previous data [212].

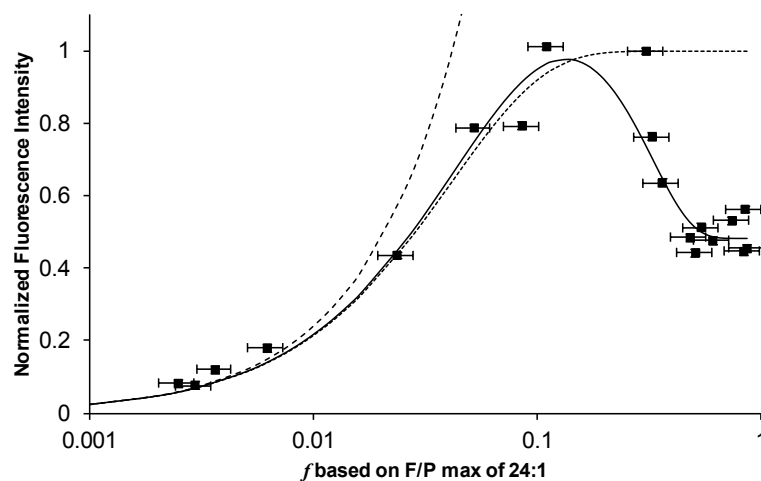


Figure 3.3.1.2: Normalized fluorescence intensity of BSA solutions as fractional labelling increased. The fluorescence was measured on a set of solutions having $Ab_{S_{494}} = 0.047 \pm 0.04$ and corrected for the amount of BSA present. The dashed line is based on the assumption of equal fluorescence intensity ($z(i) = i^1$). The dotted line is for a simple quenching model ($z(i) = i^0$). The solid line is a guide the eye.

The general trend in this data was ascribed to two processes: trap sites within the FITC population and energy transfer. The self-quenching of FITC is complex. It is known that proteins with many FITCs attached are heavily quenched but these recover in close proximity to a metal surface [215, 216]. However, to our knowledge, previous studies showing this type of behaviour in FITC labelled proteins (and proteins labelled with many other dyes) have been reported for stochastic mixtures rather than proteins labelled with a specific number of fluorophores (c.f.: [211, 212, 215-218]). As a result the behaviour of the molecules with specific numbers of fluorophores is not known.

Similarly, energy transfer in this system is complex. In the FITC-BSA system, R_0 will shift to lower values as the number of FITCs attached increases due to the known spectral shifts observed in solution. Due to the random labelling there will always be a wide range of distances. BSA is well modelled in solution as a triangular prismatic shape $8.4 \times 8.4 \times 8.4 \times 3.2$ nm [219]. Simplifying this to a globular protein 8 nm in diameter [220] and assuming that the 24 dyes evenly distribute over the surface, doubly labelled BSA will contain molecules in which the inter-FITC

distance is between 2.9 and 7.9 nm which brackets R_0 for homo-FRET. Further, over the full range of possible labelled states there are 2^{24} species and simulating all of them is a challenging problem. In general, as the number of labels increases, a concomitant increase in the density of energy transfer partners in close proximity occurs. Since some of those energy transfer partners will be trap sites, the brightness of the FITC labelled BSA will decrease. Based on these prior reports and invoking trap sites and energy transfer the general features in Figure 3.3.1.2 can be rationalized, but a full quantitative description is beyond the scope of the current study.

In the context of interpreting clustering using anisotropy the extent to which the data do not follow the assumption of equal fluorescence efficiency is striking. Based on inspection of Figure 3.3.1.3, z_i appears to follow a model in which $z_i \approx 1$ due to self-quenching processes over a limited range ($f < 0.1$). For $f > 0.1$ the applicability of all of the simple models was limited.

Several approaches to estimating the values of z_i were attempted. Unconstrained fitting of our results to equations 3.2-2 and 3.2-3 is difficult due to the limited data, the smoothness of the functions involved, and the large number of similarly valued parameters. Computed distributions for $f > 0.5$ indicated that species with $i \geq 10$ dominated these solutions. Since these solutions showed no change in normalized intensity, the z_i were assumed to be constant when $i \geq 10$. Unconstrained fitting of the remaining parameters was still unsatisfactory. Neighbouring z_i s differed greatly. A semi-empirical approach was adopted in which the z_i parameters were generated by a 4th degree polynomial over the range $i = 1$ to 10, and constant afterward. These conditions require the parameters to be “smooth” and reasonably continuous. The resulting fit can only be said to be better than existing assumptions. Although useful for guiding the eye, any parameters obtained are approximate. Further work is needed to develop robust estimates of these values for large aggregates and clusters.

The same models were applied to the prediction of measured fluorescence anisotropy (Figure 3.3.1.3). Studies of the depolarization behaviour of FITC:BSA as a function of labelling have been reported [213, 220, 221] but explicit comparisons to theoretical predictions have not, to our knowledge, appeared previously. Although our data cover a wider range of F/P than in previous studies, the measured anisotropy

of the FITC:BSA preparations were consistent with previously reported trends showing lower measured anisotropy as F/P increased [213, 220, 221]. The observed depolarization is due to FITC-FITC homo-FRET for which the R_0 is 4.4 nm [222]. The anisotropy predicted assuming $r_i = r_1/i$ in the equal fluorescence efficiency, simple quenching, and semi-empirical models was compared to the measured data. At low values of f the observed anisotropy is somewhat lower than expected due to the limitations of the assumption ($r_i = r_1/i$). At more experimentally realistic fractional labelling ($f > 0.05$) this assumption appears to hold well. It is clear the results do not correspond to an equal fluorescence intensity model and, based on Figure 3.3.1.3, there would normally be no reason to invoke it. The simple self-quenching model gave a good prediction of the observed results and, in this instance, the greatly increased complexity of the semi-empirical model yielded anisotropy predictions indistinguishable from the simple self-quenching model. The equal fluorescence intensity model under-predicted the anisotropy and if used interpretively would under-estimate the number of clustered fluorophores” [28].

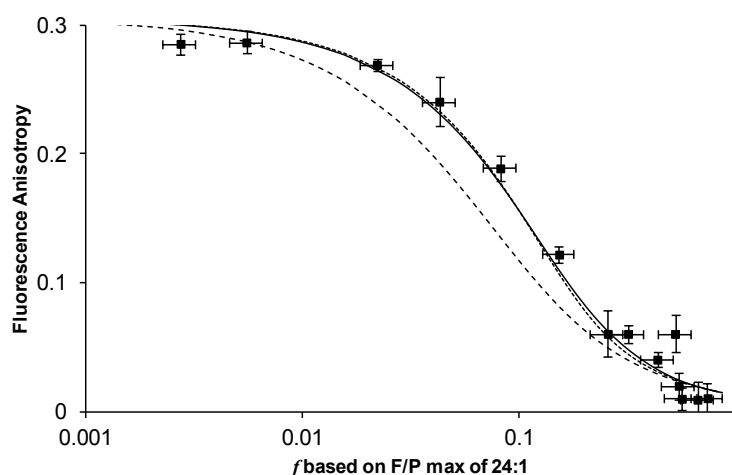


Figure 3.3.1.3: Fluorescence anisotropy of BSA solutions as fractional labelling increased. The dashed line is the predicted behaviour of a system following the assumption of equal fluorescence intensity ($z(i) = i^1$). The dotted line represents the simple quenching model ($z(i) = i^0$). The solid line is a semi-empirical fit primarily to guide the eye.

3.4 Conclusion

Existing widely applied assumptions lead to underestimation of both the predicted anisotropy and the cluster size when interpreting data from fluorophore systems exhibiting self-quenching. The theory presented here has emphasized systems restricted to randomly oriented fluorophores where the inter-fluorophore distance is $< 0.8 R/R_0$. Under these conditions, anisotropy may be readily predicted using models exhibiting enhancement, equal fluorescence, or quenching. The theory, however, can be applied to other cases by invoking the more detailed expressions for r_i provided by Runnels and Scarlata [204]. For the system studied, once the broad behaviour is known, anisotropy can be readily predicted. Variations in anisotropy with f are more easily predicted than is intensity. As noted by earlier workers, the interpretation of anisotropy is greatly enhanced by the availability of complementary data [223]. More detailed knowledge of the photophysical behaviour of fluorophores in clusters will greatly enhance interpretation of cluster size using anisotropy. In particular, the theoretical considerations provided here indicate that discrimination of cluster size is improved by unsaturated subunits (e.g. $f \neq 1$) and by fluorophores that quench. It is also likely that more detailed understanding of different types of clustering is needed: some remain constant in size so that the density of transfer partners increases like the case of BSA-FITC that has been discussed; others grow by adding subunits such that the distance to the next fluorophore remains nearly constant like DNA-fluorescein template directed assembly discussed in chapter 4.

4 Distance Dependent Non-Additivity of Fluorescence Emission and Its Effect on Anisotropy Measurements.

4.1 Introduction

DNA duplexes and four-way Holliday junction are examples of model systems in which the distances between the fluorophores are fixed and known. The system also has the flexibility needed to be designed in different sizes. It also has a known and controllable number of sites that can be labelled with fluorophores.

As explained in section 2.4.2, DNA four-way junctions are made of four single strands of DNA with semi complementary sequences that are bound to each other by a reciprocal single-stranded cross-over and have an antiparallel structure with four duplex arms. In the present study all single stranded four-way junctions were labelled with fluorescein at their 5' end to suit the required experimental objectives.

Existing approaches to modelling the anisotropy of four-way junctions would include the assumption of equal fluorescence efficiency of fluorophores when describing dye binding to subunits of a cluster. According to the assumption, the intensity of a solution of fluorescein labelled DNA molecules would not be expected to change upon induced assembly into four way junctions or bound to template DNA molecules. The Holliday four-way junction system presents a further system to

investigate the behaviour of clustered systems providing good control over distance. The range of distances provided in this model is of particular interest in the context of homo-FRET (figure 1.7.1) as it gives access to the R from 0.8 to $2 R/R_o$ unit.

4.2 Theory

4.2.1 The emission intensity of individual species in stochastic mixtures

The extent of energy migration that is measured by fluorescence anisotropy as a function of fluorophore labelling in clusters larger than dimer can give valuable information on oligomerization state if it is based on realistic assumptions.

Theories previously discussed in section 1.7.1 and 1.7.2 predicted a steady increase of intensity upon fractional labelling, however if fluorophores in close proximity undergo interactions such as self-quenching, it will not be easy to predict the intensity of their stochastic mixtures.

The emission intensities of individual labelled species with 1,2,3,..., N fluorophores, ($I_{\text{mono}}, z_2 \cdot I_{\text{mono}}, z_3 \cdot I_{\text{mono}}, \dots$) in a stochastic mixture can be found as parameters when fitting data using equation 3.2-1. Once intensities of each labelled species in the mixture is known, its anisotropy will be found using equation 3.2-2.

This means that in presence of intensity data, equation 3.2-2 can be used for any stochastic mixtures and will not be restricted to cases where $R/R_o \leq 0.8$.

A set of DNA samples were fractionally labelled with fluorescein-DNA and the applicability of the formula over a range of distances were tested.

4.2.2 Finding effective N in clusters labelled with fluorophores undergoing self quenching

The extent of interactions such as self-quenching and emission enhancement depends on the distance between the dyes, so by assuming that, for example, a triply labelled DNA has an emission that is 3 times as intense as the emission of a singly labelled DNA, the effect of the distance on the interactions of the dyes, is ignored.

The general theoretical model presented by Knox[2], states that in a system with N fluorophores, the probability of finding a molecule i (directly excited by polarized light) in excited state at time t , depends on the energy exchange between all N molecules. However, the fluorescence emission intensity of those N molecules depends on the type and extent of possible interactions that they have.

The theory suggests that when efficiency of energy transfer is high in an N -mer, both directly and indirectly excited fluorophores emit with the same probability and equation 1.7-4 gives the steady state anisotropy of such a system. In that equation it is assumed that in an N -mer 1 fluorophore is directly excited and $(N - 1)$ fluorophores are indirectly excited by polarized light. However, it is known that most dyes in close proximity interact with each other and such interactions either enhance or quench the fluorescence emission (sections 1.9 and 1.10). Therefore, N in equation 1.7.1-4 might give either lower (in case of fluorescence quenching) or higher anisotropy (in case of fluorescence enhancement) than experimental results.

In these cases, N in equation 1.7.1-4 may be replaced with a term that accounts for the behaviour of fluorophores in a cluster of a particular size

Equation 4.2.2-1

$$r_N = r_1 \frac{1 + (R_o/R)^6}{1 + q_N \cdot (R_o/R)^6} + r_{RET} \frac{(q_N - 1)(R_o/R)^6}{1 + q_N \cdot (R_o/R)^6}$$

where q_N is the apparent number of fluorophores in an N -mer.

If a cluster is large and the distance between the fluorophores is too far to let them interact, or the fluorophores do not have the affinity to react with themselves, $q_N = N$, where N is the number of emitting particles in a cluster. If the fluorophores interact, depending on the type of their interaction, then $q_N < N$ or $q_N > N$.

A simple model of $q_N = \rho \cdot N$ may be used to investigate the general behaviour of fluorophores that quench ($\rho < 1$) or enhance ($\rho > 1$) when in close proximity. Such

interactions depend on inter-probe distance (R) and knowledge of R is required to estimate the value of ρ . However, for fluorophores that do not interact with themselves, $\rho = 1$ and $q_N = N$, for all inter-probe distances. For a particular fluorophore with known self-interaction behaviour, ρ can be inversely proportional to inter-probe distances.

In the present study, 11 four-way junctions were labelled with fluorescein. Fluorescein is known to self-quench [22], and the fluorescence anisotropy as a function of cluster size was studied. The anisotropy data were then analyzed using equation 4.2.2-1.

4.3 Results and Discussion

4.3.1 DNA Strands

4.3.1.1 Intensity

As all DNA samples were titrated with the same amount of fluorescein labelled DNA, it was expected (according to the assumption of equal fluorescence emission [1]), that they would have similar intensities and show the same rate of increase with increasing ratio of labelled DNA to DNA template, (figure 4.3.1.1.1, dashed line). However the observations showed that the rate of intensity increase was not as high as predicted by the theory and was not the same for all samples. The theory previously discussed in chapter 1 and developed by equation 3.2-1, predicts a steady increase of intensity upon increasing the fluorescein to DNA ratio, by assuming that e.g. a triply labelled DNA has an emission that is 3 times as intense as the emission of singly labelled DNA. However, as discussed in chapter 3, most dyes in close proximity have some interactions with each other that either quench or enhance their fluorescence emission[28] and fluorescein in particular shows quenching [22].

The measured intensities of most samples in the present work, especially with the F/D ratio above 50%, were below the predicted values (figure 4.3.1.1.1) due to the quenching behaviour of fluorescein molecules in close proximity. However the behaviour of all the samples were not the same and the intensities of the samples

with larger sizes, where the distances between the dyes were more, showed less quenching.

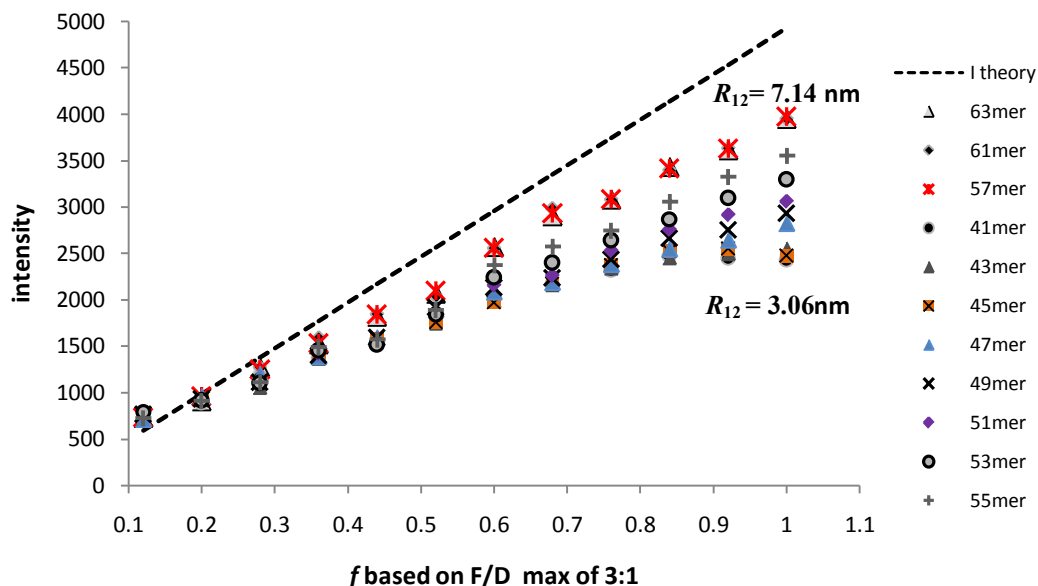


Figure 4.3.1.1.1: Comparison of intensities of 11 samples of DNA upon fractional labelling with fluorescein. The samples with mutual distances (distances between two neighbouring dyes, R_{12}) from ≈ 3.1 nm (●) to ≈ 7.1 nm (×) are shown. All the samples showed almost the same increase of intensity up to $F/D \approx 40\%$. However the intensities of shorter DNA samples increased less than expected with the shortest DNA template (●) showing the least increase upon increasing of F to D ratio. The dashed line shows theoretical intensity, calculated based on the assumption of equal fluorescence efficiency. As the distances between the dyes increased, the behaviour of their intensities became closer to the theory.

The theory presented in chapter 3, equation 3.2.3, was then used to analyze the present data. At each stage of the fractional labelling, the samples were assumed to be a stochastic mixture of differently labelled DNA molecules and the intensity of the samples with 2 or 3 labels were assumed to be a factor of the intensity of mono labelled DNA, $z_2 \cdot I_{mono}$ and $z_3 \cdot I_{mono}$ (equation 4.3.1.1-1, table 4.3.1.1.1). The samples are compared based on the distances between neighbouring dyes (figure 4.3.1.1.2).

Equation 4.3.1.1-1

$$I = 3I_{mono} f(1 - f)^2 + 3z_2 \cdot I_{mono} f^2(1 - f) + z_3 \cdot I_{mono} f^3$$

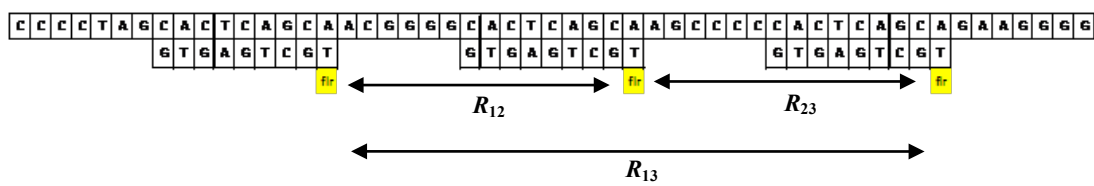


Figure 4.3.1.1.2: An example of a DNA trimer with the gap of 6 nucleotides between the repeating sequences. R_{12} and R_{23} show the distances between two neighbouring dyes and are equal. All 11 constructs were compared based on these distances that were from 30.6 to 7.14nm.

$f \backslash R_{12}, \text{\AA}$	30.6	34	37.4	40.8	44.2	47.6	51	54.4	57.8	64.6	71.4
0.12	729 ± 10	761 ± 17	711 ± 21	715 ± 38	765 ± 22	774 ± 26	794 ± 10	728 ± 12	728 ± 8	710 ± 23	728 ± 25
0.2	889 ± 28	927 ± 10	939 ± 31	959 ± 21	932 ± 16	939 ± 33	915 ± 26	912 ± 11	955 ± 11	940 ± 13	912 ± 16
0.28	1167 ± 12	1057 ± 27	1117 ± 35	1196 ± 9	1111 ± 30	1118 ± 30	1101 ± 37	1109 ± 9	1245 ± 8	1277 ± 15	1276 ± 10
0.36	1373 ± 25	1370 ± 20	1382 ± 4	1395 ± 16	1397 ± 26	1423 ± 11	1456 ± 18	1492 ± 13	1533 ± 20	1594 ± 16	1526 ± 15
0.44	1550 ± 24	1578 ± 31	1576 ± 10	1590 ± 14	1589 ± 28	1546 ± 31	1514 ± 47	1576 ± 12	1841 ± 16	1845 ± 15	1819 ± 15
0.52	1838 ± 12	1749 ± 36	1760 ± 14	1893 ± 12	1920 ± 17	1823 ± 26	1839 ± 8	1892 ± 15	2094 ± 7	2038 ± 11	2071 ± 13
0.6	2036 ± 12	1989 ± 17	1975 ± 25	2086 ± 14	2134 ± 30	2158 ± 21	2241 ± 11	2376 ± 11	2561 ± 17	2561 ± 19	2576 ± 13
0.68	2165 ± 16	2166 ± 22	2170 ± 16	2195 ± 11	2237 ± 24	2263 ± 7	2397 ± 20	2573 ± 10	2931 ± 25	2988 ± 20	2907 ± 62
0.76	2320 ± 23	2346 ± 10	2371 ± 25	2384 ± 7	2436 ± 17	2530 ± 19	2640 ± 14	2751 ± 17	3083 ± 11	3085 ± 9	3085 ± 12
0.84	2479 ± 23	2455 ± 7	2523 ± 8	2555 ± 17	2660 ± 37	2756 ± 24	2872 ± 19	3062 ± 24	3418 ± 15	3401 ± 10	3434 ± 22
0.92	2449 ± 21	2499 ± 28	2551 ± 38	2647 ± 18	2754 ± 19	2915 ± 17	3095 ± 63	3328 ± 23	3631 ± 18	3634 ± 14	3614 ± 37
1	2430 ± 46	2553 ± 25	2476 ± 57	2830 ± 26	2930 ± 23	3061 ± 22	3294 ± 6	3554 ± 20	3974 ± 12	3954 ± 19	3954 ± 37
z_2	1.412	1.351	1.366	1.374	1.377	1.337	1.345	1.41	1.658	1.677	1.653
z_3	1.528	1.582	1.587	1.71	1.786	1.893	2.034	2.193	2.42	2.409	2.413

Table 4.3.1.1.1: Emission intensities of fluorescein labelled DNA samples. The values for emission intensities were averaged out 3 measurements. The binomial distribution formula (equation 4.3.1.1-1) was used to analyze the data and the fitted parameters were the intensity of mono labelled templates, z_2 and z_3 . The values of the two latter parameters were different for different samples and are shown in table.

The fitted parameters of z_2 and z_3 were different for different samples. The values of these two parameters increased as the size of the oligonucleotides got larger and z_2 and z_3 became closer to the theoretical values of 2 and 3 respectively. This observation showed that in close proximity the interaction of the dyes were more effective and experimental data showed more deviation from the old theory at this level.

Although the values of z_2 and z_3 increased with increasing distance, they levelled off below these values (table 4.3.1.1.1, figure 4.3.1.1.3). Other mechanism of quenching, rather than local concentration (distance dependent) might be the reason for such behaviour.

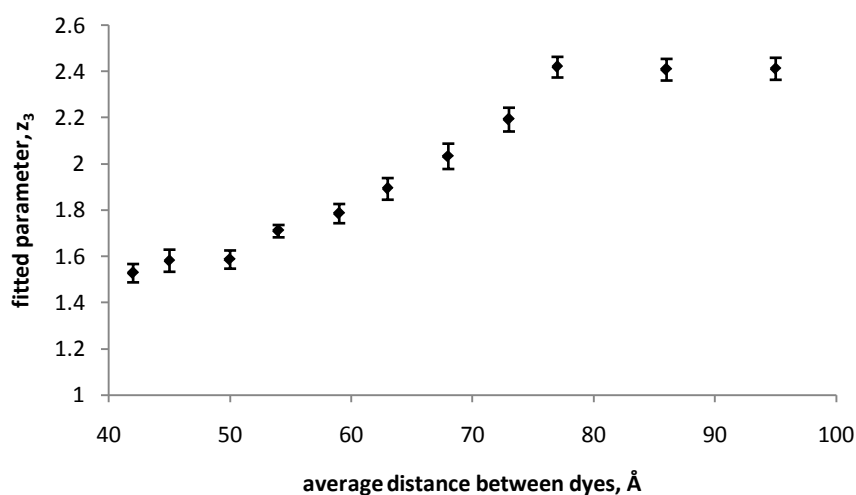


Figure 4.3.1.1.3: Comparison of the values of the fitted parameter, z_3 , for samples with different distances between dyes and consequently different extent of self quenching. Although the factor showed an increase as the distance increased it did not get the theoretical values of three.

4.3.1.2 Anisotropy

Anisotropies of the sample showed the expected trend of decrease over increasing fractional labelling. However the trend got less obvious as the distance between the neighbouring dyes increased (table 4.3.1.2.1, figure 4.3.1.2.1).

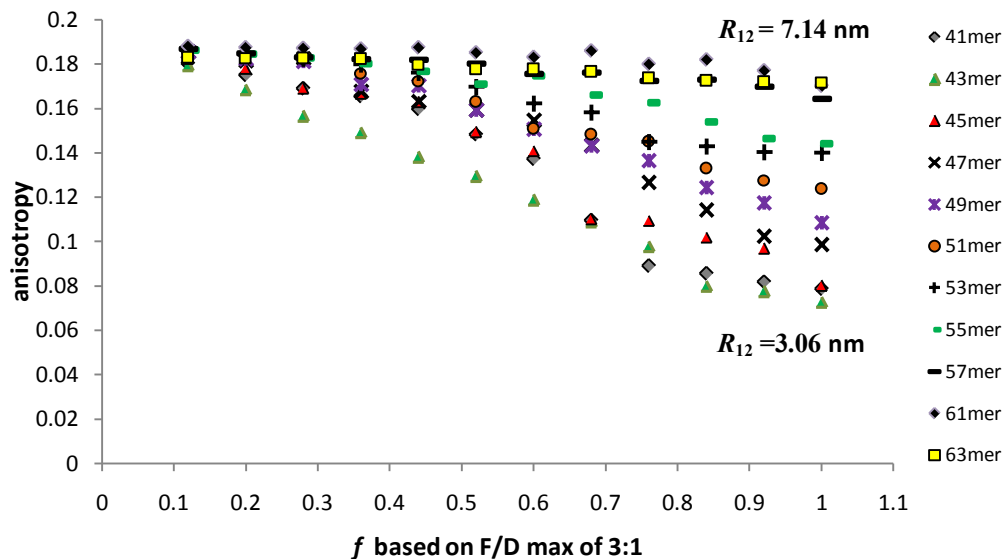


Figure 4.3.1.2.1: Comparison of anisotropies of the set of 11 different samples. All the measurements were done on the samples that were left in -20°C freezer for a couple of hours.

To avoid the reduction in anisotropy caused by molecular tumbling that can interfere with homo-FRET studies and to make sure that all fluorescein labelled DNA molecules were fused to DNA templates, samples were left in -20°C freezer for a couple of hours, and the measurements were done right after the samples were taken out of the freezer.

<i>f</i>	30.6	34	37.4	40.8	44.2	47.6	51	54.4	57.8	64.6	71.4
0.12	0.1708±0.001	0.1804±0.001	0.1824±0.004	0.1856±0.002	0.1856±0.005	0.1856±0.003	0.1862±0.001	0.1863±0.004	0.1984±0.004	0.1881±0.004	0.1829±0.001
0.2	0.1686±0.001	0.175±0.002	0.178±0.001	0.1817±0.001	0.1824±0.004	0.1843±0.005	0.1843±0.003	0.1845±0.005	0.198±0.005	0.1874±0.005	0.1827±0.001
0.28	0.1566±0.001	0.1691±0.001	0.1691±0.002	0.1826±0.001	0.1812±0.001	0.1824±0.001	0.1824±0.001	0.1829±0.005	0.1948±0.005	0.1872±0.005	0.1825±0.003
0.36	0.1493±0.001	0.1657±0.001	0.1667±0.001	0.1678±0.002	0.1708±0.001	0.1758±0.004	0.1798±0.003	0.1803±0.004	0.1966±0.004	0.187±0.004	0.1822±0.001
0.44	0.1381±0.002	0.1599±0.001	0.1629±0.002	0.1633±0.001	0.1703±0.002	0.1723±0.005	0.1761±0.003	0.1767±0.003	0.1946±0.003	0.1876±0.003	0.1798±0.006
0.52	0.1295±0.001	0.1484±0.001	0.1494±0.001	0.1593±0.002	0.1593±0.004	0.1629±0.001	0.1698±0.003	0.1708±0.003	0.1908±0.003	0.1852±0.003	0.1777±0.005
0.6	0.1189±0.001	0.1372±0.001	0.1409±0.003	0.1547±0.001	0.1508±0.005	0.1508±0.002	0.1624±0.002	0.1747±0.002	0.184±0.002	0.1832±0.002	0.1776±0.007
0.68	0.109±0.001	0.1096±0.001	0.1102±0.002	0.1434±0.001	0.1433±0.003	0.1483±0.001	0.1583±0.002	0.1661±0.001	0.1838±0.001	0.1861±0.001	0.1765±0.001
0.76	0.0979±0.002	0.0891±0.001	0.1095±0.004	0.1267±0.001	0.1367±0.004	0.1451±0.001	0.1451±0.004	0.1625±0.004	0.1747±0.004	0.1801±0.004	0.1736±0.001
0.84	0.08±0.001	0.0858±0.002	0.102±0.001	0.1145±0.001	0.1245±0.004	0.1329±0.001	0.1429±0.004	0.1538±0.015	0.1724±0.015	0.1821±0.015	0.1724±0.001
0.92	0.0775±0.001	0.0821±0.002	0.097±0.001	0.1025±0.002	0.1175±0.001	0.1276±0.001	0.1404±0.003	0.1463±0.015	0.1709±0.015	0.1771±0.015	0.172±0.007
1	0.0728±0.002	0.0788±0.002	0.0801±0.002	0.0987±0.002	0.1087±0.004	0.1237±0.003	0.1402±0.001	0.1442±0.014	0.1646±0.014	0.1701±0.014	0.1718±0.005

Table 4.3.1.2.1: Anisotropies of 12 stages of fractional labelling of 11 samples. The results shown here are averages of the results of 3 measurements

Fitted parameters of emission and z_i were used to fit the data and the anisotropies of individual species, r_1 , r_2 , r_3 were calculated for all samples (equation 4.3.1.2-1):

Equation 4.3.1.2-1

$$r(f, 3) = \frac{3 \cdot f(1-f)^2 r_1 + 3 \cdot z_2 \cdot f(1-f)^2 r_2 + z_3 \cdot f(1-f)^2 r_3}{3 \cdot f(1-f)^2 + 3 \cdot z_2 \cdot f(1-f)^2 + z_3 \cdot f(1-f)^2}$$

R_{12} , nm	3.06	3.4	3.74	4.08	4.42	4.76	5.1	5.44	5.78	6.46	7.14
r_1	0.1884	0.1939	0.1927	0.1923	0.1901	0.1918	0.1936	0.1857	0.1867	0.1856	0.1848
r_2	0.0991	0.1205	0.1342	0.1636	0.1591	0.1569	0.1675	0.1853	0.1822	0.1953	0.1783
r_3	0.0713	0.0714	0.081	0.0935	0.109	0.1231	0.1356	0.1433	0.1662	0.1727	0.171

Table 4.3.1.2.2: Anisotropies of singly labelled, r_1 , doubly labelled, r_2 , and triply labelled, r_3 , DNA trimers. r_1 , r_2 , r_3 were fitted parameters using equation 4.4.1.2-1 and information (z_2 , z_3) obtained from intensity measurements.

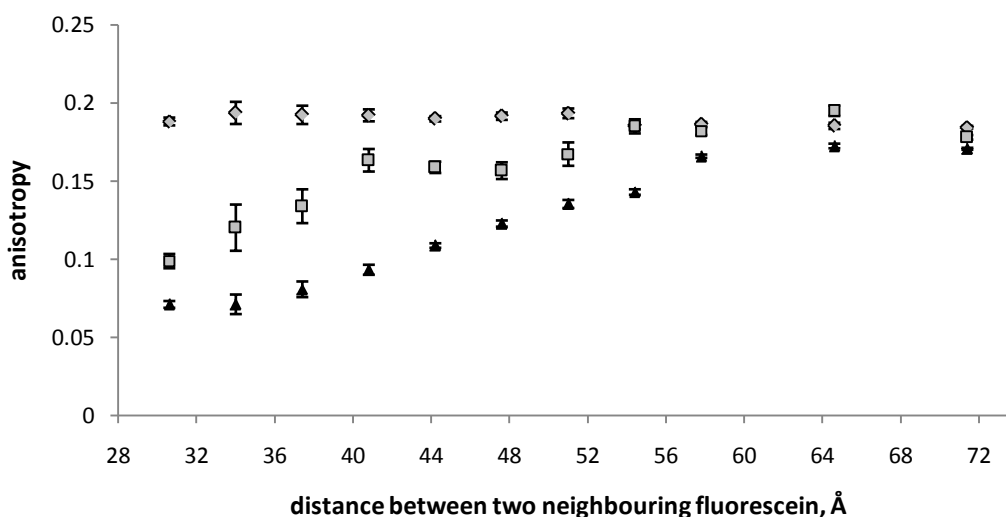


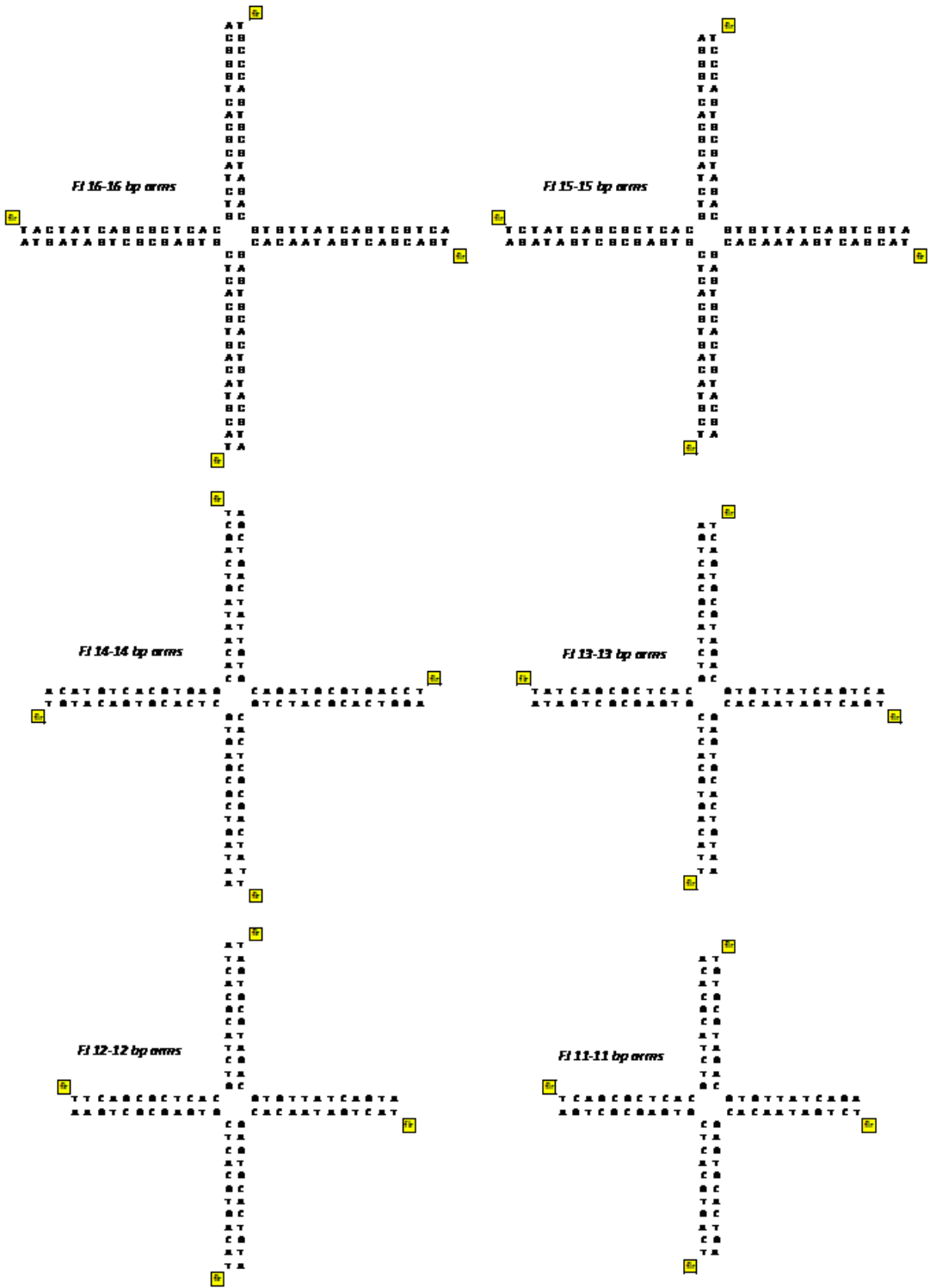
Figure 4.3.1.2.2: Comparison of 3 fitted parameters of data analysis: r_1, r_2, r_3 that show the anisotropies of different constructs with different numbers of labels: one label, r_1 , (◆), two labels, r_2 , (■) and three labels, r_3 , (▲).

Anisotropy of the mono labelled DNA templates of all samples were almost the same, indicating that at low temperatures that molecular motions are less, differences in molecular weights do not make a noticeable change in fluorescence. The anisotropies of doubly labelled samples however, were lower for smaller construct because of higher chance of resonance energy transfer. The trend of increase was less obvious than that of triply labelled species (r_3) because r_2 was an average of anisotropies of two forms of doubly labelled species, 66% with the distance of R_{12} (or R_{23}) between the fluorophores and 33% with the distance of R_{13} .

If anisotropies of partly labelled species are known, their inter-probe distances that are either the distance between the reacting sites of a template structure or the distances between the subunits of a cluster, will be known.

4.3.2 Four-way junctions

Four-way junctions were generated as a model system to study homo-FRET at varying distances (figure 4.3.2.1). A series of 11 sets of labelled oligonucleotides that differed by only two nucleotides, 12 to 32 mers spanning the range, (figure 2.6.5.1) were prepared and their emission anisotropy measured (figure 4.3.2.1).



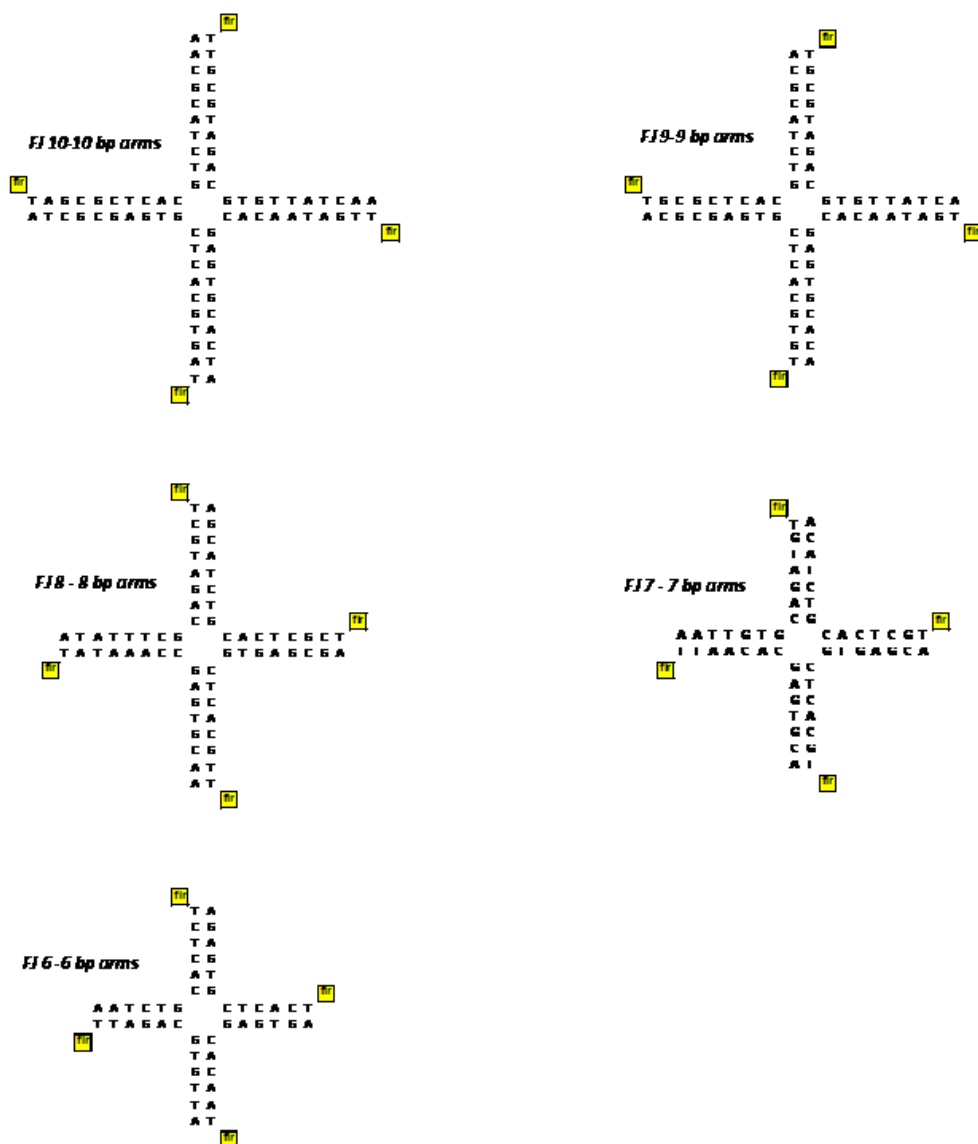


Figure 4.3.2.1: Structures of 11 fluorescein-labelled four-way junctions

The results presented in figure 4.4.2.1 and table 4.4.2.1 revealed that a change of two nucleotides in length didn't influence the anisotropy of the molecule. The anisotropies of the unassembled oligonucleotides were only slightly different from each other. Upon hybridization and formation of four-way junctions, the anisotropy increased as might be expected as the mass of the junctions increased four times relating to unassembled oligonucleotides. However, the increasing trend was not constant for all junctions, was less for smaller junctions and reversed for FJ6. By considering the fact that formation of junctions may bring the fluorescein molecules into a range for excitation energy transfer, the trend can be explained. In the case of a

small junction with an arm length of 6 base pairs (FJ6), where the homo-FRET efficiency was approximately 90%, the anisotropy decrease compare to oligonucleotides (table 4.3.2.1 and figure 4.3.2.2).

junction	anisotropy	oligonucleotide	anisotropy
FJ 16	0.0781 ± 0.0007	32-mer	0.0623 ± 0.0039
FJ 15	0.075 ± 0.0008	30-mer	0.0583 ± 0.0049
FJ 14	0.0739 ± 0.0015	28-mer	0.0575 ± 0.0047
FJ 13	0.0720 ± 0.0010	26-mer	0.0563 ± 0.0032
FJ 12	0.0715 ± 0.0007	24-mer	0.0558 ± 0.0030
FJ 11	0.0696 ± 0.0021	22-mer	0.0555 ± 0.0027
FJ 10	0.0664 ± 0.0015	20-mer	0.0538 ± 0.0037
FJ 9	0.0636 ± 0.0017	18-mer	0.0528 ± 0.0013
FJ 8	0.0575 ± 0.0022	16-mer	0.0520 ± 0.0026
FJ 7	0.0490 ± 0.0013	14-mer	0.0485 ± 0.0028
FJ 6	0.0433 ± 0.001	12-mer	0.0490 ± 0.0021

Table 4.3.2.1: Anisotropies of oligonucleotide were measured before and after hybridization

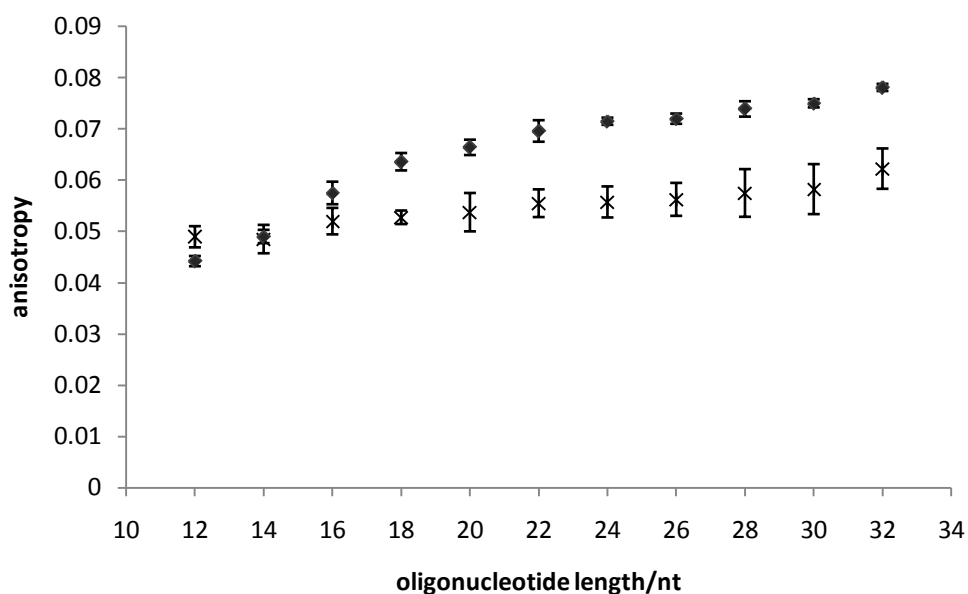


Figure 4.3.2.2: The anisotropies of free oligonucleotides of the lengths 12 to 32 nucleotides long (*) and the resulting four-way junctions, FJ6 to FJ16 (◆); There was a slight change in anisotropy with the change in the molecular weight of the oligonucleotides. Fluorescence anisotropy increased when 4 oligonucleotides joined to form junctions; however such increases were modified for the smaller junctions due to the high possibility of energy transfer between the dyes on the arms. The anisotropies of oligonucleotides were averaged out of the anisotropies of four different strands.

To confirm homo-FRET, the anisotropy measurements were repeated on frozen samples where rotational diffusion and the consequent depolarization were reduced. All four-way junctions were left in a -30°C freezer (in 384-well plates) for a couple of hours and the anisotropies immediately measured 24 times over a period of 17 minutes and 30 seconds, during which they thawed. Freezing the samples was done to minimize rotational diffusion and its consequent effect on anisotropy. The same trends observed at room temperature, existed at low temperatures when rotational diffusion was minimized. At both temperatures the anisotropy of the small junctions was below those of the longer constructs and varied according to their different FRET efficiencies. This suggests homo-FRET to be length-dependent depolarization. It was also obvious that when FRET efficiency became low for larger constructs, the anisotropy converged at both very low temperatures and room temperature showing that the slight increase in size did not change the rotational correlation times considerably (figure 4.3.2.2).

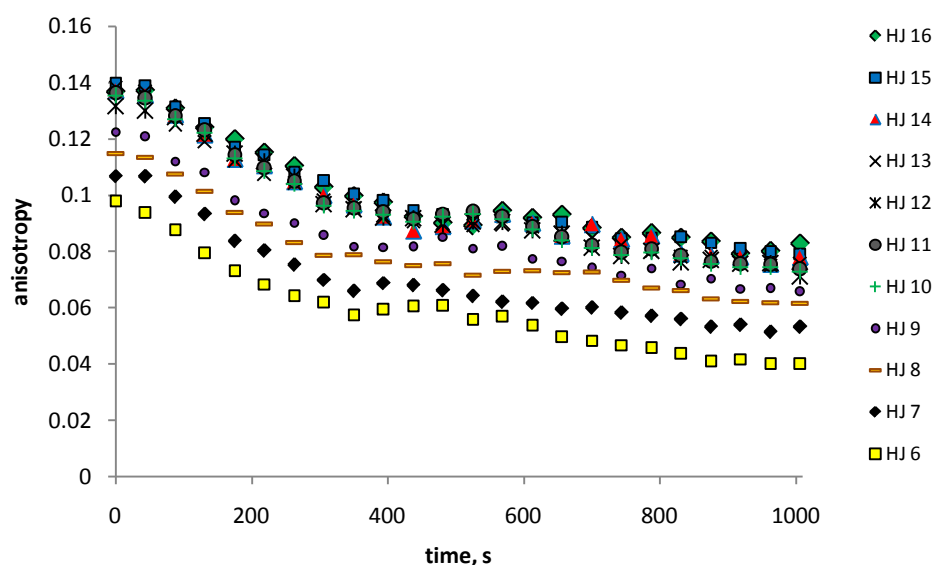


Figure 4.3.2.2: The graph shows the anisotropy change of 11 four-way junction samples upon temperature changes from approximately -30°C to room temperature during 24 measurements, over 1006 seconds. Sample \square has the arm length of 6 bp and the FRET efficiency of approximately 92%. Homo-FRET depolarizes the emission of the samples with higher FRET efficiencies even when they are frozen. Data set \blacklozenge , $-$, \bullet belong to junctions with arm length of 7, 8 and 9 bp and FRET efficiency of 86, 61 and 49% respectively and their anisotropies were different on this basis. For the rest of the junctions, where FRET efficiencies were below 30%, anisotropies were not very different from each other as the main variable was the viscosity of the water that was changing during the course of the time and temperature changing.

Another way to verify the occurrence of energy transfer in the junctions is by titration with magnesium ion. In the presence of positive metallic ions, junctions fold into the stacked X-structure[164]. Different amounts of buffer solution containing magnesium ions were added to FJ6 and FJ16 and their anisotropy measured (figure 4.4.2.3). The addition of Mg^{2+} ion was expected to gradually change the conformation to the folded form, bringing the arms closer together. Mg^{2+} did not influence the efficiency of the energy transfer in FJ6, as the distance between the fluorescein molecules was approximately 3.4 nm (<0.8 of R/R_0) [23]. In FJ16, however, the fluorescein molecules were initially farther apart and upon folding of the arms, they, two by two, allowing energy transfer. From junction folding as a function of magnesium concentration was observed as a reduction in anisotropy ascribed to increased energy transfer (table 4.3.2.2 and figure 4.3.2.3).

[Mg]²⁺, (μM)	FJ 16	FJ 6
0	0.0742 ± 0.0006	0.0422 ± 0.0003
10	0.0728 ± 0.0005	0.0417 ± 0.0008
20	0.0722 ± 0.0003	0.0433 ± 0.0005
30	0.0706 ± 0.0002	0.0416 ± 0.0002
40	0.0698 ± 0.0001	0.0431 ± 0.0004
50	0.0698 ± 0.0005	0.0414 ± 0.0005
60	0.0654 ± 0.0003	0.0409 ± 0.0002
70	0.0637 ± 0.0004	0.0418 ± 0.0002
80	0.0634 ± 0.0002	0.0421 ± 0.0002
90	0.0617 ± 0.0002	0.0416 ± 0.0001
100	0.0619 ± 0.0003	0.0441 ± 0.0001
110	0.0596 ± 0.0008	0.0415 ± 0.0002

Table 4.3.2.2: Anisotropies of FJ6 and FJ16 at different salt concentrations.

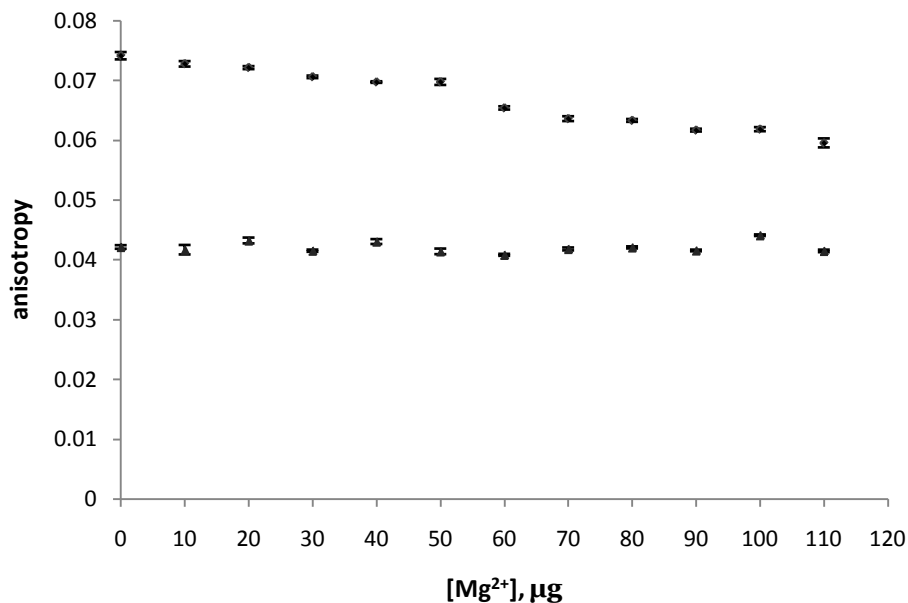


Figure 4.3.2.3: Anisotropy of FJ16 decreased upon titration with magnesium chloride solution. As concentration of Mg^{2+} FJ16 increased the junction folded more and energy transfer between the dyes happened more efficiently. In FJ6 however progression of folding did not change the energy transfer efficiency as the distance between the dyes was already less than $0.8 R_0$. All the measurements were done within 10 minutes after salt addition[155].

4.3.3 Distances

In a square planar structure (figure 4.3.3.1), the mutual distance of the dyes on the two sides (c, b) is less than the distance along the diameter (a). However where the size of the junctions allows the mutual distances of the dyes to be less than $0.8 R/R_0$, (e.g. in FJ6 and FJ8,) these differences would not be distinguished as the anisotropy would stay constant (equation 1.7-4) [23]. In larger junctions, the dyes do not interact equally along different distances and the difference in efficiency of energy transfer between mutual dyes would change the probability of energy transfer.

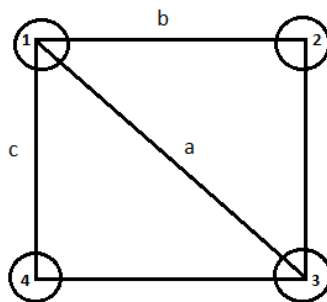


Figure 4.3.3.1: In smaller junctions $R/R_o < 0.8$ the difference between the efficiencies of energy transfer through sides ($1 \rightarrow 2$, $1 \rightarrow 4$) and through diameter ($1 \rightarrow 3$) is negligible. For FJ9 to FJ16, where the mutual distances of the dyes were beyond $0.8R_o$, FRET efficiencies along the sides and diameter were considerably different; e.g. For FJ16 the energy transfer was approximately 8 times less efficient through the diameter.

4.3.4 Self-quenching

4.3.4.1 Intensity

All the fluorescein labelled oligonucleotide samples were prepared with the same concentration ($25\mu\text{M}$) and their emission intensities measured before and after making four-way junctions. The emission intensities of the free oligonucleotides were similar, but the resulting four-way junctions showed variable emission intensities with the shortest showing signs of quenching. The intensities of four-way junctions were generally lower than the intensities of the labelled oligonucleotides; however, there was a gradual increase in intensity with the increase in size of the junction (figure 4.3.4.1.1).

This may be understood if upon hybridization, the fluorescein molecules local environment changed. In the new arrangement, the fluorescein molecules were closer to each other allowing the possibility of self-quenching and, consequently, they showed behaviour deviating from assumption of equal fluorescence efficiency[23]. The local concentrations were higher in smaller four-way junctions; where the arms were short and the proximity of the dyes was able to facilitate self-quenching. It was assumed that in FJ16, where the average inter-probe distance was approximately 8.8 nm, there was almost no self-quenching. As a result its emission intensity was very close to that of free oligonucleotides. The same fluorescence intensity was expected for all other junctions in the absence of self-quenching (table 4.3.4.1.1).

junction	intensity	oligonucleotide	intensity
FJ 16	34970 ± 859	32-mer	35142 ± 361
FJ 15	34469 ± 476	30-mer	34877 ± 219
FJ 14	33907 ± 1048	28-mer	35449 ± 316
FJ 13	33243 ± 532	26-mer	34923 ± 526
FJ 12	31680 ± 948	24-mer	34623 ± 791
FJ 11	30826 ± 692	22-mer	35451 ± 469
FJ 10	30569 ± 508	20-mer	34472 ± 437
FJ 9	30409 ± 828	18-mer	34835 ± 831
FJ 8	30131 ± 808	16-mer	34522 ± 699
FJ 7	29578 ± 618	14-mer	34292 ± 418
FJ 6	25439 ± 1056	12-mer	35383 ± 629

Table 4.3.4.1.1: Fluorescence intensities of free oligonucleotides and their resulting four-way junctions were measured at the same PMT gain of 50. The results were averaged out of six measurements.

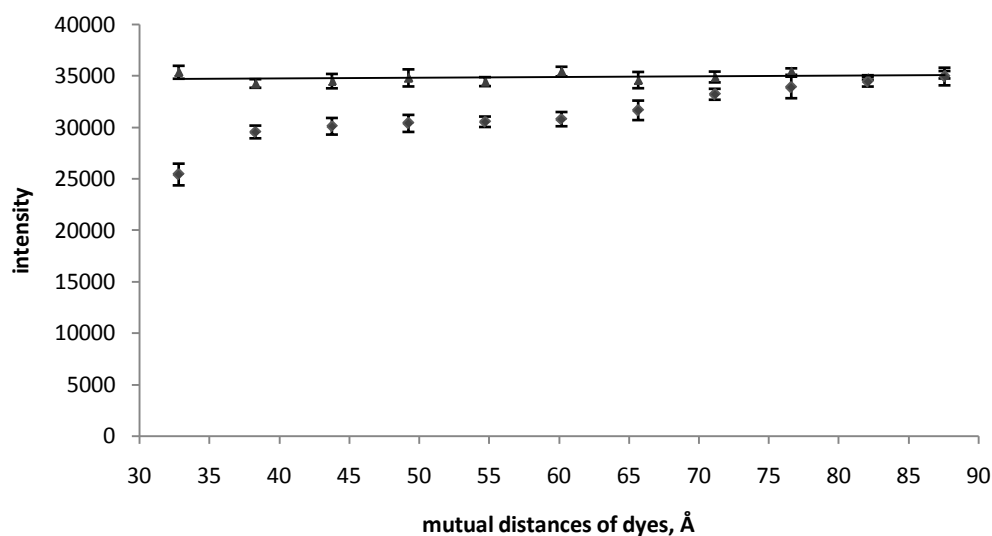


Figure 4.3.4.1.1: Comparison of fluorescence emission intensities of fluorescein labelled DNA molecules before (▲) and after (◆) generating four-way junctions. In spite of having equal molar concentrations and the same number of dyes per clusters, fluorescence emission intensities did not match. The intensities increased as the average mutual distance of fluorescein molecules increased from FJ6, 3.3 nm to FJ16, 8.8 nm, (◆) because the local dye concentration got less as molecules got bigger and self-quenching occurred less. It was assumed that for FJ16 there was no self-quenching and the intensity was assumed to be the expected fluorescence intensity in the absence of self-quenching for all other samples, because its intensity was approximately the same fluorescence intensity as free oligonucleotides (▲).

4.3.4.2 Fitting anisotropy data

To fit the anisotropy data to theory based on the assumption of equal fluorescence efficiency, equation 1.7.1-4 may be used. For all data points $r_1 = 0.077$ and $r_{et} = 0.016$ and R was the average distance between fluorescein molecules in each four-way junction. As described in chapter 3, when interpreting anisotropy data, self-quenching might cause misinterpretation of the cluster size by underestimating the number of labelled subunits, N .

In anisotropy measurements in junctions the same inconsistency was observed. While all the junctions had four labelled arms ($N = 4$), the theoretical model of $N = 2$ gave a better fit (figure 4.3.4.2.1). It seemed as if due to self-quenching the number of emitting dyes became less and anisotropy did not decrease as much as predicted by theory.

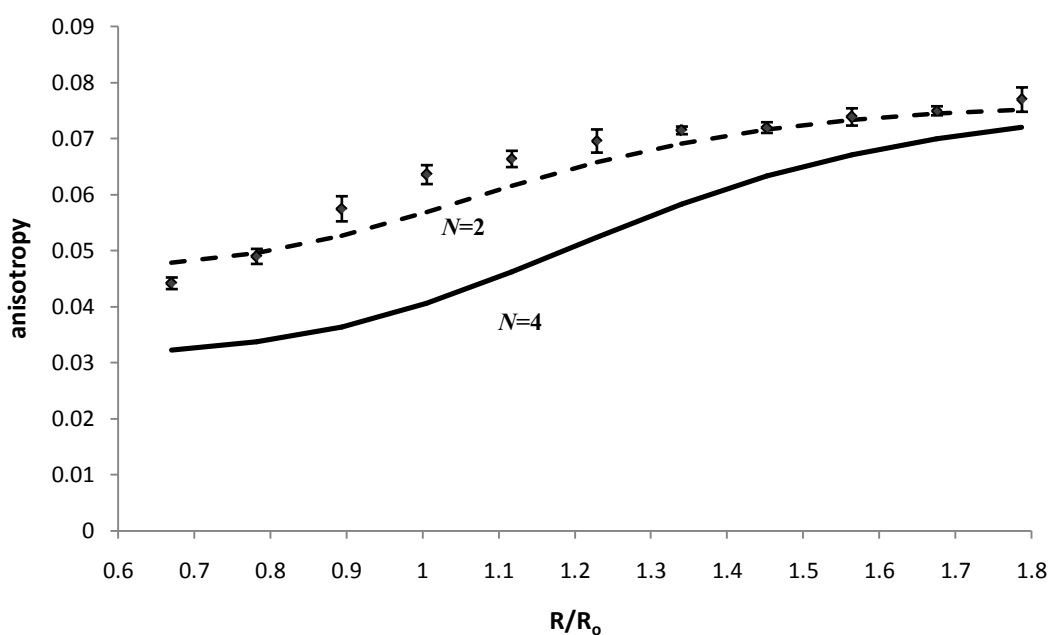


Figure 4.3.4.2.1: Direct comparison, based on equation 1.7.1-4, $N=4$ (solid line), $N=2$ (dashed line) and the anisotropy data (\blacklozenge). For both simulations $r_1 = 0.077$, $r_{RET} = 0.016$, R was the average distance between fluorescein molecules (square planar model). It seemed as if the theory predicts the cluster to be a dimer rather than a tetramer. Self-quenching caused the contribution of the dark fraction to decrease the apparent N to 2. As the value of the anisotropy of fluorescein is low it can be assumed that that κ^2 and R_0 have the same values for all the fluorescein on all the four-way junctions [164].

Such inconsistencies were expected to be more obvious for smaller junctions, where self-quenching was more probable.

The issue might be due to the fact that in the formula based on the assumption of equal fluorescence efficiency (equation 1.7-4) for a cluster with 4 labelled subunits, N is equal to 4 for all clusters independent of their size or distance between fluorophores. The theory does not predict interactions between clustered fluorophores resulting in brightness changes and therefore under-predicts the anisotropies, similar inconsistencies have been reported before [28]. As the sizes of the junctions increased, self-quenching became less probable and the difference between results and the theoretical model became less (figure 4.3.4.2.1).

Therefore equation 1.7-4 was modified by a term accounting for the behaviour of the fluorophores in a cluster of a particular size, and was rewritten as equation 4.2.2-1. The equation was then used to fit the data (figure 4.3.4.2.2). The ratio of R/R_o was used to estimate q_N because these two values seemed to be directly proportional, the shorter the distance the more effective the interaction. It was assumed that q_N changed with R/R_o and the empirical values for q_N were calculated (table 4.3.4.2-1). The distance ratios increased by the absolute value of 0.114 from one junction to the next.

arm, bp	R _{sides} , nm	R _{diameter} , nm	R _{average} , nm	R/R ₀	E%	q _N	r _{theory}	r _{experiment}
6	2.88	4.08	3.28	0.67	91.7	2.883	0.0388	0.0442 ± 0.001
7	3.37	4.76	3.83	0.782	81.4	2.995	0.0405	0.0490 ± 0.0013
8	3.85	5.44	4.38	0.893	66.3	3.107	0.0436	0.0575 ± 0.0022
9	4.33	6.12	4.92	1.005	49.2	3.218	0.0482	0.0636 ± 0.0017
10	4.81	6.8	5.47	1.117	34	3.33	0.0538	0.0664 ± 0.0015
11	5.29	7.48	6.02	1.228	22.5	3.442	0.0595	0.0696 ± 0.0021
12	5.77	8.16	6.57	1.34	14.7	3.553	0.0646	0.0715 ± 0.0007
13	6.25	8.84	7.11	1.452	9.6	3.665	0.0685	0.0720 ± 0.0010
14	6.73	9.52	7.66	1.563	6.4	3.777	0.0713	0.0739 ± 0.0015
15	7.21	10.2	8.21	1.675	4.3	3.888	0.0733	0.075 ± 0.0008
16	7.69	10.88	8.76	1.787	3	4	0.0747	0.077 ± 0.0022

Table 4.3.4.2.1: The theoretical model with the q_N values, calculated based on increasing R/R_0 to fit the measured anisotropy of a set of 11 four-way junctions. The base length of 0.34 nm is considered when calculating R_s . Distances between the dyes increased by 0.112 nm and the distance-dependent self-quenching decreased with the same rate.

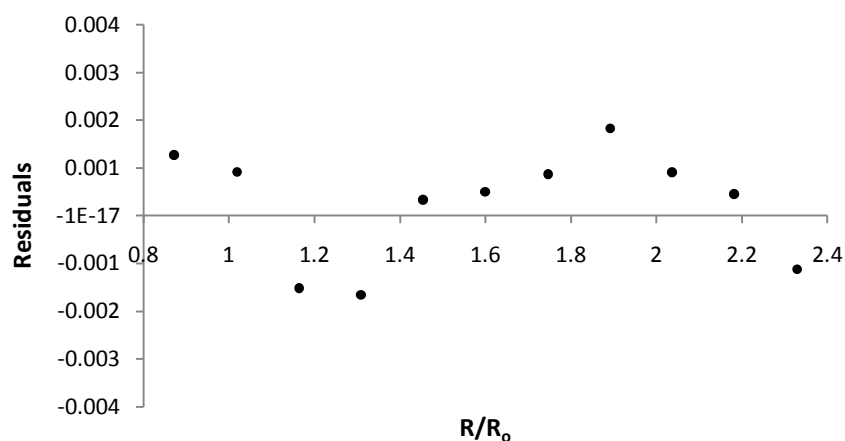
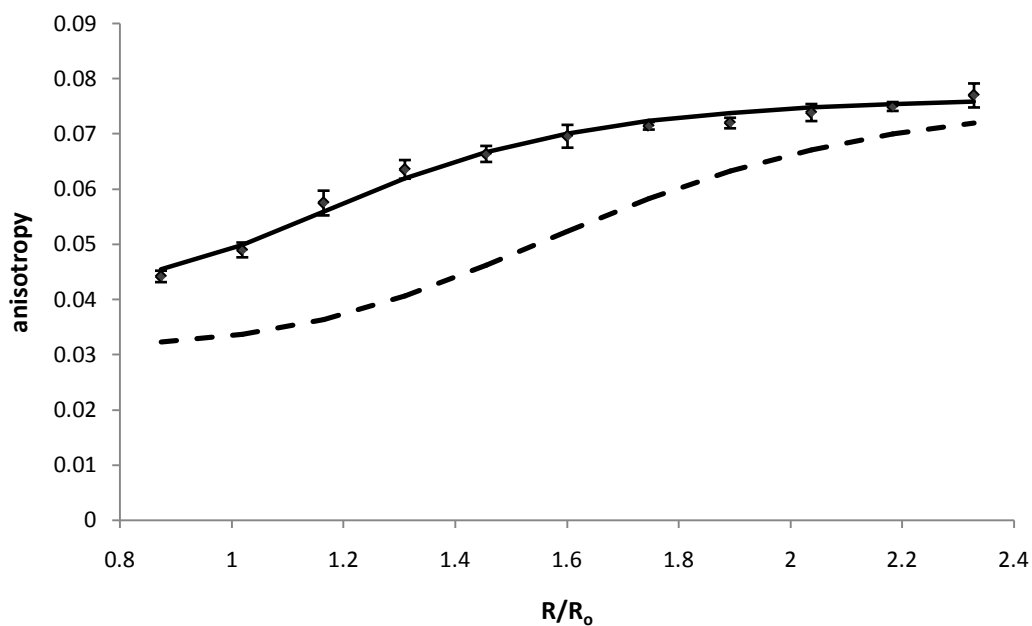


Figure 4.3.4.2.2: Comparison of two different fits. Theoretical fit,(dashed line), based on equation 1.7.1-4 with $N = 4$, and fit based on equation 4.2.2-1,with varying q_N , (solid line). R_0 was the parameter to fit the data and its final value was solved as 3.76 nm.

The parameter to fit was R_0 as the value of R_0 is not constant and may vary if the quantum yield of the fluorophore changes in different compounds [66]. The fitted R_0 of the empirical fit in figure 4.3.4.2.2 was approximately 3.76 nm. Based on the fitted R_0 , table 4.3.4.2.1 was rewritten as follows (table 4.3.4.2.2):

arm, bp	(R/R ₀)	E%	q_N	r_{theory}
6	0.873	69.3	2.54	0.0388
7	1.019	47.2	2.69	0.0405
8	1.164	28.7	2.84	0.0436
9	1.31	16.5	2.98	0.0482
10	1.455	9.5	3.13	0.0538
11	1.601	5.6	3.27	0.0595
12	1.746	3.4	3.42	0.0646
13	1.892	2.1	3.56	0.0685
14	2.037	1.4	3.71	0.0713
15	2.183	0.9	3.85	0.0733
16	2.328	0.6	4	0.0747

Table 4.3.4.2.2:Parameter q_N recalculated according to the new R_0 . The values of the parameters were slightly less than what estimated before. The difference became less as the size the junctions increased.

Methods based on distance-dependent fluorescence self-quenching, as a function of local concentration, have been widely used to study swelling or shrinking of cells upon water volume changes. Fluorophores have been injected into the cells and the extent of their fluorescence intensity as function of cell volume investigated [224-226]. To show the applicability of DNA origami as a well-controlled scaffolding material, photofunctional origami nanoclusters have been designed and quenching behaviour of Cy5 in the proximity of gold nanoparticles is observed and it is shown that gold nanoparticles exhibit measurable quenching effects. The dyes are spaced to have mutual distances of 5 nm to 100 nm and effective quenching up to 22 nm is shown[227].

The intensity data can also be used in similar cases to find an empirical fit for the data. In these cases the ratio of the emission intensity of each species to the total intensity (without quenching) can be calculated and the ratio can be used as a correction factor for N .

The interaction of the dyes influences the fluorescence intensities of individual dyes. Such interactions, either fluorescence quenching or enhancement, are stronger when the dyes are in close contact, N should be regarded as a relative rather than an absolute concept. In the examined series of four-way Holliday junctions, as the inter-probe distances increased, dyes interaction, quenching, became less and the value of q_N got closer to 4.

4.4 Conclusion

The proposed model gives a general formula for the existing theory [23] and will be useful to quantify clusters using homo-FRET, especially if the assumption of fluorescence additivity in clusters does not apply, either due to self-quenching or emission enhancement.

Self-quenching is a concentration (distance) dependent phenomenon and its extent shows how closely the fluorophores are packed in clusters. Self quenching causes misinterpretation of the cluster size by underestimating the number of labelled subunits, N [28]. The correction factor, q_N , introduced here, has been applied in the present study to correct for the dark fraction of the dyes after self-quenching and its value, was estimated based on the distances of fluorophores.

5 Conclusion

Fluorescence anisotropy is widely applied to study aggregate formation in living cells [228]. There are a number of well applied theories [1, 2, 23, 24] to quantify cluster sizes. The theories are based on a number of assumptions and are restricted to randomly oriented fluorophores with “equal fluorescence efficiency”. The assumption states that the emission behaviour of dyes in close proximity with other fluorophores of the same type is the same as the free dyes, so to predict the intensity of a cluster of n fluorophores, the intensity of a single emitting unit can be multiplied by n . This assumption simplifies descriptions of anisotropy behaviour of clusters and the anisotropy trends as the fractional labelling of the cluster changes. However it is well understood that fluorescent dyes, if their mutual distance allows, interact with themselves and such interactions either enhance or quench their emissions [22] so in any of these cases the intensity of the fluorophore would not follow the additivity assumption of the theory.

Although self-quenching of fluorescein in clusters of labelled melittin has been observed and discussed by Runnels and Scarlata, its effect on cluster quantification has not been considered when analyzing anisotropy data [23].

If dyes, in close proximity, show quenching behaviour, the intensity of the ensemble would be less than expected. Such an inconsistency causes the anisotropy to be under-predicted and the size of the cluster to be under-estimated. On the other hand if the intensity of the fluorophores is enhanced, the size of the cluster would be overestimated.

The anisotropy of multi-labelled clusters is determined by the extent of energy transfer (homo-FRET) which in turn is a function of the number of the fluorophores and the distance between them. Although the distance dependency of resonance energy transfer is well described and well tested, there has been no consistent picture about how the distance may influence other interactions such as emission enhancement or self quenching of the dyes which in turn determines the effective or apparent N .

Intensity measurements of multi-labelled clusters reveal the type of interaction that takes place between the dyes. The theory presented here can use the information obtained from intensity data to analyze anisotropy data of multiply labelled systems, with the assumption that the fluorophores are randomly oriented. Information obtained from intensity measurements can be used to a) find effective $N(q_N = \rho \cdot N)$ that is particularly important in small clusters where the distance between the fluorophores allow interaction such as self quenching, b) find out the intensity of singly, doubly, triply, ... labelled species in stochastic mixtures, that depending on the photophysics of the dye might be greater than, less than or equal to $i \cdot I_{\text{mono}}$, ($i=1,2,3,\dots$).

For a cluster of a particular size that has undergone fractional labelling, if fluorescence intensity data of the stochastic mixture of each stage of labelling is present, the intensity of differently labelled species can be determined as fitted parameters. By knowing the intensity of differently labelled species in a stochastic mixture the study of the anisotropy of the system becomes possible, the anisotropy of the individual species in the stochastic mixture can be found and the study will not be restricted to cases where $R/R_0 < 0.8$.

The anisotropy data of the individually labelled species can then be used to figure out the distance between the dyes and their relative orientations.

The theoretical models are used to analyze the anisotropy data of FITC labelled BSA. As FITC molecules undergo quenching when in proximity, the existing theoretical models failed to fit anisotropy data of BSA over fractional labelling with FITC. The model was then modified and a correction factor was introduced to count for intensity behaviour, named as z_i (equation 3.2-1,-2). DNA model systems were then fractionally labelled with fluorescein and the new theoretical model was used to fit the data and the intensity and anisotropy of individual species in stochastic mixtures were successfully found out. By finding anisotropies of individual, partly labelled species, in a stochastic mixture, more detailed information about the structures of the molecules such as distances between their reacting sites would be obtained. In the present work for example, r_2 and r_3 would be used to calculate distances between neighbouring fluorophores. To do more robust studies however, constructs with known structures must be used.

To find out distance dependent non-additivity and its effects on intensity and anisotropy, DNA four way junctions in a range of different sizes, labelled with fluorescein on each arm, were chosen as model systems. The intensities of four way junctions labelled with fluorescein changes with the size of the construct and are the lowest for the smallest constructs. A correction factor, q_N , was introduced to the existing formula to count for distance dependent quenching. The values of q_N were empirically estimated based on changes in the distances between the dyes in different four way junctions.

In the present study, the importance of considering the photophysical properties of the fluorophores has been mainly discussed for systems undergoing fractional labelling or when the intensity and anisotropy of a set of similar clusters of different sizes are being compared. It will also be very useful to study the anisotropy of single systems (not in stochastically defined ensembles), with known photophysical properties, undergoing homo-FRET.

If similar systems with different sizes are labelled with the same number of the same dye, the distance between the dyes can be calculated or experimentally verified using the presented theory, because the extent of these interactions, e.g. quenching [227], depends on the distance between the fluorophores.

The applicability of the models has been tested by analyzing the anisotropy data of an assembled tetrameric cluster of fluorescent proteins as well[28].

Some of the present studies on DNA have been done at a very low temperature. As fluorescence emission is temperature dependent [229], the individual observations and results might not be simply generalized to any condition. Similar fluorescence studies in systems with higher rotational correlation times may allow for measuring homo-FRET in the absence of rotational diffusion at room temperature and this is the area of work that is currently being done on Lysozyme labelled with Alexa flour 488.

Although assumptions such as equal fluorescence efficiency simplify the theoretical treatment of clustering, they restrict their applications and may cause misinterpretation if not applied carefully. For example the other assumption of the theory is the assumption of random orientation of the fluorophores that is not always

valid either, e.g. for fluorescent proteins when the rotational correlation times are high in comparison with lifetime and the energy is not completely depolarized through rotational diffusion [4, 67]. This is an important area of work which has partly been covered [4] and needs more extensive work in future.

Such considerations are crucial when designing and making optimal fluorophores for studying protein interactions while making clusters and in studies about receptor activation, plaque formation, or similar processes underlying disease states. In particular, such studies improve *in vivo* methods that involve imaging and anisotropy [230-234].

References

1. Weber, G., Daniel, E. , *Cooperative effects in binding by bovine serum albumin. II. The binding of 1-anilino-8-naphthalenesulfonate. Polarization of the ligand fluorescence and quenching of the protein fluorescence.* Biochemistry, 1966. **5**: p. 1900-1907.
2. Knox, R.S., *Theory of Polarization Quenching by Excitation Transfer.* Physica 1968. **39**: p. 361-386.
3. Ciccotosto G.D. , K.N., Chow T.T.Y., Chon J.W.M. , Clayton A.H.A. , *Aggregation Distributions on Cells Determined by Photobleaching Image Correlation Spectroscopy.* Biophysical Journal 2013. **104**: p. 1056-1064.
4. Bader, A.N., *Homo-FRET Imaging as a Tool to Quantify Protein and Lipid Clustering.* ChemPhysChem, 2011. **12**: p. 475-483.
5. Chan, F.T.S., Kaminski, C. F. & Kaminski Schierle, G. S. , *HomoFRET Fluorescence Anisotropy Imaging as a Tool to Study Molecular Self -Assembly in Live Cells.* ChemPhysChem, 2011. **12**: p. 500-509.
6. Xu, B., Jin, C., Deng, Y., Liu, W., Yang, T., Feng, S., Xu, Z. , *Alpha-Synuclein Oligomerization in Manganese-Induced Nerve Cell Injury in Brain Slices: A Role of NO-Mediated S-Nitrosylation of Protein Disulfide Isomerase.* Molecular Neurobiology, 2014.

7. Verinaa, T., Schneiderb, J.,S., Guilarte, T.R., *Manganese exposure induces α -synuclein aggregation in the frontal cortex of non-human primates*. Toxicology Letters, 2013. **217**: p. 177–183.
8. Lynn, D.G., Meredith, S. C., Burkoth, T.S., Benzinger, T.L.S, Urban, V.,Morgan, D.M. ,Gregory, D.M. , Thiyagarajan, P. , Botto, R.E., *Structure of the β -Amyloid (10-35) Fibril*. J. Am. Chem. Soc., , 2000. **122**: p. 7883-7889.
9. Burkoth T. S., B.T.L.S., Urban V., Morgan D. M., Gregory D. M., Thiyagarajan P., Botto R. E. , Meredith S. C.,Lynn D. G. , *Structure of the β -amyloid (10-35) fibril*. J. Am. Chem. Soc., 2000 **122**: p. 7883-7889.
10. Lyubchenko, Y.L., Kim, B. H., Krasnoslobodtsev A. V., Yu J. , *Nanoimaging for protein misfolding diseases*. Wiley Interdiscip. Rev. Nanomed. Nanobiotechnol. , 2010. **2**: p. 526-544.
11. Stephens D. J., A.V.J., *Light Microscopy Techniques for Live Cell Imaging*. Science 2003. **300**: p. 82-86.
12. Dai X. W. , Y.Z.L., Eccleston M. E. , Swartling J., Slater N. K. H. , Kaminski C. F. , *Fluorescence intensity and lifetime imaging of free and micellar-encapsulated doxorubicin in living cells*. Nanomed. Nanotechnol, 2008. **4**: p. 49-56.
13. Esposito A., S.S., Schierle G. S. K., Elder A. D., Diaspro A., Wouters F. S., Kaminski C. F., Iliev A. I., *Quantitative fluorescence microscopy techniques*. Methods Mol. Biol. , 2009. **586**: p. 117-42.
14. A.E., J., *Fluorescence Approaches for Determining Protein Conformations, Interactions and Mechanisms at Membranes*. Traffic, 2005. **6**: p. 1078–1092.
15. Yan Y., M.G., *Analysis of protein interactions using fluorescence technologies*. Current Opinion in Chemical Biology 2003, 7:635–640, 2003. **7**: p. 635-640.
16. Clegg, R.M., Holub, O., Gohlke, C., *Fluorescence lifetime-resolved imaging: measuring lifetimes in an image*. Methods Enzymol, 2003. **360**: p. 509-542.
17. Haustein E., S.P., *Single-molecule spectroscopic methods*. Curr. Opin. Struct. Biol., 2004. **14**: p. 531-540.
18. Maa, L., Yanga, F., Zhenga, J., *Application of fluorescence resonance energy transfer in protein studies* Journal of Molecular Structure, 2013. **1077**: p. 87–100.
19. Sun Y., R.C., Jyothikumar V., Periasamy A., *Förster resonance energy transfer microscopy and spectroscopy for localizing protein–protein interactions in living cells*. Cytometry Part A: Special Issue: Microscopy of Molecular Interactions, 2013. **83**: p. 780-793.

20. Kozer, N., C. Henderson, J. T. Jackson, E. C. Nice, A. W. Burgess, and A. H. A. Clayton. , *Evidence for extended YFP-EGFR dimers in the absence of ligand on the surface of living cells.* . Physical Biology 2011. **8**.
21. Levitt, J.A., D. R. Matthews, S. M. Ameer-Beg, and K. Suhling. , *Fluorescence lifetime and polarization-resolved imaging in cell biology.* . Current Opinion in Biotechnology 2009. **20**: p. 28-36.
22. Lakowicz, J.R., *Principles of fluorescence spectroscopy.* 2006: Springer.
23. Runnels, L.W., Scarlata, S. F. , *Theory and application of fluorescence homotransfer to melittin oligomerization.* Biophysical Journal, 1995. **J69**: p. 1569–1583
24. Yeow, E.K.L., Clayton, A. H. A. , *Enumeration of Oligomerization States of Membrane Proteins in Living Cells by Homo-FRET Spectroscopy and Microscopy: Theory and Application* Biophysical Journal, 2007. **92**: p. 3098–3104
25. Shankar, G.M., Li, S. M. , Mehta, T. H., Garcia-Munoz, A., Shepardson, N. E. , Smith, I., Brett ,F. M., Farrell, M. A., Rowan, M. J., Lemere, C. A. , Regan, C. M., Walsh, D. M. , Sabatini, B. L. , Selkoe, D. J. , *Amyloid- β protein dimers isolated directly from Alzheimer's brains impair synaptic plasticity and memory.* Nat. Med., 2008. **14**.
26. Lesn, S., Koh, M. T. , Kotilinek, L. , Kaye, R., Glabe, C. G. , Yang, A. , Gallagher, M. , Ashe, K. H. ,, Nature 2006. **440**.
27. Bader, A.N., Hofman E. G., Voortman J. , van Bergen en Henegouwen P. M. P. , Gerritsen H. C.,, *Homo-FRET Imaging Enables Quantification of Protein Cluster Sizes with Subcellular Resolution.* Biophysical Journal 2009. **97**: p. 2613–2622.
28. Zolmajd-Haghighi, Z., Hanley, Q.S., *When One Plus One Does Not Equal Two: Fluorescence Anisotropy in Aggregates and Multiply Labeled Proteins.* Biophysical Journal, 2014. **106**: p. 1457–1466.
29. Sieber, J., Lang T., *Anatomy and Dynamics of a Supramolecular Membrane Protein Cluster.* Science, 2007. **317**: p. 1072-1076.
30. Roy, N.H., Chan, J., Lambele, M., Thali, M. , *Clustering and Mobility of HIV-1 Env at Viral Assembly Sites Predict Its Propensity To Induce Cell-Cell Fusion.* Journal of Virology 2013. **87**: p. 7516–7525.
31. Peckys, D.B., Baudoin, J. P., Eder, M. , Werner, U., de Jonge, N., *Epidermal growth factor receptor subunit locations determined in hydrated cells with environmental scanning electron microscopy.* Scientific Reports, 2013: p. 1-6.

32. Mujumdar, R.B., Ernst, L. A., Mujumdar, S. R., Waggoner A. S., *Cyanine dye labeling reagents containing isothiocyanate groups*. *Cytometry*, 1989. **10**: p. 11-19.
33. Matveeva, E.G., Terpetschnig, E. A., Stevens, M., Patsenker L., Kolosova, O. S., Gryczynski, Z., Gryczynski, I., *Near-infrared squaraine dyes for fluorescence enhanced surface assay*. *DYES AND PIGMENTS AN INTERNATIONAL JOURNA*, 2009. **L80**: p. 41-46.
34. Gruber, H.J., Hahn, C. D., Kada G., Riener C. K., Harms G. S., Ahrer W. , Dax T. G., Knaus H.G. , *Anomalous fluorescence enhancement of Cy3 and Cy3. 5 versus anomalous fluorescence loss of Cy5 and Cy7 upon covalent linking to IgG and noncovalent binding to avidin*. . *Bioconjug. Chem.* , 2000. **11**: p. 696-704.
35. Hungerford, G., Benesch, J., Mano, J. F. & Reis, R. L. , *Effect of the labelling ratio on the photophysics of fluorescein isothiocyanate (FITC) conjugated to bovine serum albumin*. *Photochemical & Photobiological Sciences*, 2007. **6**: p. 152-158.
36. Neisch, A.L., and R. G. Fehon. , *Ezrin, Radixin and Moesin: key regulators of membrane–cortex interactions and signaling*. *Current Opinion in Cell Biology*, 2011. **23**: p. 377-382.
37. Fábrián, Á., Szöllősi, János, *Optimizing fluorescence resonance energy transfer measurements*. *Optoelectronics, Instrumentation and Data Processing*, 2013. **49**: p. 298-304.
38. Jin, Z., Y. Li, R. Pitti, D. Lawrence, V. C. Pham, J. R. Lill, and A. Ashkenazi. , *Cullin3-Based Polyubiquitination and p62-Dependent Aggregation of Caspase-8 Mediate Extrinsic Apoptosis Signaling*. . *Cell*, 2009. **137**: p. 721-735.
39. Ganguly, S., A.H.A. Clayton, and A. Chattopadhyay, *Organization of higher-order oligomers of the serotonin_{1A} receptor explored utilizing homo-FRET in live cells*. *Biophysical journal*, 2011. **100**(2): p. 361-368.
40. Peckys D.B., B.J.P., Eder M., Werner U. , de Jonge N. , *Epidermal growth factor receptor subunit locations determined in hydrated cells with environmental scanning electron microscopy*. *Scientific Reports*, 2013: p. 1-6.
41. Endres N.F., E.K., Das R., Kovacs E. ,Kuriyan J., *Regulation of the catalytic activity of the EGF receptor*. *Current Opinion in Structural Biology* 2011. **21**: p. 777-784.
42. Ahn, M., De Genst E., Schierle G. S. K. , Erdelyi M. , Kaminski C. F., Dobson C. M., Kumita J. R., *Analysis of the Native Structure, Stability and Aggregation of Biotinylated Human Lysozyme*. . *PLoS ONE* 2012. **7**.

43. Ecroyd, H., Carver, J.A., *Crystallin proteins and amyloid fibrils*. Cellular and Molecular Life Sciences, , 2009. **66**: p. 62-81.
44. Devauges, V., C. Marquer, S. Lécart, J.-C. Cossec, M.-C. Potier, E. Fort, K. Suhling, and S. Lévêque-Fort. , *Homodimerization of Amyloid Precursor Protein at the Plasma Membrane: A homoFRET Study by Time-Resolved Fluorescence Anisotropy Imaging*. . PLoS ONE 2012. **7**.
45. Kaminsky, Y.G., M. W. Marlatt, M. A. Smith, and E. A. Kosenko. , *Subcellular and metabolic examination of amyloid- β peptides in Alzheimer disease pathogenesis: Evidence for A β 25–35*. . Experimental Neurology 2010. **221**: p. 26-37.
46. Van Ham, T.J.e.a., *Towards Multiparametric Fluorescent Imaging of Amyloid Formation: Studies of a YFP Model of α -Synuclein Aggregation*. . Journal of Molecular Biology, 2010. **395**: p. 627-642.
47. Muchowski, P.J., Ramsden, R., Nguyen, Q., Arnett, E.E., Greiling, T.M., Anderson, S.K., Clark, J.I. , *Noninvasive measurement of protein aggregation by mutant huntingtin fragments or alpha-synuclein in the lens*. . J Biol Chem 2008. **283**: p. 6330-6336.
48. Truscott, R.J., *Age-related nuclear cataract-oxidation is the key*. . Exp Eye Res 2005. **80**: p. 709-725.
49. Claxton, D.P., Zou, P. ,McHaourab, H.S., *Structure and orientation of T4 lysozyme bound to the small heat shock protein alpha-crystallin*. . J Mol Biol 2008 **375**: p. 1026-1039.
50. Valeur, B., *Molecular Fluorescence: Principles and Applications*. . 2002: Wiley VCH.
51. Jameson, D.M., Croney, J. C. , *Fluorescence Polarization: Past, Present and Future*. Combinatorial Chemistry & High Throughput Screening, 2003. **6**: p. 167-176.
52. Jameson, D.M., Croney, J. C. , Moens P. D., *Fluorescence: basic concepts, practical aspects, and some anecdotes*. Methods Enzymol 2003. **360**: p. 1-43.
53. Weber, G., *Polarization of the fluorescence of macromolecules. 1. Theory and experimental method*. . Biochem, 1952. **J51**: p. 145-155.
54. Cehelnik, E.D.M., K. , *Polarization effects on fluorescence measurements*. . Journal of Research of National Bureau of Standard A.Physics and Chemistry, 1974. **79A**: p. 1-15.
55. Cercek, L., Cercek, B. & Ockey, C. H. , *Fluorescein excitation and emission polarization spectra in living cells: changes during the cell cycle*. Biophys, 1978. **J23**: p. 395-405.

56. Mann, T.L.K., U. J. , *Fluorescence polarization spectroscopy in protein analysis*. Analyst, 2003. **128**: p. 313-317.
57. Lukas, T.J., Burgess, W. H., Prendergast, F. G., Lau, W. & Watterson, D. M., *Calmodulin binding domains: characterization of a phosphorylation and calmodulin binding site from myosin light chain kinase*. . Biochemistry, 1986. **25**: p. 1458-1464.
58. Kupstat, A., Ritschel, T. & Kumke, M. U. , *Oxazine Dye-Conjugated DNA Oligonucleotides: Förster Resonance Energy Transfer in View of Molecular Dye–DNA Interactions*. . Bioconjugate Chem., 2011. **22**: p. 2546-2547.
59. Sauer, M., Hofkens, J., Enderlein, J., *Handbook of Fluorescence Spectroscopy and Imaging, From Ensemble to Single Molecule*. 2010: WILEY-VCH.
60. Vogel, S.S., Thaler, C., Koushik ,S.V., *Fanciful FRET*. Sci. STKE, 2006.
61. Forde, T.S., Hanley, Q. S., *Following FRET through five energy transfer steps: spectroscopic photobleaching, recovery of spectra, and a sequential mechanism of FRET*. . Photochemical & Photobiological Sciences 2005. **4**: p. 609-616.
62. Wouters, F.S., Verveer, P. J., Bastiaens, P.I.H. , *Imaging biochemistry inside cells*. TRENDS in Cell Biology, 2001. **11**: p. 203-211.
63. Poland SP, K.N., Coelho S, Tyndall D, Walker RJ, Devauges V, Morton PE, Nicholas NS, Richardson J, Li DD, Suhling K, Wells CM, Parsons M, Henderson RK, Ameer-Beg SM., *Time-resolved multifocal multiphoton microscope for high speed FRET imaging in vivo*. Optics Letters, 2014. **39**: p. 6013-6016.
64. Truong, K., Ikura, M. , *The use of FRET imaging microscopy to detect protein–protein interactions and protein conformational changes in vivo*. . Current Opinion in Structural Biology, 2001. **11**: p. 573-578.
65. Kirsch F. , E.T., Ziolkowska J., Herrmann A., *Analyse eines unkonventionellen Vitamin-Transporters*. BIO spektrum, 2013. **18**: p. 493-496.
66. Stryer, L., Haugland, R. P., *Energy Transfer: A Spectroscopic Ruler*. Proc Natl Acad Sci U S A (Biochemistry), 1967. **58**: p. 719-726.
67. Bader, A.N., Hofman, E. G. , van Bergen en Henegouwen P.M. P. , Gerritsen H.C. , *Imaging of protein cluster sizes by means of confocal time-gated fluorescence anisotropy microscopy*. OPT EXPRESS 2007. **15**: p. 6934-6945.
68. Koushik S.V., B.P.S., Vogel S.S., *Anomalous Surplus Energy Transfer Observed with Multiple FRET Acceptors*. PLoS ONE, 2009. **4**: p. 1-11.

69. Corry B. , J.D., Rigby P. , *A Flexible Approach to the Calculation of Resonance Energy Transfer Efficiency between Multiple Donors and Acceptors in Complex Geometries*. Biophysical Journal, 2005. **89**: p. 3822–3836.
70. Raicu V. , *Efficiency of Resonance Energy Transfer in Homo-Oligomeric Complexes of Proteins*. J Biol Phys., 2007. **33**: p. 109-127.
71. Istvan F.A. , *Optimizing fluorescence resonance energy transfer*, in *Doctoral School of Molecular Medicine* 2013, University of Debrecen. p. 76.
72. Dietrich A., B.V., Muller C. , Sauer M., *Fluorescence resonance energy transfer (FRET) and competing processes in donoracceptor substituted DNA strands: a comparative study of ensemble and single-molecule data*. Reviews in Molecular Biotechnology, 2002. **82**: p. 211-231.
73. Jares-Erijman, E.A., Jovin, T. M., *FRET Imaging*. Nat.Biotechnol, 2003. **21**: p. 1387-1395.
74. Crosby K.C., P.M., Hink M.A., Zeelenberg C.H.C. , Adjobo-Hermans M.J.W., Gadella T.W.J., *Quantitative Analysis of Self-Association and Mobility of Annexin A4 at the Plasma Membrane*. Biophysical Journal, 2013. **104**: p. 1875-1885.
75. Lo J. , Y.C.M., *Homo-FRET Imaging of CEACAM1 in Living Cells using Total Internal Reflection Fluorescence Polarization Microscopy*. Fluorescence polarization microscopy, 2012.
76. Lakowicz, J.R., Malicka, J., D'Auria, S. & Gryczynski, I. , *Release of the self-quenching of fluorescence near silver metallic surfaces*. . Analytical Biochemistry, 2003. **320**: p. 13-20.
77. Demchenko, A.P., *Advanced Fluorescence Reporters in Chemistry and Biology 2: Molecular Constructions, Polymers and Nanoparticles*. 2010: Springer.
78. Hermanson, G.T., *Bioconjugate techniques*. 2008: Academic Press.
79. Jameson, D.M., Ross, J . A . *Fluorescence Polarization/Anisotropy in Diagnostics and Imaging*. Chem. Rev., 2010. **110**: p. 2685-2708.
80. Agranovich, V.M., Galanin, M. D. , *Electronic excitation energy transfer in condensed matter*. 1982: North-Holland Pub. Co.
81. Mielczarek, E.V., Greenbaum, E. S. , *Biological physics*. 1993: Springer.
82. Szabó Á., H., G., Szollosi, J. , Nagy, P. , *Quantitative Characterization of the Large-Scale Association of ErbB1 and ErbB2 by Flow Cytometric Homo-FRET Measurements*. . Biophysical Journal, 2008. **95**: p. 2086-2096.

83. Varma, R., Mayor, S. , *GPI-anchored proteins are organized in submicron domains at the cell surface*. Nature, 1998. **394**: p. 798-801.
84. Blackman, S.M., Piston, D. W. , Beth, A. H., *Oligomeric State of Human Erythrocyte Band 3 Measured by Fluorescence Resonance Energy Homotransfer*. . Biophysical Journal, 1998. **75**: p. 1117-1130.
85. Lidke, D.S., Nagy P. , Barisas B. G., Heintzmann R., Post J. N., Lidke K. A., Clayton A. H. A. , Arndt-Jovin D. J., Jovin T. M., *Imaging molecular interactions in cells by dynamic and static fluorescence anisotropy (rFLIM and emFRET)*. Biochem. Soc. Trans, 2003. **31**: p. 1020-1027.
86. Ganguly, S., Clayton, A. H. A. & Chattopadhyay, A. , *Organization of Higher-Order Oligomers of the Serotonin1A Receptor Explored Utilizing Homo-FRET in Live Cells*. Biophys 2011. **J100**: p. 361-368.
87. Tramier, M., Coppey-Moisan, M. , *Fluorescence anisotropy imaging microscopy for homo-FRET in living cells*. Methods Cell Biol., 2008. **85**: p. 395-414.
88. Dix, J.A.V., A. S. , *Mapping of fluorescence anisotropy in living cells by ratio imaging. Application to cytoplasmic viscosity*. . Biophysical Journal, 1990. **57**: p. 231-240.
89. Gough, A.H.T., D. L. , *Fluorescence anisotropy imaging microscopy maps calmodulin binding during cellular contraction and locomotion*. . The Journal of Cell Biology, 1993. **121**: p. 1095 –1107
90. Pal'chikova I. G., O.y.L.V., Kamanina N. V. , Makarov S. N., Smirnov E. S., *Finding fluorescence polarization anisotropy from digital microimages of cells*. Optoelectronics, Instrumentation and Data Processing, 2013. **49**: p. 102-113.
91. Resch-Genger, U., *Standardization and quality assurance in fluorescence measurements I: techniques*. . 2008: Springer.
92. Sharma, P., R. Varma, R. C. Sarasij, Ira, K. Gousset, G. Krishnamoorthy, M. Rao, and S. Mayor. , *Nanoscale Organization of Multiple GPI-Anchored Proteins in Living Cell Membranes*. Cell Cell, 2004. **116**: p. 577-589.
93. Lakowicz JR, M.J., D'Auria S, Gryczynski I. , *Release of the self-quenching of fluorescence near silver metallic surfaces*. . Anal Biochem, 2003. **320**: p. 13–20.
94. Malicka J, G.I., Lakowicz JR. , *Enhanced emission of highly labeled DNA oligomers near silver metallic surfaces*. . Anal Chem 2003. **75**(4408–4414).
95. Lakowicz JR, M.J., Huang J, Gryczynski Z, Gryczynski I., *Ultrabright fluorescein-labeled antibodies near silver metallic surfaces*. . Biopolymers 2004. **74**: p. 467–475.

96. Frederic, k.F.W., Knox, R. S., *Theory of Polarization Quenching by Excitation Transfer II. Anisotropy and Second-Neighbour Considerations*. Molecular Physics 1971. **22**: p. 385-402.
97. Haugland, R.P., *Handbook of fluorescent probes and research chemicals*. 9th ed. 1996: Molecular Probes Inc, Eugene, OR.
98. Waggoner, A., *Covalent labeling of proteins and nucleic acids with fluorophores*. . Methods Enzymol 1995. **246**: p. 362–373.
99. Panchuk-Voloshina, N., R. P. Haugland, J. Bishop-Stewart, M. K. Bhalgat, P. J. Millard, F. Mao, W.-Y. Leung, and R. P. Haugland. , *Alexa dyes, a series of new fluorescent dyes that yield exceptionally bright, photostable conjugates*. Journal of Histochemistry & Cytochemistry, 1999. **47**: p. 1179-1188.
100. Song X, S.B., *Rapid assay for avidin and biotin based on fluorescence quenching*. Anal Chim Acta 2001. **442**: p. 79–87.
101. Goto Y, H.Y., *Mechanism of the conformational transition of melittin*. Biochemistry 1992. **31**: p. 732–738.
102. Cuppoletti, A., Y. Cho, J.-S. Park, C. Strässler, and E. T. Kool. 2005. , *Oligomeric fluorescent labels for DNA*. . Bioconjug. Chem., 2005. **16**: p. 528-534.
103. Voss Jr, E.W., C. Workman, and M. Mummert. , *Detection of protease activity using a fluorescence-enhancement globular substrate*. . BioTechniques 1996. **20**: p. 286-291.
104. Parfenov, A., I. Gryczynski, J. Malicka, C. D. Geddes, and J. R. Lakowicz. , *Enhanced fluorescence from fluorophores on fractal silver surfaces*. . The Journal of Physical Chemistry 2003. **B 107** p. 8829-8833.
105. Anderson, G.P., N. L. Nerurkar. , *Improved fluoroimmunoassays using the dye Alexa Fluor 647 with the RAPTOR, a fiber optic biosensor*. . Journal of immunological methods 2002. **271**: p. 17-24.
106. Gholami, Z., L. Brunsveld, and Q. Hanley. , *PNA-Induced assembly of fluorescent proteins using DNA as a framework*. . Bioconjug. Chem. , 2013.
107. Okamoto A, I.T., Saito I. , *Pyrene-labeled oligodeoxynucleotide probe for detecting base insertion by excimer fluorescence emission*. J Am Chem Soc 2004. **126**: p. 8364–8365.
108. Yamana K, I.T., Ohtani Y, Sato S, Nakamura M, Nakano H. , *Bis-pyrene-labeled oligonucleotides: sequence specificity of excimer and monomer fluorescence changes upon hybridization with DNA*. Bioconjugate Chem 2002. **13**: p. 1266–1273.

109. Wang W, H.J., Wang LQ, Li LS, Shaw WJ, Li ADQ., *Dynamic B–B stacked molecular assemblies emit from green to red colors*. . Nano Lett 2003. **3**: p. 455–458.
110. Birks, J.B., *Photophysics of aromatic molecules*. 1970: John Wiley & Sons, New York.
111. Bennett M.K., G.-A.J.E., Elferink L.A., Peterson K., Fleming A.M., Hazuka C.D., Scheller R.H. , *The syntaxin family of vesicular transport receptors* Cell 1993. **74** p. 863–73.
112. Gautier I. , M.T., C. Durieux, J. Coppey,R. B. Pansu,J-C. Nicolas,K. Kemnitz, M. Coppey-Moisan, *Homo-FRET Microscopy in Living Cells to Measure Monomer-Dimer Transition of GFP-Tagged Proteins*. Biophysical Journal 2001. **80**: p. 3000–3008.
113. Yeow, E.K.L., Ghiggino, K.P., Reek, J.N.H. , Crossley, M.J., Bosman, A.W. , Schenning A. P. H. J. , Meijer, E.W., *The Dynamics of Electronic Energy Transfer in Novel Multiporphyrin Functionalized Dendrimers: A Time-Resolved Fluorescence Anisotropy Study*. J. Phys. Chem. B 2000. **104**: p. 2596-2606.
114. Seeman N.C. , *DNA engineering and its application to nanotechnology*. TIBTECH NOVEMBER, 1999. **17**: p. 437-442.
115. Seeman N.C. , *DNA NANOTECHNOLOGY: Novel DNA Constructions*. Annu. Rev. Biophys. Biomol. Struct. , 1998. **27**: p. 225–48.
116. Levi, V.G.F., F. L. , *Reversible fast-dimerization of bovine serum albumin detected by fluorescence resonance energy transfer*. . Biochimica et Biophysica Acta (BBA) - Proteins & Proteomics, 2002. **1599**: p. 141-148.
117. Schumaker, V.N., *Advances in protein chemistry*. 1994: Academic Press.
118. Squire, P.G., Moser, P. & O’Konski, C. T. , *Hydrodynamic properties of bovine serum albumin monomer and dimer*. . Biochemistry, 1968. **7**: p. 4261-4272.
119. Groza R.C., C.A., Ryder A.G, *A fluorescence anisotropy method for measuring protein concentration in complex cell culture media*. Analytica Chimica Acta, 2014. **821**: p. 54–61.
120. Mir, M.M., Fazili, K. M. & Abul Qasim, M. , *Chemical modification of buried lysine residues of bovine serum albumin and its influence on protein conformation and bilirubin binding*. . Biochim. Biophys. Acta, 1992. **1119**: p. 261-267.
121. Anfinsen, C.B.E., J. T. , *Advances in Protein Chemistry*. 1995: Academic Press.
122. Sadler, P.J.T., A., *Proton NMR studies of bovine serum albumin*. . European Journal of Biochemistry, 1992. **205**: p. 631-643.

123. Carter, D.C., He, X. M. , Munson, S. H., Twigg, P. D., Gernert, K. M. , Broom, M. B., Miller, T. Y. , *Three-dimensional structure of human serum albumin*. Science 1989. **244**: p. 1195-1198.
124. Tayyab, S., Qasim, M. A. , *A correlation between changes in conformation and molecular properties of bovine serum albumin upon succinylation*. J. Biochem., 1986. **100**: p. 1125-1136.
125. A.F.S.A., H., *Quantitation of conformational changes on chemical modification of proteins: Use of succinylated proteins as a model*. . Archives of Biochemistry and Biophysics 1967. **121**: p. 652-664.
126. Huang B.X., K.H.Y., Dass C., *Probing Three-Dimensional Structure of Bovine Serum Albumin by Chemical Cross-Linking and Mass Spectrometry*. J Am Soc Mass Spectrom 2004. **15**: p. 1237-1247.
127. Li, D.H., Zhu, Q.Z., Ye, D., Fang, Y. , Xu, J.G. , *A rapid method for the determination of molar ratio of fluorophore to protein by fluorescence anisotropy detection* Analytica Chimica Acta, 1999. **389**: p. 85-88.
128. Martin, M.M., Lindqvist, L. , *The pH dependence of fluorescein fluorescence*. Journal of Luminescence, 1975. **10**: p. 381-390.
129. Wu, S., Dovichi, N. J. , *High-sensitivity fluorescence detector for fluorescein isothiocyanate derivatives of amino acids separated by capillary zone electrophoresis*. Journal of Chromatography 1989. **A480**: p. 141-155.
130. Klugerman, M.R., *Chemical and Physical Variables Affecting the Properties of Fluorescein Isothiocyanate and Its Protein Conjugates*. . The Journal of Immunology, 1965. **95**: p. 1165-1173.
131. Schultz, N.M.K., R. T., *Rapid immunoassays using capillary electrophoresis with fluorescence detection*. . Anal. Chem., 1993. **65**: p. 3161-3165.
132. James W., G., *Conjugation of antibodies with fluorochromes: Modifications to the standard methods*. . Journal of Immunological Methods, 1976. **13**: p. 215-226.
133. Banks, P.R., Paquette, D. M. , *Comparison of three common amine reactive fluorescent probes used for conjugation to biomolecules by capillary zone electrophoresis*. Bioconjug. Chem., 1995. **6**: p. 447-458.
134. Ma H., S., W., Dong, S., Wang, K., Jia, J., Chen S. , *N-Terminal Specific Fluorescence Labeling and its Use in Local Structure Analysis of Proteins (Invited Review)*. Current Chemical Biology 2008. **2**: p. 249-255.

135. Mckinney, R.M., Spillane, J. T. & Pearce, G. W. , *Factors Affecting the Rate of Reaction of Fluorescein Isothiocyanate with Serum Proteins*. The Journal of Immunology, 1964. **93**, : p. 232-242.
136. Cherry W. B., M.R.M., Emmel V. ,M., Spillane J. T., Hebert A., Bertie Pittman B., *Evaluation of Commercial Fluorescein Isothiocyanates Used in Fluorescent Antibody Studies*. Biotechnic & Histochemistry, 1969. **44**: p. 179-186.
137. Maiti, P.K., Cagin, T., Wang, G., Goddard, W. A., *Structure of PAMAM Dendrimers: Generations 1 through 11*. Macromolecules 2004. **37**: p. 6236-6254.
138. Ghiggino, K.P., *The Dynamics of Electronic Energy Transfer in Novel Multiporphyrin Functionalized Dendrimers: A Time-Resolved Fluorescence Anisotropy Study*. J. Phys. Chem. , 2000. **B104**: p. 2596–2606.
139. Seeman N.C., Molecular Biotechnology 2007. **37**: p. 246-257.
140. Woźniaka A. K. , S., G. F., Grubmullerb H., Seidel C. A. M. , Oesterhelta F., *Single-molecule FRET measures bends and kinks in DNA*. Biophysics, 2008. **105**: p. 18337–18342.
141. Pinheiro A.V, H.D., Shih W.M, Yan H., *Challenges and opportunities for structural DNA nanotechnology*. nature nanotechnology, 2011. **6**: p. 763-772.
142. Storhoff J.J. , M.C.A., *Programmed Materials Synthesis with DNA*. Chem. Rev. , 1999. **99**: p. 1849-1862.
143. Ha T., E.T., Ogletree D. F. , Chemla D. S., Selvin P. R. , Weiss S., *Probing the interaction between two single molecules: Fluorescence resonance energy transfer between a single donor and a single acceptor*. Proc. Natl. Acad. Sci. USA, 1996. **93**: p. 6264-6268.
144. Jares-Erijman EA, J.T., *Determination of DNA helical handedness by fluorescence resonance energy transfer*. . J Mol Biol, 1996. **257**: p. 597–617.
145. Clegg R.M., M.A.I.H., Zechel A., Lilley D.M.J., *Observing the helical geometry of double-stranded DNA in solution by fluorescence resonance energy transfer*. Biophysics, 1993. **90**: p. 2994-2998.
146. Toth K. , S.V., Langowski J., *DNA curvature in solution measured by fluorescence resonance energy transfer*. Biochemistry 1998. **37**: p. 8173–8179.
147. Neubauer H., G.N., Berger S., Schaffer J., Eggeling C., Tuma J., Verdier L., Seidel C.A. M. ,Griesinger C., Volkmer A., *Orientalional and Dynamical Heterogeneity of Rhodamine 6G Terminally Attached to a DNA Helix Revealed by NMR and Single-*

- Molecule Fluorescence Spectroscopy*. J. AM. CHEM. SOC., 2007. **129**: p. 12746-12755.
148. Kumke, M.U., Li, G. , McQown, L.B. , Walker, T. , Linn, C.P. , *Hybridization of Fluorescein-Labeled DNA Oligomers Detected by Fluorescence Anisotropy with Protein Binding Enhancement*. Anal. Chem., 1995. **67**: p. 3945-3951.
 149. Vamosi, G., Gohike, C. , Clegg, R.M. , *Fluorescence Characteristics of 5-Carboxytetramethylrhodamine Linked Covalently to the 5' End of Oligonucleotides: Multiple Conformers of Single-Stranded and Double-Stranded Dye-DNA Complexes*. Biophysical Journal 1996. **71**: p. 972-994.
 150. Kelbauskas L., W.N., Lohr D., *DNA sequence-dependent variation in nucleosome structure, stability, and dynamics detected by a FRET-based analysis*. Biochem. Cell Biol. , 2009. **87**: p. 323–335.
 151. Boeneman K., P.D.E., Blanco-Canosa J.B., Dawson P.E., Melinger J.S., Ancona M., Stewart M.H., Susumu K., Huston A., Medintz I.L., *Self-Assembled Quantum Dot-Sensitized Multivalent DNA Photonic Wires*. J. AM. CHEM. SOC., 2010. **132**: p. 18177–18190.
 152. Holliday R., *A mechanism for gene conversion in fungi*. Genetical Research, 1964. **5**: p. 282-304.
 153. Evans D.H. , K.R., *Construction of a Synthetic Holliday Junction Analog and Characterization of Its Interaction with a Saccharomyces cerevisiae Endonuclease That Cleaves Holliday Junctions*. The Journal of Biological Chemistry, 1987. **262**: p. 9160-9165.
 154. Murchie, A.I.H., Carter, W. A. , Portugal, J. , Lilley, D. M. J., *The tertiary structure of the four-way DNA junction affords protection against DNase I cleavage*. Nucleic Acids Research, , 1990. **18**: p. 2599-2606.
 155. Clegg R.M. , M.A.I.H., Zechel A., Carlberg C., *Fluorescence Resonance Energy Transfer Analysis of the Structure of the Four-Way DNA Junction*. Biochemistry, 1992. **31**: p. 4846–4856.
 156. Duckett, D.R., Lilley, D.M.J., *The structure of DNA junctions and their interaction with enzymes*. European Journal of Biochemistry, 1992. **207**: p. 285-295.
 157. Stahl F.W., *The Holliday Junction on Its Thirtieth Anniversary*. Genetics, 1994. **138**: p. 241-246.
 158. McKinney S.A., D.A.C., Lilley D.M.J., Ha T., *Structural dynamics of individual Holliday junctions*. nature structural biology, 2003. **10**: p. 93-97.

159. Lilley, D.M.J., *Structure of helical junctions in nucleic acids*. Quarterly Reviews of Biophysics, 2000. **33**: p. 109–159.
160. Joo C. , M.S.A., Lilley D. M. J. , Ha T., *Exploring Rare Conformational Species and Ionic Effects in DNA Holliday Junctions Using Single-molecule Spectroscopy*. J. Mol. Biol. , 2004 **341**: p. 739–751.
161. Lilley D.M.J. , *All changes at Holliday junctions*. Proc. Natl. Acad. Sci. USA, 1997. **94**: p. 9513-9515.
162. Walter, F., Murchie, A. I. H., Duckett, D. R. , Lilley, D. M. J., *Global structure of four-way RNA junctions studied using fluorescence resonance energy transfer*. RNA, 1998. **4**: p. 719–728.
163. Duckett D.R, M.A.I.H., Lilley D.M.J, *The role of metal ions in the conformation of the four-way DNA junction*. The EMBO Journal, 1990. **9**: p. 583-590.
164. Clegg R.M. , M.A.I., Lilley D.M., *The solution structure of the four-way DNA junction at low-salt conditions: a fluorescence resonance energy transfer analysis*. Biophysical journal, 1994. **66**: p. 99-109.
165. Ho, P.S., Eichman, B.F. , *The crystal structures of DNA Holliday junctions*. Current Opinion Struct. Biol., 2001. **11**: p. 302-308.
166. Grainger, R.J., Murchie, A. I. H., Lilley, D. M. J., *Exchange between Stacking Conformers in a Four-Way DNA Junction*. Biochemistry 1998. **37**: p. 23-32.
167. Murchie A. I. H., C.R.M., v.KE., D.D. R., D.S. ,Lilley D. M. J. , *Fluorescence energy transfer shows that the four-way DNA junction is a right-handed cross of antiparallel molecules*. Nature, 1989. **341**: p. 763-766.
168. McKinney, S.A., Déclais, A. C., Lilley, M.J., Ha T., *Structural dynamics of individual Holliday junctions*. Nature, 2002. **10**: p. 93-97.
169. Pascal, T.A., Goddard, W. A., M.P.K, Vaidehi, N., *Role of Specific Cations and Water Entropy on the Stability of Branched DNA Motif Structures*. J. Phys. Chem. B., 2012. **159**: p. 12159-12167.
170. Lilley, D.M.J., *Structure of helical junctions in nucleic acids*. Quarterly Reviews of Biophysics, 2000. **33**: p. 109-159.
171. Ortiz-Lombardía M, G.A., Eritja R, Aymamí J, Azorín F, Coll M, *Crystal structure of a DNA Holliday junction*. Nature, 1999. **6**: p. 913-917.
172. Nollmann, M., Stark, W.M., Byron, O., *Low-Resolution Reconstruction of a Synthetic DNA Holliday Junction*. Biophysical Journal 2004. **86**: p. 3060–3069.

173. Sabir, T., Magennis, S. W., *Global Structure of Forked DNA in Solution Revealed by High-Resolution Single-Molecule FRET*. J. Am. Chem. Soc. , 2011. **133**: p. 1188-1191.
174. Wang J.C., *Helical repeat of DNA in solution*. Biochemistry, 1978. **76**: p. 200-203.
175. Trifonov, E.N., Sussman, J. L. , *The pitch of chromatin DNA is reflected in its nucleotide sequence (deformation of DNA/dinucleotides/correlation analysis)*. Biochemistry, 1980. **77**: p. 3816-3820.
176. Shida, T., Iwasaki, H., Shinagawa, H., Kyogoku, Y., *Characterization and Comparison of Synthetic Immobile and Mobile Holliday Junctions*. J. Biochem. , 1996. **119**: p. 653-658.
177. Seeman N. C. , *Nucleic acid junctions and lattices*. J.Theor.Biol, 1982. **99**: p. 237-247.
178. Hohng, S., Joo, C., Ha, T., *Single-Molecule Three-Color FRET*. Biophysical Journal 2004. **87**: p. 1328–1337.
179. Gough, G.W., Lilley, D. M. J., Nature 1985. **313**, : p. 154-156.
180. Miick S.M., F.R.S., Millar D.P., Chazin W.J., *Crossover isomer bias is the primary sequence-dependent property of immobilized Holliday junctions*. Proc. Natl. Acad. Sci. USA Biophysics, 1997. **94**: p. 9080–9084.
181. Gopaul D.N., G.F., Van Duyne G.D., *Structure of the Holliday junction intermediate in Cre-loxP site-specific recombination*. The EMBO Journal 1998. **17**: p. 4175–4187.
182. Stuhmeier F, H.A., Clegg R.M, Diekmann S., *Fluorescence Energy Transfer Analysis of DNA Structures Containing Several Bulges and their Interaction with CAP*. J.Mol.Biol, 2000. **302**: p. 1081-1100.
183. Maleki S., R., C. A. , Hurlburt B. K., *Analysis of the DNA-Binding Properties of MyoD, Myogenin, and E12 by Fluorescence Anisotropy*. Biochemistry 2002. **41**: p. 10888-10894.
184. Hogan M. , W.J., Austin R. H. , Monitto C. L. , Hershkowitz S. , *Molecular motion of DNA as measured by triplet anisotropy decay (flexible rod/local motion)*. Biophysics, 1982. **79**: p. 3518-3522.
185. Dexheimer T.S. , S.A.G., Fivash M.J. , Fisher R.J. , Pommier Y. , *The DNA binding and 30-end preferential activity of human tyrosyl-DNA phosphodiesterase*. Nucleic Acids Research, 2010. **38**: p. 2444–2452.
186. Ameloot M, v.M., Acuña A, Valeur B, *Fluorescence anisotropy measurements in solution: Methods and reference materials (IUPAC Technical Report)*. Pure Appl. Chem, 2013. **85**: p. 589–608.

187. Bollag, D.M., Rozycki, M. D. , Edelstein, S. J. , *Protein methods*. 1996: Wiley-Liss.
188. Skoog, D.A., West, D. M., Holler, F. J. , Crouch, S. R. , *Analytical Chemistry: An Introduction*. . 1999: Brooks Cole.
189. Togashi, D.M., Ryder, A. G. , *Assessing protein-surface interactions with a series of multi-labeled BSA using fluorescence lifetime microscopy and Förster Energy Resonance Transfer* Biophys. Chem., 2010. **152**: p. 55-64.
190. Rahman, Q.I., Schmeisser, G. , *Characterization of the speed of convergence of the trapezoidal rule*. . Numerische Mathematik, 1990. **57** , : p. 123–138
191. Staiano, M., *Nanostructured Silver-Based Surfaces: New Emergent Methodologies for an Easy Detection of Analytes* ACS Appl. Mater. Interfaces, 2009. **1**: p. 2909–2916.
192. Kibbe, W.A. *OligoCalc: an online oligonucleotide properties calculator*. Nucleic Acids Research 2007; 35, Web Server issue:[W43–W46].
193. Owczarzy, R., Vallone, P.M., Gallo, F.J., Paner, T.M., Lane, M.J., Benight, A.S. , *Predicting sequence-dependent melting stability of short duplex DNA oligomers*. Biopolymers, 1997. **44**: p. 217–239.
194. SantaLucia, J.J., *A unified view of polymer, dumbbell, and oligonucleotide DNA nearest-neighbor thermodynamics*. Proc. Natl Acad. Sci. USA, 1998. **95**: p. 1460–1465.
195. Squire, A., Verveer, P.J., Rocks, O., Bastiaens, P. I.H. , *Red-edge anisotropy microscopy enables dynamic imaging of homo-FRET between green fluorescent proteins in cells* J STRUC BIO, 2004. **147**: p. 62.
196. Wright, A.K.T., M. R., *Hydrodynamic structure of bovine serum albumin determined by transient electric birefringence*. Biophys, 1975. **J15**: p. 137-141.
197. Lehninger, A.L., Nelson, D. L., Cox M. M., *Lehninger Principles of Biochemistry* 4ed. 2004: W.H. Freeman & Company. 1119.
198. Brewer, J.M., Weber, G. , *The reversible dissociation of yeast enolase*. Proc Natl Acad Sci USA 1968. **59**: p. 216-223.
199. Highsmith, S., Cohen. J. A., *Spatial organization of calcium ATPase molecules in sarcoplasmic reticulum vesicles*. Biochemistry 1987. **26**: p. 154-161.
200. Huang, S., Squier, T. C. , *Enhanced Rotational Dynamics of the Phosphorylation Domain of the Ca-ATPase upon Calcium Activation*. Biochemistry 1998. **37**: p. 18064-18073.

201. Yao, Q., Chen, L. T. L., Li J., Brungardt, K., Squier, T. C., Bigelow, D. J., *Oligomeric Interactions between Phospholamban Molecules Regulate Ca-ATPase Activity in Functionally Reconstituted Membranes*. *Biochemistry* 2001. **40**: p. 6406-6413.
202. Melo, A.M., Fedorov, A., Prieto, M., Coutinho, A., *Exploring Fluorescence Lifetime and Homo-FRET Measurements to Monitor Lysozyme Oligomerization in Anionic Lipid Membranes: Relation to "Amyloid-Like" Fibril Formation*. *Biophysical Journal* 2012. **102**: p. 433a-434a.
203. Melo, A.M., Fedorov, A., Prieto, M., Coutinho, A., *Exploring homo-FRET to quantify the oligomer stoichiometry of membrane-bound proteins involved in a cooperative partition equilibrium*. *Phys. Chem. Chem. Phys.*, 2014: p. 18105-18117.
204. Runnels, L.W. and S.F. Scarlata, *Theory and application of fluorescence homotransfer to melittin oligomerization*. *Biophysical Journal*, 1995. **69**(4): p. 1569-1583.
205. Nguyen, T.A., et al., *Fluorescence polarization and fluctuation analysis monitors subunit proximity, stoichiometry, and protein complex hydrodynamics*. *PLoS ONE*, 2012. **7**(5): p. e38209.
206. Gholami, Z., L. Brunsveld, and Q. Hanley, *PNA-Induced assembly of fluorescent proteins using DNA as a framework*. *Bioconjugate chemistry*, 2013. **in press**.
207. Carter, D.C., et al., *Three-dimensional structure of human serum albumin*. *Science* (New York, N.Y.), 1989. **244**(4909): p. 1195-1198.
208. Huang, B.X., H.-Y. Kim, and C. Dass, *Probing three-dimensional structure of bovine serum albumin by chemical cross-linking and mass spectrometry*. *Journal of the American Society for Mass Spectrometry*, 2004. **15**(8): p. 1237-1247.
209. Matveeva, E.G., et al., *Near-infrared squaraine dyes for fluorescence enhanced surface assay*. *Dyes and Pigments*, 2009. **80**(1): p. 41-46.
210. Mujumdar, R.B., et al., *Cyanine dye labeling reagents containing isothiocyanate groups*. *Cytometry*, 1989. **10**(1): p. 11-19.
211. Gruber, H.J., et al., *Anomalous fluorescence enhancement of Cy3 and cy3.5 versus anomalous fluorescence loss of Cy5 and Cy7 upon covalent linking to IgG and noncovalent binding to avidin*. *Bioconjugate chemistry*, 2000. **11**(5): p. 696-704.
212. Voss Jr, E.W., C. Workman, and M. Mummert, *Detection of protease activity using a fluorescence-enhancement globular substrate*. *BioTechniques*, 1996. **20**(2): p. 286-291.

213. Hungerford, G., et al., *Effect of the labelling ratio on the photophysics of fluorescein isothiocyanate (FITC) conjugated to bovine serum albumin*. Photochemical & photobiological sciences: Official journal of the European Photochemistry Association and the European Society for Photobiology, 2007. **6**(2): p. 152-158.
214. Frath, D., et al., *Chemistry on Boranils: An Entry to Functionalized Fluorescent Dyes*. Organic Letters, 2012. **14**(18): p. 4774-4777.
215. Lakowicz, J.R., et al., *Release of the self-quenching of fluorescence near silver metallic surfaces*. Analytical biochemistry, 2003. **320**(1): p. 13-20.
216. Parfenov, A., et al., *Enhanced fluorescence from fluorophores on fractal silver surfaces*. The Journal of Physical Chemistry B, 2003. **107**(34): p. 8829-8833.
217. Panchuk-Voloshina, N., et al., *Alexa dyes, a series of new fluorescent dyes that yield exceptionally bright, photostable conjugates*. Journal of Histochemistry & Cytochemistry, 1999. **47**(9): p. 1179-1188.
218. Anderson, G.P. and N.L. Nerurkar, *Improved fluoroimmunoassays using the dye Alexa Fluor 647 with the RAPTOR, a fiber optic biosensor*. Journal of immunological methods, 2002. **271**(1): p. 17-24.
219. Ferrer, M.L., et al., *The conformation of serum albumin in solution: a combined phosphorescence depolarization-hydrodynamic modeling study*. Biophysical Journal, 2001. **80**(5): p. 2422-2430.
220. Benesch, J., et al., *Fluorescence probe techniques to monitor protein adsorption-induced conformation changes on biodegradable polymers*. Journal of colloid and interface science, 2007. **312**(2): p. 193-200.
221. Li, D.-H., et al., *A rapid method for the determination of molar ratio of fluorophore to protein by fluorescence anisotropy detection*. Analytica chimica acta, 1999. **389**(1): p. 85-88.
222. Krishnan, R., R. Varma, and S. Mayor, *Fluorescence methods to probe nanometer-scale organization of molecules in living cell membranes*. Journal of Fluorescence, 2001. **11**(3): p. 211-226.
223. Yeow, E.K.L. and A.H.A. Clayton, *Enumeration of oligomerization states of membrane proteins in living cells by homo-FRET spectroscopy and microscopy: theory and application*. Biophysical journal, 2007. **92**(9): p. 3098-3104.
224. Hamann, S., Kiilgaard, J.F., Litman, T., Alvarez-Leefmans, F.J., Winther, B.R., Zeuthen, T., *Measurement of Cell Volume Changes by Fluorescence Self-Quenching*. Journal of Fluorescence, 2002. **12**: p. 139-145.

225. Tinel, H., Wehner, F., Kinne, R.K. H., *Cell Volume Measurements Using Confocal Laser Scanning Microscopy*. *Fluorescence Microscopy and Fluorescent Probes* 1996: p. 273-277.
226. Fenton, R.A., Moeller, H. B.,Nielsen, S. , de Groot, B. L., Rutzler, M., *A plate reader-based method for cell water permeability measurement*. *Am J Physiol Renal Physiol* 2009. **298**: p. F224-F230.
227. Schreiber, R., Do, J., Roller, E., Zhang, T., Schüller, V. J., Nickels, P. C., Feldmann J., Liedl T., *Hierarchical assembly of metal nanoparticles, quantum dots and organic dyes using DNA origami scaffolds*. *Nature Nanotechnology*, 2014. **9**: p. 74–78.
228. Kaminski-Schierle, G.S., Sauer, M., Kaminski, C.F., *Probing Amyloid Aggregation and Morphology In Situ by Multiparameter Imaging and Super-Resolution Fluorescence Microscopy*, in *Bio-nanoimaging: Protein Misfolding & Aggregation*. 2014. p. 105-120.
229. Bowen, E.J., Sahu, J., *The Effect of Temperature on Fluorescence of Solutions*. *J. Phys. Chem.*, 1959. **63**: p. 4–7.
230. Clayton, A.H.A., et al., *Dynamic fluorescence anisotropy imaging microscopy in the frequency domain (rFLIM)*. *Biophysical Journal*, 2002. **83**(3): p. 1631-1649.
231. Zhou, Y., J.M. Dickenson, and Q.S. Hanley, *Imaging lifetime and anisotropy spectra in the frequency domain*. *Journal of microscopy*, 2009. **234**(1): p. 80-88.
232. van Ham, T.J., et al., *Towards multiparametric fluorescent imaging of amyloid formation: Studies of a YFP model of α -synuclein aggregation*. *Journal of molecular biology*, 2010. **395**(3): p. 627-642.
233. Esposito, A., et al., *Design and application of a confocal microscope for spectrally resolved anisotropy imaging*. *Optics express*, 2011. **19**(3): p. 2546-2555.
234. Brasselet, S., et al., *Imaging Molecular Order in Cell Membranes by Polarization-Resolved Fluorescence Microscopy*, in *Fluorescent Methods to Study Biological Membranes*. 2013, Springer. p. 311-337.